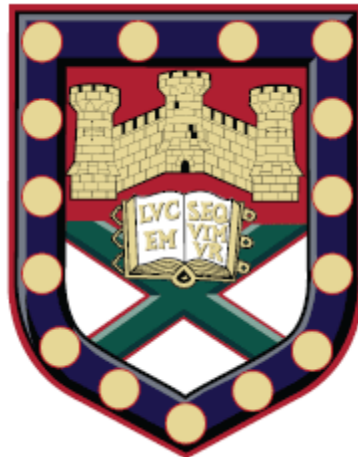


**Modelling landslide sediment and hazard cascades with limited data
availability following large typhoon events in the Philippines**



Submitted by Chloe Magenta Bird, to the University of Exeter as a thesis for the degree of Masters by Research in Physical Geography, May 2023.

This thesis is available for Library use on the understanding that it is copyright material and that no quotation from the thesis may be published without proper acknowledgement.

I certify that all material in this thesis which is not my own work has been identified and that any material that has previously been submitted and approved for the award of a degree by this or any other University has been acknowledged.

Abstract

Despite landslides acting as a dominant source of sediment within river catchments, the impact of sediment transport and delivery following an extreme weather event on channel geomorphological change is not yet well understood. This research builds on existing studies by investigating the Abuan River catchment in the Philippines following Typhoon Lawin in 2016 and Typhoon Kammuri in 2019. Each event triggered thousands of landslides varying in magnitude, of which a large proportion following Typhoon Lawin produced landslide runouts connecting to the channel network. When considering the associated uncertainty and data availability, Typhoon Lawin was selected for further investigation of the impact of landslide sediment input on changes in channel geomorphology.

Traditionally, geomorphic channel change is determined through calculated change in active channel width which is assessed alongside stream power across the catchment. Stream power alone failed to explain changes in lateral channel change observed from satellite imagery across the Abuan River catchment. This research builds on existing studies to incorporate the influence of landslide sediment fluxes through the use of *r.avaflow*, a computational multi-phase mass simulation model. With a digital elevation model only available prior to the landslide event, methods used in previous studies were unattainable and therefore an empirical formula was used to derive landslides depths to be input into the model. Additional key parameters were based on a previous study also conducted in the Philippines or calibrated to observed channel changes. Modelled results with the inclusion of landslide sediment, demonstrated high consistency with lateral channel changed observed with large depths of

deposition and a dominance of erosion upstream. Sensitivity analysis alongside a test run without the inclusion of landslides validated the choice of parameter values used. Results highlighted the importance of a multi-phase model approach to simulate channel morphological change in mountainous and tropical catchments with high rates of landslide sediment delivery.

This study improves the understanding of geomorphic hazard following a typhoon event by integrating the impact of landslide sediment influx into existing understanding of processes influencing of geomorphic channel change.

Acknowledgements

Firstly I would like to thank my supervisors, Georgie Bennett, Diego Panici and Rolf Aalto, for their continued support while conducting this research.

Throughout they took the time to meet with me both in person and online to share relevant insights as well as provide guidance on my research endeavours. I would also like to thank collaborators of the SCaRP project for sharing various data resources with me and being such a welcoming research group. Additionally, thank you to David Hein-Griggs for helping me to overcome technical challenges and sharing his expertise throughout this research. I would also like to thank my friends and family who supported, motivated and encouraged me throughout this research.

i. **Table of Contents**

Section	Heading	Page
i	Table of Contents	4
ii	Table of Figures	9
iii	Table of Tables	13
iv	Tale of Equations	14
v	List of Accompanying Material	14
1	INTRODUCTION	15
1.1	Project Rationale	15
1.2	Literature Review	18
1.2.1	The landslide hazard cascade	18
1.2.2	Influence of landslides on channel form and processes	19
1.2.3	Interaction between landslides and communities	21
1.2.4	Landslide analysis	23
1.2.5	Landslides triggered by typhoons	26
1.2.6	Investigation of geomorphic impacts of floods	28
1.2.7	Sediment cascades	30
1.2.8	Landslide sediment composition and flow characteristics	30
1.2.9	Controls on channel morphology	33
1.2.10	Sediment cascade and channel geomorphology	36
1.2.11	Processes influencing changes in channel geomorphology	38
1.2.12	Modelling landslide-flood hazard cascades	43
1.3	Aim, Research Questions and Objectives	55
1.3.1	Aim	55
1.3.2	Hypothesis	55

1.3.3	Research questions	55
1.3.4	Objectives	55
1.4	Study Site	56
1.4.1	The Philippines	56
1.4.2	The Abuan River Watershed	56
1.4.3	Geological Characteristics	58
1.4.4	Sub-Area Modelled Site	62
1.5	Typhoon Events	63
1.5.1	Typhoon Lawin	64
1.5.2	Typhoon Kammuri	65
2	METHODOLOGY	67
2.1	Data Collection	67
2.1.1	Digital Elevation Model	67
2.1.2	DEM Co-Registration	69
2.1.3	Satellite Imagery	70
2.1.4	Rainfall Data	73
2.2	Data Analysis	74
2.2.1	Creating a landslide inventory	74
2.2.2	Mapping active river channels	75
2.2.3	Uncertainty associated with human error	78
2.2.4	Topographic analysis	78
2.2.5	Landslide depth estimation	79
2.2.6	Rainfall-runoff analysis	81
2.2.7	Discharge and stream power analysis	82
2.2.8	Sediment input from landslides analysis	84

2.2.9	Modelling the sediment cascade	84
3	RESULTS	94
3.1	Landslide Inventory	94
3.1.1	Typhoon Lawin	94
3.1.2	Typhoon Kammuri	95
3.1.3	Landslide magnitude-frequency	95
3.1.4	Landslide density	98
3.2	Geomorphic change in Abuan River Network	99
3.2.1	Active Channel Width (ACW)	104
3.2.2	River Abuan	106
3.2.3	Sub-catchment identified for modelling	110
3.2.4	Rainfall, discharge and topographic factors	111
3.3	Stream Power	113
3.3.1	River Abuan	115
3.3.2	Study area	115
3.3.3	Comparison of ACW, stream power and sediment input from landslides	117
3.4	r.avaflow model outputs	120
3.4.1	Topographic changes in channel geomorphology modelled following Typhoon Lawin	120
3.4.2	Comparison of modelled to observed changes in ACW	122
3.4.3	Sediment depth and velocity of different phases over time	124
3.4.4	Assessment of the inclusion of landslides	128

3.4.5	Sensitivity Analysis	130
4	DISCUSSION	136
4.1	Relative geomorphic impacts of Typhoons Lawin and Kammuri on Abuan catchment	136
4.1.1	Differences in landslide characteristics between typhoon events	136
4.2	Landslide contribution to lateral channel widening during typhoon events	138
4.2.1	Stream power and changes in ACW	140
4.2.2	Influence of landslides on changes in ACW	141
4.3	Effectiveness of r.avaflow to simulate the effects of typhoon induced landslides on channel geomorphology	144
4.3.1	Modelled with the inclusion of landslides and runouts	144
4.3.2	Simulations without the inclusion of landslides	148
4.3.3	Sensitivity analysis	149
4.4	Additional research considerations, limitations and improvement	152
4.4.1	Seasonal variability	152
4.4.2	Data availability and lack of fieldwork analysis	153
4.4.3	Limiting factors and associated uncertainty of ACW	154
4.4.4	Channel confinement	156
4.4.5	Assumptions and uncertainty of landslide sediment input	159

4.4.6	Topographic change of lateral channel extents	160
4.5	Model Limitations	162
4.5.1	Upstream sediment input	162
4.5.2	Model inputs	164
4.5.3	Suitability of r.avaflow	164
4.6	Future Research	165
4.6.1	Consideration of the influence of previous landslides on follow-up landslides	165
4.6.2	Additional study sites	166
4.6.3	Fieldwork data collection	167
4.6.4	Application of data	168
5	CONCLUSION	169
6	APPENDICES	175
6.1	Appendix A	175
6.2	Appendix B	176
6.3	Appendix C	177
6.4	Appendix D	179
6.5	Appendix E	180
7	BIBLIOGRAPHY	181

ii. Table of Figures

Figure	Heading	Page
1	INTRODUCTION	
1.1	Map of observed tracks the global spatial distribution of tropical cyclones over 150 years up until September 2006 by Nasa (2006).	17
1.2	Figure 1.2: A classification of landslides in line with Varnes (1978) by Mouratidis (2010).	21
1.3	Flowchart of landslide map creation by Jaboyedoff et al. (2012).	25
1.4	Hierarchical structure over different time scales of controlling factors influencing river morphodynamics by Rhoads (2020).	51
1.5	Schematic diagram of the framework of r.avaflow produced by Mergili et al. (2017).	51
1.6	Results of simulations by Bennett et al. (submitted) using r.avaflow	52
1.7	Model output results from Panici et al. (in review) of topographic change of Antamok River	53
1.8	Sensitivity analysis of r.avaflow modelling by Panici et al. (in review)	54
1.9	Map of River Abuan catchment with insert map of location in the Philippines	58
1.10	Lithology and land use cover maps of Abuan River catchment	61

1.11	Close up of Google Earth satellite imagery highlighting channel geomorphology	62
1.12	Map of study site selected for modelling magnified	63
2	METHODOLOGY	
2.1	Magnified views of satellite imagery used to delineate landslides and channel width	77
2.2	Total and peak intensity event rainfall on 19 th October 2016 over first 24 hours Typhoon Lawin made landfall	82
2.3	Location of observation points along the section of channel modelled	89
3	RESULTS	
3.1	Landslide inventories following Typhoon Lawin (with runouts) and Typhoon Kammuri	96
3.2	Power law magnitude frequency distribution curves for landslides inventories following both typhoon events	97
3.3	Landslide density maps following both typhoon events	98
3.4	Delineated channel networks before and after each typhoon event	100
3.5	Areas of interest of dramatic changes in channel width across the Abuan river network	101
3.6	Channel mapping following Typhoon Lawin overlaying PlanetLabs satellite imagery at AOI 1-3	102

3.7	Channel and landslide mapping following Typhoon Lawin overlaying Google Earth satellite imagery at AOI 1-3	103
3.8	Maps of changes in active channel width across the Abuan River network following both typhoon events	105
3.9	Patterns of changes in active channel width, stream power and landslide sediment flux following Typhoon Lawin along River Abuan	108
3.10	Patterns of changes in active channel width, stream power and landslide sediment flux following Typhoon Kammuri along River Abuan	109
3.11	Maps of discharge, elevation and slope gradient calculated across Abuan River network	112
3.12	Comparison of changes in active channel width and stream power calculated across the Abuan River network	114
3.13	Patterns of changes in active channel width, stream power and landslide sediment flux following Typhoon Lawin along study site selected for modelling	116
3.14	Topographic change of study site modelled for Test 1	121
3.15	Location of transect lines along the study site selected for modelling	123

3.16	Graph comparing simulated channel width of Test 1 to that observed	124
3.17	Elevation and average velocity of sediment contributions at observation points along the channel modelled	127
3.18	Topographic change of study site modelled for Test 0	129
3.19	Graph comparing simulated channel width of Test 0 to that observed	130
3.20	Sensitivity analysis of topographic change of study site modelled comparing Tests 1-5	133
3.21	Graph comparing simulated channel width of sensitivity analysis comparing Tests 1-5 to that observed	134
5	CONCLUSION	
5.1	Schematic flow diagram of analysis of changes in geomorphology with new conceptual framework of including the effects of landslides	174
6	APPENDICES	
E	Graph quantifying change in elevation along cross section found ~3500 km downstream along the channel modelled	180

iii. Table of Tables

Table	Heading	Page
2	METHODOLOGY	
2.1	Satellite imagery sources	73
2.2	Landslide dataset and parameter for scaling relationship	81
2.3	Input parameter for r.avaflow	88
2.4	Parameters tested in sensitivity analysis	92
3	RESULTS	
3.1	Descriptive statistics of both landslide inventories	97
3.2	Statistics of active channel width change across Abuan River network	106
3.3	Statistics of active channel width change along Abuan River channel	110
3.4	Derived topographic, discharge and slope statistics across River Abuan network	113
3.5	Derived stream power, sediment contribution and active channel statistics along the River Abuan	118
3.6	Statistics comparing changes in active channel width between Tests 1-5 to observed	135
6	APPENDICES	
A	Parameters selected when creating DEM in DSM-OPT service	175

B	Total and average intensity of rainfall on the day Typhoon Lawin made landfall at each satellite rainfall cell location	176
C	Changes in ACW comparing pre- and post- channel width following Typhoon Lawin and Typhoon Kammuri	177
D	Comparison of simulated (Tests 0-5) and observed channel widths along modelled study site	179

iv .Table of Equations

Equation	Heading	Page
2	METHODOLOGY	
2.1	Active channel width calculation	78
2.2	Scaling relationship to derive landslide volume	80
2.3	Stream power calculation	84

v. List of Accompanying Material

1. Manuscript of Panici et al. (in review) - Observations and computational multi-phase modelling show complex tropical channel changes downstream from rainfall-triggered landslides

1. Introduction

1.1 Project Rationale

Typhoons are tropical cyclones with the addition of characteristic high intensity winds in excess of 118 kph, intensifying to a super typhoon with winds exceeding 220 kph (van der Meide and Pagaran, 2017). In line with climate change projections, the frequency and intensity of extreme rainfall weather events is expected to rise, thereby increasing the associated risk of flood and landslide hazards (Gariano and Guzzetti, 2016). It is estimated that the intensity and frequency of future tropical cyclones is going to increase by 2-11% by 2100 and change in their trajectories increasing the associated hazards (Sevieri and Galasso, 2020). Asia is disproportionately vulnerable to typhoon-induced landslide events (Bankoff, 1999) and more specifically the Philippines due to the fact it is a meteorological and geological world disaster hotspot (Shaw et al., 2010). Due to the Philippines' volcanic archipelago it experiences a high frequency of earthquakes and is vulnerable to tropical cyclones (Figure 1.1) increasing the vulnerability to landslide events (Nolasco-Javier et al., 2015). It is inflicted by a quarter of all typhoons globally which develop from tropical cyclones originating in the west of the northern Pacific Ocean (van der Meide and Pagaran, 2017).

Increased frequency and intensity of these extreme weather events leads to a greater associated landslide and flood hazard which influences the evolution of landscapes by enhancing erosion and driving channel widening (Ruiz-Villanueva et al., 2018). Changes in channel geomorphology pose a significant threat to riparian communities as can lead to the destruction of infrastructure along the channel (Ruiz-Villanueva et al., 2014, Wohl et al., 2010). Ever

increasing pressures of population growth drives land use change through urbanisation of embankment construction (Wyżga, 1997) and deforestation to cultivate land for farming. Encroachment of communities onto riverbanks provides reasoning for the increased vulnerability and high economic losses associated with landslide and flood induced channel widening. The relationship between hillslope characteristics and river dynamics plays a crucial role in sediment characteristics downstream (Korup et al., 2010). Therefore, it is important to further understand the link between landslide sediment input and transport on changes in channel geomorphology (Church, 2006). The temporal assessment of changes in channel geomorphology following an extreme weather event supports river management projects. This helps to improve existing and create new mitigation efforts aiming to protect vulnerable communities.

Numerous studies have used remote sensing data, such as satellite imagery, to collate inventories of landslides following extreme events, such as typhoons (Abancó et al., 2020, Jones et al., 2023). These inventories are used in different ways to conduct landslide hazard assessment, for example by investigating landslide magnitude frequency distributions and spatial landslide susceptibility (Eco et al., 2015, Jones et al., 2023, Rabonza et al., 2016). Other studies quantify sediment budgets from extreme events and rates of sediment delivery to the river network by landslides (Rathburn et al., 2017, Sutherland et al., 2002). However, the investigation of the role of landslides on geomorphic channel change during extreme events is in its infancy (e.g. Panici et al. in review; Bennett et al. submitted). These studies leverage new open source numerical modelling tools to demonstrate the role of landslides in channel widening during flood events through mechanisms of flow bulking by sediment

and temporary damming of the flow by sediment. This research will focus on applying similar tools to evaluate the hypothesis that landslides contribute to channel widening in floods and must be considered to accurately simulate flood channel widening. Research will be conducted in a new region of the Philippines forming part of the Simulating Cascading Rainfall-Triggered Landslide Hazards in the Philippines (SCaRP) project. Findings presented will have implications for management and mitigation of flood hazards along confined mountain channels.

Tracks and Intensity of All Tropical Storms

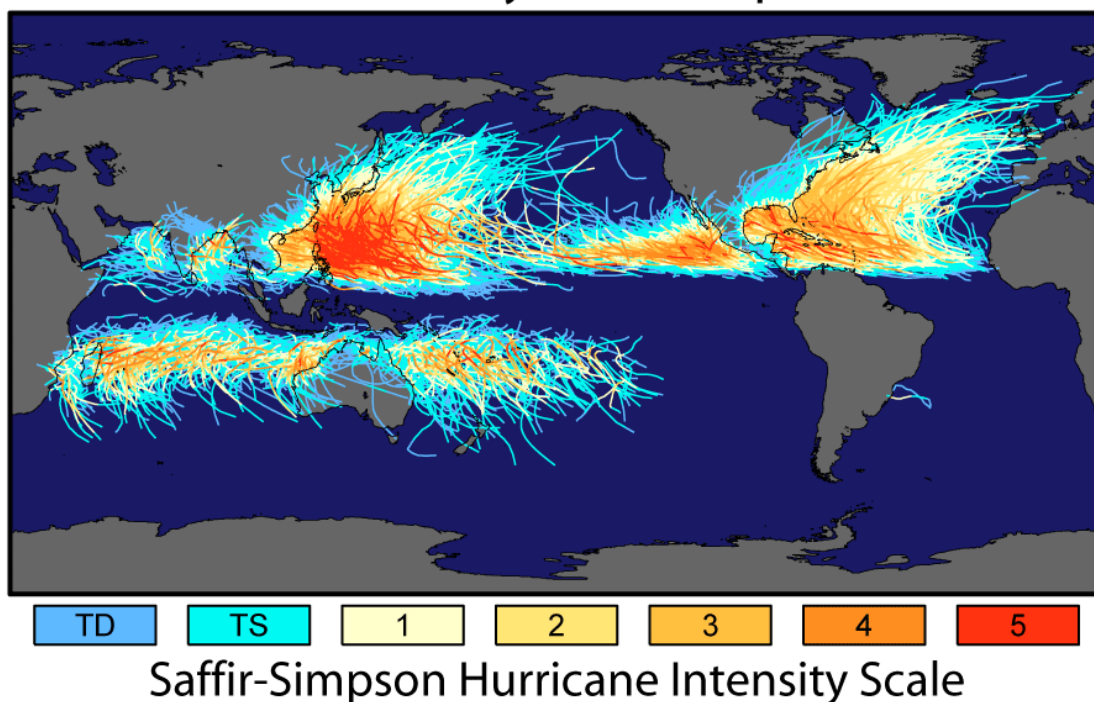


Figure 1.1: Map tracking the global spatial distribution of tropical cyclones over 150 years prior to September 2006 by Nasa (2006).

1.2 Literature Review

1.2.1 The landslide hazard cascade

Landslides are a dominant mechanism of sediment transfer and play a crucial role in controlling channel morphology and sediment cascades (Brardinoni et al., 2009). They are defined as the mass movement of debris downslope due to a number of different environmental and anthropogenic factors across a landscape (Reichenbach et al., 2018). Landslides occur when poorly consolidated sediment becomes saturated, such as from a heavy rainfall event (Stephenson et al., 2018). Extreme rainfall lowers soil cohesion which causes the surge of displaced material once the resistive shear stresses of the slope are exceeded by the shear strength, e.g. gravity (Iverson, 1997). Shallow slides are defined as new or reactivated failures of slopes of less than 2 m in depth (Mondini et al., 2011). These shallow debris slides may evolve and propagate downslope to form debris flows (Guthrie and Evans, 2004). When sediment combines with water and transverses down a slope at a high velocity, unsteady surges with high concentrations of large rock fragments have the ability to entrain large amounts of material (Berzi et al., 2010, Mondini et al., 2011).

Geologic and topographic factors influence the susceptibility of a landscape to incur a landslide. Landcover characteristics play a critical role in the occurrence of debris flows (Pradhan et al., 2010). In addition, different land use types control slope stability which is particularly dependent on vegetation cover characterising the hydrological as well as mechanical factors of the landscape (Reichenbach et al., 2014). Soil characteristics also determine the stability of slopes as they alter the hydrological characteristics of the landscape system (Van Asch et al., 1999). Soil type is widely considered in conjunction with slope gradient and elevation as collectively these influence the level of saturation

during heavy rainfall events, affecting the shear stress and stability of the slope (Fan et al., 2016). Changes in these factors can increase the likelihood of landslide occurrence, such as deforestation and urbanisation of slopes altering the geologic composition and slope angle, increasing the risk of the hazard imposed on local populations (Melillo et al., 2018). Although these factors precondition the landscape, and landslides can occur stochastically with no apparent trigger, it is abrupt changes in the environment that trigger mass landslide events (Jakob and Lambert, 2009), such as earthquakes or extreme weather events.

To evaluate the change in landscapes caused by mass wasting events, it is important to quantify the number, area and volume of landslides to identify associated processes, susceptibility and hazard across the catchment (Guzzetti et al., 2009). For the purpose of this investigation, in line with the existing mapping criteria of landslide inventories of the SCaRP project, every landslide is to be mapped, including those with an area smaller 10 m². Despite this being time consuming research, it is important to create inventories following more recent landslide events to learn about the evolution of landscapes and update or infill existing inventories (Malamud et al., 2004). Improvement in the understanding of landscapes will help inform local authorities to create the most appropriate warning and evacuation strategies to best mitigate the risks associated with landslide hazard (Church, 2006).

1.2.2 Influence of landslides on channel form and processes

Landslides play a key role in the evolution of mountain basins as sediment can be supplied to river channels via various hillslope mechanisms (Oguchi et al., 2001). Landslides are categorised by the type of movement (fall, topple, slide,

spread or flow) and whether they are rock, debris or soil based as shown in Figure 1.2 (Hunggr et al., 2014; Mouratidis, 2010; Varnes, 1978). The impacts of landslides however varies as a function of landslide type, connectivity with the fluvial system and transport as well as storage capacity of the fluvial system (Clapuyt et al., 2019, Gran and Czuba, 2017). Therefore, the effects of landslides on river dynamics is highly variable and depends predominantly on the volume of sediment delivery (Korup, 2005). There are also other factors to consider, such as landslide-channel connectivity, including population (landslide frequency), areal (landslide area) and volumetric (landslide volume) connectivity and the velocity, angle and direction of landslide entry which are all linked to the topography and lithology of the landscape (Li et al., 2016, Liu et al., 2021).

In some cases, landslides may have only a minor impact on the channel (Kirschbaum and Stanley, 2018). Alternatively, landslides can supply enough sediment to dramatically change, most frequently lower, the slope angle of the river channel (Ferguson et al., 2015, Tseng et al., 2015). On an even larger scale, in extreme cases the channel may become dammed following a large supply of sediment blocking the flow (Catane et al., 2012), dramatically altering the downstream channel flow regime (Chen et al., 2017, Kumar et al., 2019). Downstream of a dam, flood hazard increases as if it were to fail, the sudden release of stored water causes an increase in discharge and flash flooding (Catane et al., 2012, Wang et al., 2017). The most frequent mechanism of large scale sediment transfer occurs as a result of debris flows (Bardinoni et al., 2009), which this investigation will focus on, due to their long runout distances and connectivity with the river network.



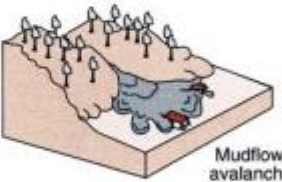


MECHANISM		MATERIAL			VELOCITY
		Rock	Fine-grained soil	Coarse-grained soil	
Slide	 Earth slump	Slump	Earth slump	Debris slump	Slow (days to weeks)
	 Block glide	Block glide <i>Down the plane of inclined rock layers where inclination is parallel to slope.</i>	Earth slide	Debris slide	
Flow	 Mudflow, avalanche	Rock avalanche	Mudflow, avalanche	Debrisflow, avalanche	Very rapid (minutes)
	 Creep	Creep	Creep	Creep	
Fall	 Rockfall	Rockfall	Earthfall	Debrisfall	Extremely rapid (seconds)

Figure 1.2: A classification of landslides in accordance with Varnes (1978) by Mouratidis (2010).

1.2.3 Interaction between landslides and communities

Landslides are only hazardous when interact with human activity (Karsli et al., 2009). They are known to cause a large amount of loss to both life and infrastructure annually (Mergili et al., 2017) of which the socioeconomic costs tend to be significantly higher than commonly reported (Schuster, 1996). This is

likely due to the fact landslides are frequently reported as multi-hazard scenarios that collaboratively assess numerous natural hazards, e.g. earthquakes, hurricanes, wildfires and floods. Therefore the impact directly associated with landslides is not fully understood (Kjekstad and Highland, 2009). As a result, it is important to analyse the impact of landslides and the induction of secondary hazardous events, such as flooding, to understand the overall impact on the landscape.

It is estimated that slope failure accounts for approximately (~)14% of all casualties attributed to natural hazards (Froude and Petley, 2018) with landslides causing ~1000 deaths and property damage of ~\$4bn annually (Karsli et al., 2009). The true socioeconomic cost is however not fully known as factors associated with natural hazards that both directly and indirectly affect a population, are much more difficult to quantify than just physical factors alone (Kjekstad and Highland, 2009). For example Eidsvig et al. (2014) reports that a community is directly impacted by the loss of buildings which indirectly results in the socioeconomic loss of income for workers of which both the physical and socioeconomic can be quantified. However, there are additional underlying factors that influence a community's ability to endure a natural hazard. Different climatic variables will affect slopes and landslide types in varying ways (Froude and Petley, 2018, Gariano and Guzzetti, 2016). This investigation will focus on the impact of physical processes that drive geomorphic change to be able to quantify and better understand the nature of the hazard imposed on the landscape. In turn, this will help to reduce the socioeconomic costs associated with this type of hazard.

1.2.4 Landslide analysis

To assess landslide risk, studies must first compile a landslide inventory before additional and more specific analysis can occur. Spatial landslide databases are useful in determining magnitude-frequency relations of landslides at a given time which may be a continuous record or following a singular event (Corominas and Moya, 2008). Following a landslide event, inventories may only include landslides directly attributed to the event or may also be comprised of relic or historical landslides dependent on the purpose of the analysis (Picarelli et al., 2005).

To conduct such inventories, in recent years traditional methods of in-field data collection, such as field surveys, have been replaced due to improvements in technology through the use of remotely sensed data, such as satellite imagery and aerial photography (Reichenbach et al., 2018). The attainment of high-resolution topographic surveys has promoted new applications and ways of analysing the earth's surface to detect geomorphic change, such as digital elevation model (DEM) analysis to create a DEM of difference (DoD) or derive slope gradient and elevation characteristics (Tarolli, 2014). Analysis of surveys before and after extreme events, such as typhoon induced landslides, allows investigation into the processes which caused changes in the topography observed driving the evolution of landscapes as a result of each event (Tseng et al., 2015).

Identifying the timing and location of landslide events over large extents presents a challenge as the occurrence of landslides is influenced by varying geologic and atmospheric conditions that lead to slope failure and it can be difficult to precisely understand all conditions (Kirschbaum and Stanley, 2018).

In addition, landslide events may occur in succession and care must be taken when attributing delineated landslides to specific events. Historic landslide scours may remain visible, for example in places where vegetation recovery rates are low, so human error in mapping landslides following specific events must be accounted for. Jaboyedoff et al. (2012) presents a step by step framework to create and validate landslide inventories (Figure 1.3). Despite this global landslide inventories are heterogenous and mapped based on varying criteria as there is no universal framework informing landslide studies due to differences in data availability (Karsli et al., 2009, Kjekstad and Highland, 2009). It is important to continue to contribute to the global landslide inventory and set out the criteria in which landslides have been mapped to better inform analysis of landslide hazard.

From these inventories, landslides are categorised by their size and frequency due to the fact they are influenced by different forces. For example resistance in large landslides is controlled by friction whereas in small landslides cohesion acts as the dominant resistant force (Brardinoni and Church, 2004, Guns and Vanacker, 2014). Often within the literature size-frequency distributions are quantified through conceptual models such as cumulative frequency, probability density and frequency density distributions to assess scaling of landslide hazard (Tebbens, 2020). It is understood that landslide distribution follows a power law function based on the area and volume across large scale events (Brardinoni and Church, 2004, Guthrie and Evans, 2004, Guzzetti et al., 2002, Korup, 2005). Such scaling can occur spatially, geometrically and temporally with studies conducted predominately following large rainfall or earthquake triggered landslide events (Tebbens, 2020).

In addition, volumetric data is required to assess the impact of landslides following an extreme weather event. Ideally, a DEM from before and after the event are obtained to extract the differences in elevation and calculate the volume of each landslide identified (Bennett et al., 2012). This is however not always attainable as may not cover the region or time period required. Larsen et al. (2010) investigated the relationship between landslide area and volume by compiling numerous inventories globally. From this, an empirical formula was created using a scaling exponent to calculate volume of landslide from the area of failure. The use of this equation overcomes the requirement of DEMs or any inability to conduct fieldwork to calculate landslide volumes. Research into the controls of landslide volume-area scaling by Larsen et al. (2010) emphasised the importance of distinguishing between soil and bedrock landslides. Therefore, the geology of the landscape must be identified initially to best inform the scaling exponent used to estimate the volume of landslides.

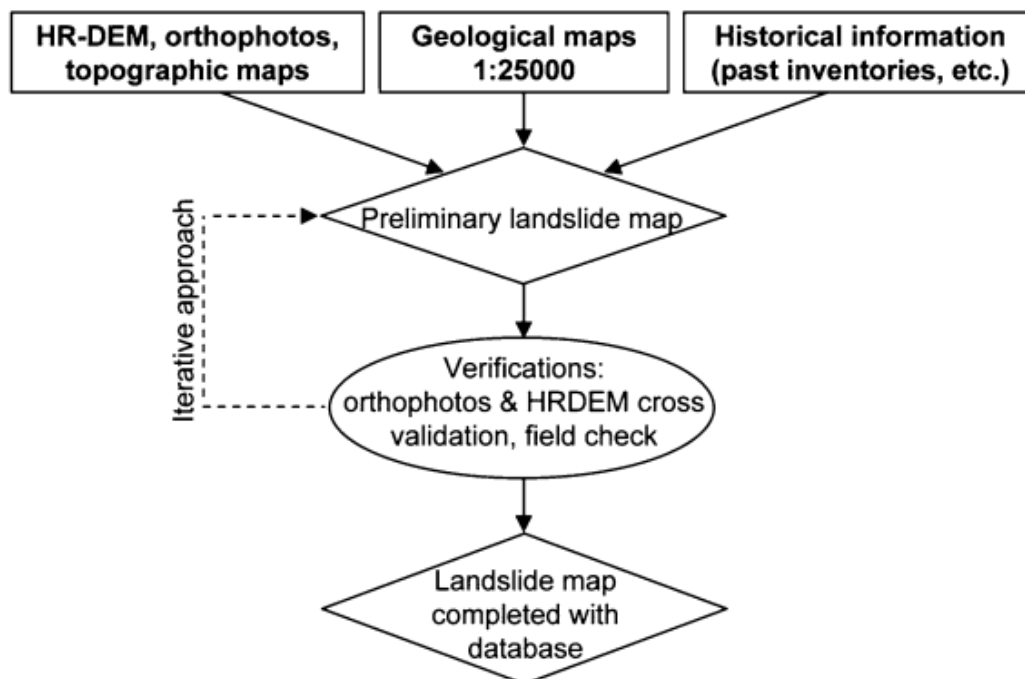


Figure 1.3: Flowchart of landslide map creation by Jaboyedoff et al. (2012).

1.2.5 Landslides triggered by typhoons

Climate change and predicted increases in warming will alter the hydrological cycle with higher atmospheric moisture from evaporation of oceans due to increased sea surface temperature (SST). This will provide a sustained energy source for more intense and prolonged storms over the ocean with the ability to make landfall (Jakob and Lambert, 2009). Although most reports are in agreement of an increase in the frequency and intensity of these events, there are high levels of uncertainty associated as to the magnitude of this increase and therefore the associated hazards (Pecchi et al., 2020). Mitigation efforts depend on the geographic area, the spatial scale of the hazard and needs of the community impacted (Kirschbaum and Stanley, 2018).

Hazard varies globally, with most landslide prone areas found along the Himalayan Belt, in Central America and the Philippines (Kjekstad and Highland, 2009). The intensity and frequency of natural hazards is expected to vary regionally as a result of changes in oceanic warming from El Nino and La Nina, sea level from retreating ice extents and soil moisture change across all continents (Chang, 2020). Predicted changes in these climatic conditions are anticipated to be more pronounced in environments at higher elevations, such as mountainous regions (Beniston, 2005). In addition this will have a profound impact on coastal regions.

In the Philippines, typhoons are most likely to occur during El Nino years due to the anomalous oceanic warming and alterations in SST. The higher SST, the greater the observed typhoon activity known as the 'ENSO-typhoon' hypothesis (Elsner and Liu, 2003). These favourable conditions intensify tropical cyclones into typhoons, however are weakened by vertical winds as opposed to

strengthened with horizontal winds defining the trajectory of the typhoon (van der Meide and Pagaran, 2017). Most damage is associated when typhoons make landfall and traverse across landscapes, of which the northernmost island of Luzon is reported to have experienced more typhoons than any other island in the Philippines.

Sudden changes to hillslopes as a result of extreme weather events can trigger landslides (Jakob and Lambert, 2009, Malamud et al., 2004). Tropical cyclones, or typhoons as reported in the Pacific, influence the geomorphology of the landscape. This occurs through a combination of wind and flood hazard (Stephenson et al., 2018) and landslide hazards (Chigira et al., 2013), causing most damage when all hazards occur concurrently (Catto and Dowdy, 2021). The mobilisation of sediment as a result of landslides influences the landscape across varying spatial scales, which has a knock on effect on fluvial systems further altering the geomorphology of channels downstream (Yanites et al., 2018).

Typhoon induced landslides act as a dominant mechanism for sediment transfer and are therefore a key driver of changes in channel morphology. They alter the amount of sediment entrained, transported and stored altering the flood risk downstream over time (Bagnardi et al., 2016, Nones, 2019). In the context of this investigation, debris flows will be categorised as the primary hazard inducing the secondary event of channel erosion and flooding in the form of cascade hazard. Due to the secondary impact of flooding on the geomorphology of channels, it is important to quantify and understand the effect of landslide sediment and hazard cascades to help understand the movement of sediment through river systems (Sutherland et al., 2002). This study will

support ongoing research into landslides in the Philippines but, vary from existing research by focusing on the role of sediment transfer on channel evolution. Current research by Panici et al. (in review) investigates the effects of Typhoon Mangkhut in September 2018 and this research aims to build upon these findings to better understand the role of sediment cascades following typhoon events.

1.2.6 Investigation of geomorphic impacts of floods

Morphologic changes are determined by both driving (discharge and slope gradient) and resisting forces (bed and bank resistance) (Bizzi and Lerner, 2015). Changes are most commonly investigated through analysis of stream power, which was first introduced by Bagnold (1960) who defines total stream power as the capacity of a river to cause geomorphological change as a product of slope gradient and discharge. By including width into the calculation, it allows for the application of unit stream power across a stream for a given discharge and slope gradient (Thompson and Croke, 2013). Unit stream power can be expressed as the potential energy expenditure per unit weight of water (Yang and Stall, 1974). Stream power used as a measure of the energy of the river flow at a given moment and its probability threshold provides an indication as to the value required to break resistive forces. This demonstrates the potential of the river discharge to erode channel banks and bed or below which would favour deposition. This indicates the channel's capacity to transport sediment and can therefore be used as a method to identify channel stability thresholds (Bizzi and Lerner, 2015). High rates of stream power indicate higher rates of erosion as a result of a higher gradient of a steeper channel associated with geomorphologic development. Stream power does not account for resistive forces however is accounted for (although implicitly) in the stream power

threshold. On the counter side, sections with low stream power or where there are abrupt decreases are likely to cause deposition. Changes in channel width can be more subtle than changes in flood flow and stream power which suggests additional controls on the locations of erosion and deposition (Gartner et al., 2015). Identification of areas of abrupt change in stream power highlights areas sensitive to intense erosion or deposition where river management strategies should be focused.

Stream power however only considers the fluid part of the flow and neglects the potential role of sediment supply on flow dynamics and subsequent channel erosion. To model stream power, assumptions are made that channel changes are influenced by only fluvial processes and that river-incision is the limiting process for topographic change in the mountain basin (Korup et al., 2010).

These assumptions are limiting and neglect the role of potential additional factors, such as sediment supply, driving channel change. Increasingly, studies are focusing on the importance of sediment supply on channel erosion, such as Finnegan et al. (2007), Mueller and Pitlick (2013) and Brenna et al. (2023).

Therefore, when changes in channel geomorphology observed differ from stream power calculated it can be inferred that there are other driving factors influencing channel change. This study aims to investigate other factors influencing channel geomorphology, primarily the influence of sediment delivery by landslides into river channels. This will provide a new conceptual way of understanding channel change to build on existing models which solely focus on fluvial driven processes.

1.2.7 Sediment cascades

The understanding of landslide sediment cascades and their characteristics has been investigated within the literature with differing ideas on the landslide characteristics as they propagate downslope. Increasingly geomorphologists are considering sediment connectivity across the landscape, linking processes from source to sink in the catchment (Bracken et al., 2015, Croke et al., 2005, Wainwright et al., 2011). Erosion, entrainment and deposition increase the volume of sediment cascade which alters their destructive potential and hazard associated (Santi et al., 2008). Mobility is determined by the energy of the landslide and ability to entrain sediment which can dramatically increase the overall volume downslope (Haas and Woerkom, 2016).

To model landslides, their ability to erode as well as entrain sediment is required to analyse their resultant mass increase which is directly linked to landslide hazard limiting mitigation efforts. Mechanical controls of erosion and entrainment of landslides as well runouts is not yet fully understood and as a consequence underestimated (Dietrich and Krautblatter, 2019). Long-runout landslides are common in mountainous terrains and the threat posed by them is linked to their high mobility (Heim, 1932, Pudasaini and Krautblatter, 2021). Therefore, these are to be mapped separately to account for the difference in characteristics from landslides. In addition, this helps eliminate the overestimation of landslide volume by separately mapping landslide scar areas from associated areas of runout.

1.2.8 Landslide sediment composition and flow characteristics

Landslide masses are formed by three distinct phases, solid, fine-solid and fluid, and the volume of entrainment of a landslide is highly dependent on the

composition of these masses (McArdell and Sartori, 2021). These components in the mixture of mass flow behave differently in response to basal boundary conditions, phase interaction and parameters of material. The solid component is comprised of coarse granular sediment such as boulders, cobbles and gravel, whereas fine-solid is consists of sand and particles larger than clay and silt which combined with water comprise the fluid component (Pudasaini and Mergili, 2019). Each of these sediment types are referred to as layers or phases. For the purpose of this investigation, we term solid material as phase one, fine-solid as phase two and fluid as phase three.

Previously within the literature hypotheses were proposed as to the reasoning behind the accelerated flow by Shaller and Shaller (1996). Initially, it was suggested that runouts are comprised of a fluidising component, such as air, water or vapour which act as lubricants and reduce the frictional forces acting on the sediment hence the greater mobilisation experienced (Legros, 2002). In contrast, Fahnstock (1978) suggested that entrapped air may instead act as a cushion to support and stabilise sediment as opposed to fluidising them. Contrarily, Hsu (1975) hypothesised that runouts incorporate fine particles which can fluidise and transport coarser debris. Numerous additional hypotheses exist and have been investigated through modelling to assess landslide properties such as viscosity and yield strength.

The role of both inter-porous fluids and sediment immersed fluids are not yet fully understood however there are a number of theories of how the presence of fluid mobilises sediment. Firstly incorporation of the fluid component reduces the solid friction coefficient such that landslides can travel larger distances than without a fluid component (Legros, 2002). This is achieved by partially

supporting the particles, thereby reducing the granular stress imposed (Bagnold, 1960). Alternatively, it has been suggested that fluidisation is caused by vaporisation of water at the bed when the pore fluid pressure gradient in the bed is lithostatic (Goguel, 1978). This strongly reduces the friction coefficient and thus enhances the overburden mass and flow sediment.

While in specific cases certain hypotheses of sediment mobilisation characteristics have worked, there is no widely recognised explanation for landslide mobility. It can however be understood that a combination of solid, fine-solid and fluid materials form the initial landslide whereas in the runout, fluid is not bonded to the solid matrix and fine-solid material can move independently from phase one (Iverson, 1997, McArdell et al., 2007, Schraml et al., 2015). Therefore, when assessing landslides, the role of fine-solid and solid sediment as well as fluids must all be carefully considered.

Assessment must consider the exchange in momentum as a result of shearing and rubbing between solid and fine-solid particles (Meyrat et al., 2022).

Shearing interactions between the particles and the ground cause the solid matrix to dilate such that the space between particles may either increase or decrease (Buser and Bartelt, 2009). This in turn affects the volume of the overall sediment and causes the density to change between phases. This occurs when the landslide is no longer in a steady state as the sediment leaves the slope and enters the runout zone (Meyrat et al., 2022). Transfer between these states determines the velocity of the flow as well as the density and is dependent on the amount of void space. This investigation aims to aid existing research to improve understanding of sediment cascades by accounting for

both fine-solid and solid material in landslides and runout generation as well as the interaction between phases.

1.2.9 Controls on channel morphology

Rivers are a vital part of the hydrological cycle and are key players in driving changes in the landscape through their evolution over time (Rhoads, 2020), despite only occupying a small percentage of the Earth's land surface (Whipple, 2004). Over time, changes in channel morphology are determined by varying factors such as tectonic uplift, fluvial erosion and climate change (extreme weather events, such as floods and landslides). Rhoads (2020) depicted the influence of these controlling factors on changes in river morphology over time as seen in the flow chart of Figure 1.4. Changes in river channels are determined by differences in sediment supply (frequency, volume and grain size), transport capacity (slope, discharge) and the direct or indirect effects of riparian vegetation (influencing bank strength, rates of runoff) (Montgomery and Buffington, 1998). This leads to changes in the slope, depth, width, velocity, roughness and grain size of the channel (Leopold and Maddock, 1953).

Hydraulic geometry has been studied in great depth over the past fifty years as its understanding is fundamental in the overall evolution of fluvial landscapes (Spotila et al., 2015). There are numerous factors which influence the pattern of the geometry of a river channel; tectonics, land use, riparian vegetation cover, stability of channel banks and locally built structures (Parida et al., 2017). To quantify channel change, width is often investigated, approximated as full channel width (Finnegan et al., 2005). Active channel width (ACW) is defined as the area of the channel occupied by flow and unvegetated sediment bars (Liébault and Piégay, 2002). It is understood that sediment supply conditions

are critical in understanding spatial patterns of ACW and therefore changes in channel geomorphology (Bertrand and Liébault, 2019).

ACW is highly dependent on various controlling factors and is therefore an evolving parameter which indicates changes in channel geomorphology. It is important to investigate the controls affecting ACW to gain a broader understanding of processes acting on the river across larger scales, for example the influence of uplift and changes in climate (Wobus et al., 2006). ACW is controlled by tectonic, topographic, lithologic and climatic changes. These controls act across different scales and therefore there can be locally varied resulting in different processes acting along different stretches of the river network (Spotila et al., 2015). For the width of a channel to increase, bank erosion needs to occur at the point where stream power exceeds the channel boundary resistance threshold (Parida et al., 2017). The threshold varies and is influenced by several controls. With low bank stability if the shear stress is greater than the cohesive strength, lateral erosion will occur resulting in the widening of a channel (Pitlick et al., 2013). Alongside natural processes acting along the river, anthropogenic activity also influences bank stability and therefore ACW. For example, the introduction of dams has a major influence on channel geometry as can control sediment and water fluxes. In addition, land use change across the floodplain has a direct impact on bank stability, potentially lowering the threshold of lateral erosion.

This may vary downslope as sediment also plays a key role in local channel width variation, such as following a mass wasting event being investigated here. Large amounts of sediment can either be transported further downstream or locally deposited largely influencing the morphology across the long profile of

the river. This alters the sediment calibre and degree of sorting which effects the ability to shield the channel from erosion (Gasparini et al., 1999, Robinson and Slingerland, 1998). Dependent on these factors, sediment input from cascades and mass wasting events can either be supply or transport limited altering the geomorphology of the river. Most commonly assessments of changes in channel geomorphology will focus on the width of the channel as can be achieved via conducting ground surveys or through remotely sensed satellite imagery. This investigation aims to improve the understanding of changes in ACW by investigating the effect of mass wasting events and landslide sediment fluxes on channel width change using remotely sensed data.

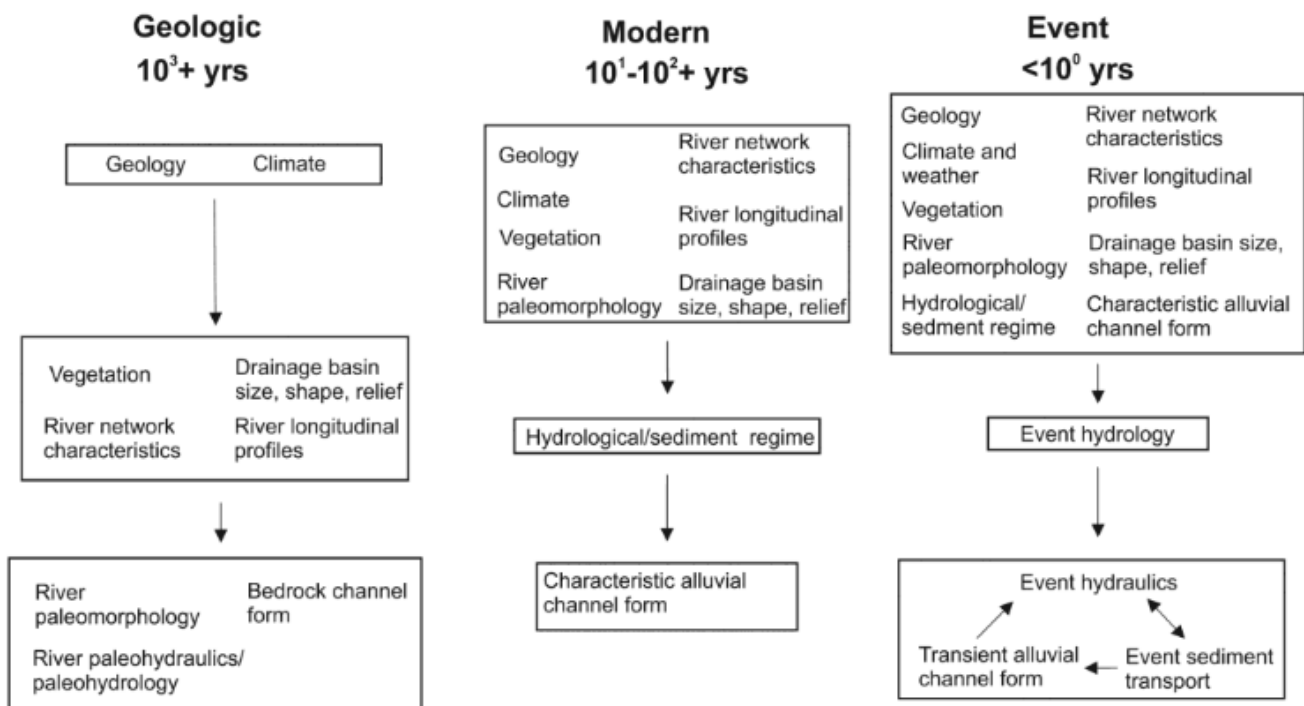


Figure 1.4: Hierarchical structure over different time scales of controlling factors influencing river morphodynamics by Rhoads (2020).

1.2.10 Sediment cascade and channel geomorphology

Channel morphology indicates the interaction between the stability of the bed and bank material compared to the force of water running through a landscape (Benke and Cushing, 2011). To understand the ability of landslide events of different magnitudes and frequencies to mobilise sediment, investigation into the dominant forces acting on the landscape needs to be conducted (Reid and Page, 2003). Channel morphology changes naturally via erosion and deposition causing the widening or narrowing of the channel making it either shallower or deeper altering the flood risk across the catchment (Agency, 2021). Upland rivers are active geomorphic systems which produce high sediment yields globally (Milliman and Syvitski, 1992). This is due to steeper channel gradients resulting in dynamic geomorphic processes which generate high rates of sediment production, transfer and deposition leading to increase geomorphic change (Johnson and Warburton, 2002). The relative influence of sediment cascades is however dependent on the dominant source of sediment production in the channel, such as gully or streambank erosion (Page et al., 1999). If these are already high within the channel network the relative contribution of landslide sediment cascades will be lower and vice versa.

Extreme weather events impact riverbed and bank erosion, channel widening, sediment deposition over bank and destruction of protective infrastructure (Langhammer, 2010, Magilligan, 1992, Prosser et al., 2000, Williams and Costa, 1988). Therefore, changes in channel geomorphology following extreme weather events can have significant impacts on society and infrastructure surrounding upland rivers and the effects can propagate to downstream communities (Davies and Korup, 2010). Flood surges and debris flows inducing sediment cascades have the ability to dramatically alter river dynamics through

different processes. For example, altering the transport capacity through changes in the vegetation cover, infiltration capacity and transport capacity as a result of the destabilisation of slopes (Benda and Dunne, 1997, Tseng et al., 2015). Sediment transport can however be limited as a result of excessive amounts of sediment entering the channel causing the diversion or burial of channels or creation of dams (Korup, 2005).

Although evidence suggests sediment cascades have a direct geomorphic control on river channels, further research is required to understand the influence of sediment cascades on changes in channel geomorphology (Korup et al., 2010). Research investigating the controls of geomorphic change following extreme weather events is most commonly reported for flood events (Joyce et al., 2018). Studies of flood events also tend to overlook the role of sediment instead focusing on changes in geomorphology linked to magnitude-frequency relationships, hydraulic forces (discharge, stream power, shear stress) catchments characteristics (e.g. channel confinement) and anthropogenic modifications (Lewin, 2013, Righini et al., 2017, Thompson and Croke, 2013, Wolman and Gerson, 1978). In comparison, only a few studies investigated the role of sediment cascades following flood events (Johnson, 2016, Joyce et al., 2018) and investigation following typhoon-induced landslide events is an area of research in its infancy (e.g. Panici et al., in review). Therefore, this research will enhance existing studies to better understand processes acting on the hillslope and fluvial morphologies which are traditionally separate areas of research (Korup, 2005).

1.2.11 Processes influencing changes in channel geomorphology

As the long profile of river networks defines the spatial relief of mountainous environments, a large proportion of research has focused on the controls of change along river channels (eg Tarboton et al., 1992 and Whipple and Tucker, 1999). There are different concepts as to the drivers of channel change over time and consequently basin evolution. Previous concepts have focused on the influence of fluvial driven processes including fluvial bedrock incision and channel widening (Korup, 2009). The rate of bed rock incision is commonly understood as a power-law function of mean bed shear stress which has led to the development of stream power modelling. If fluvial incision and widening defines the relief, this therefore acts as the rate-limiting process indicating the threshold of slope relief (Safran et al. 2005). Feedback loops however also exist between the rates of fluvial incision, channel widening and likelihood of landslides. High rates of incision will steepen riverbanks, destabilising hillslopes and will lead to the increase of landslides and visa versa (Korup et al. 2009). Flood events are often responsible for extreme rates of channel change along river corridors (e.g. Rathburn et al., 2017). Through the assessment of flood events, it is understood that changes in channel geomorphology depends largely on the magnitude and frequency of extreme weather events (Anderson and Calver, 1977). Large extreme weather events exude a greater influence on the ability of the river network to transport sediment. This is due to increased discharge and therefore presents a greater stream power to erode the valley floor and riverbanks,

There is an ongoing debate as to whether the magnitude or duration of stream power above a threshold has a greater control on channel geomorphic change (e.g. Magilligan et al., 2015). Other studies suggest geomorphic change can be

explained by the result of gradients in stream power (e.g. Gartner et al., 2015). Flood water may also transport and deposit large quantities of sediment influencing channel morphology (Joyce et al., 2018). Several studies have been unable to find a simple relationship between stream power and channel geomorphic change and have invoked other factors such as bed-packing geometry at the time of a flood (East et al. 2018) and sediment input by landslides (e.g. Bennett et al., submitted, Panici et al., in review).

Channel evolution and landslides has thus far been rarely quantified over large spatial or temporal scales. Therefore, little is understood of their influence and the extent sediment budgets can change within fluvial systems. Large landslides have the ability to reduce hillslope gradients along the long profile of a river and contribute to changes in active channel width of the river through the deposition of transported debris (Roering et al., 2005). Landslides with large runouts also have the ability to destruct valley floors through scouring and the vast deposition of debris (Shang et al., 2003).

The geomorphic efficiency of a landslide can be characterised by the rate and volume of sediment excavated then efficiently delivered to the channel which contributes to the overall sediment budget (Korup et al. 2009). The amount of sediment produced is a function of their magnitude and frequency (Reid and Page, 2002), hence the need to create landslide inventories. The overall contribution of larger landslides is less commonly investigated compared to small shallow landslides (Korup, 2009). Extreme rainfall events, such as that being studied here following a typhoon event, often generate greater peaks in landslide sediment delivery into the fluvial system (e.g. Abanco et al., 2021; Rathburn et al., 2017). Large uncertainty exists surrounding the amount of

sediment delivered to the channel, especially within models (Brardinoni and Church, 2004). This provides context to the nature of this research as often only the fluvial processes acting within a river basin are modelled, neglecting the potential impact of mass wasting sediment inputs, eg from landslides. This research aims to provide a new conceptual modelling approach to investigate the inclusion of landslide sediment when analysing changes in channel geomorphology following an extreme weather event. Traditional flood models

The assessment of flood hazard has evolved considerably over time through adjustments and improvements of numerous models. These can simulate changes in fluid dynamics following a flood event, with only recent advancements starting to include the role of sediment. Flood models use a momentum and conservation of mass approach (Blade et al., 2012). When assessing a cross section of river between two cross sections (or, if you use 2D models, in the 2D domain) the flood model follows these two laws; 1 - the amount of water entering and exiting must be conserved and 2 - the forces acting on the fluid (or exerted by the fluid on the solid boundary) need to balance each other or if unbalanced they will accelerate/decelerate the flow (Begnudelli et al., 2008). 1D models can be used to simulate the movement of water in rivers and are often used to understand the impact of floods, however, are unable to fully capture the intricacies of interactions between flood waters and the riparian environment (Kumar et al., 2023). Therefore, although more computationally expensive, 2D models may instead be used which simulate both cross-sectional and longitudinal water flow.

HEC-RAS is the most widely used hydraulic model worldwide which was initially used to model 1D flow through river networks provided freely by the US Army

Corps of Engineers. It is used primarily by engineers for channel flow analysis and floodplain delineation. Recent updates combine the existing modelling capabilities with 2D flow to enable the simulations of floodplains as well as complex river systems of flow and sediment (Patel et al., 2017). HEC-RAS is capable of simulating water surface profiles in varied steady and unsteady scenarios with the ability to simulate the consequences of obstructions, such as a bridges or weirs. Several studies have used HEC-RAS to simulate the inundation of a flood requiring only basic inputs such as river discharge, channel resistance and channel geometry. Numerous studies have simulated the effects of extreme weather events on changes in channel geomorphology, primarily as a consequence of flooding, such as Khattak et al. (2016). Khattak provided a case study of the Kabul River by modelling peak floods in 2010 to create floodplain maps of vulnerable areas. As with other studies, the use of HEC-RAS is designed to model floods and neglects potential sediment contributions from mass wasting flows such as landslides. Sediment transport in this model requires the application of 50-year old equations (Meyer-Peter and Müller, 1948) by giving an estimation of sediment transported in the river. Despite advances, traditional flood models are not fit for purpose to include large instantaneous sediment releases into the channel, such as landslides. Alternatively, when assessing channel geomorphological change, researchers also opt to use TUFLOW. This is able to handle large-scale data sets once again only requiring basic data sets of land cover statistics, topography and water level at the start of the simulation (BMT, 2016). This 2D model simulates the spatial pattern of the depth and velocity of channel flow through the use of numeric algorithms. It varies from HEC-RAS as in addition to flooding can simulate urban drainage, coastal hydraulics and track water quality. Numerous

studies have used this model to better understand inland floods, such as Fahad et al. (2020) who used this model to simulate heavily impacted areas of New Jersey, USA, following Hurricane Sandy in 2012. Outputs generated were similar to that observed and were useful in creating damage assessments for that particular type of extreme weather event. Although useful for modelling the impact of flooding in response to extreme weather events, this approach once again neglects sediment contribution. Advances in TUFLOW allow the use of modules such as sediment transport (Pasternack and Hopkins, 2017). Such advances in this module include the ability to model multiple sediment fractions at once, bedload transport, morphological bed evolution and feedback systems. Smith et al. (2019), used this extension to further understand bed sorting and armouring from the East Fork River, USA. The model was used to estimate channel stability in terms of patterns of erosion and deposition within the channel of which the modelled results agreed with that observed. Although appropriate for use in this study, the sediment transport module of TUFLOW is confined to the channel and is unable to simulate the sudden release of sediment from landslides within the floodplain for example. Therefore an alternate model is required for this research until further advances are made.

Additionally, researchers have used Sediment and River Hydraulics (SRH-2D) to model the hydraulics, sediment, vegetation and temperature of river systems (Lai, 2008). This builds upon the previous version (SRH-W) to include modules related to sediment focusing specifically on 2D modelling. It is capable of simulating flows from multiple streams, flood routing over any terrain, overspill of banks and morphological assessments of bed erosional potential. Among other studies, Ho et al. (2021), used SRH-2D to simulate geomorphological change across two rivers in Taiwan. Using the sediment module, results were

effective in stimulating bed elevation change over time following the typhoon induced rainfall. Despite also researching channel change following a typhoon event, this model is only able to simulate the consequence of flood induced change as opposed to the role of landslide sediment. Once again, this model is not compatible with the aims of this research as although it includes a sediment extension, it is once again confined to the channel. Therefore, this model is unable to fully simulate the effects of a sudden release of sediment from landslides and also fails to reflect the different characteristics of landslide sediment.

Although some of these traditional flood models may include sediment transport, they only consider erodible sediment on the channel and equations employed are based on experiments that studied mild sediment transport (e.g., Meyer Peter-Muller equation). None of these really considers sediment input that is as intense as the product of a landslide. The relationship between water and sediment is simplified within these models, neglecting any momentum exchange; however, when there's large sediment input like a landslide this cannot be neglected.

1.2.12 Modelling landslide-flood hazard cascades

There is a large range of differing modelling approaches used to investigate mass movements which provide a greater insight on the complexity of fluid dynamics within a given landscape. The ability to anticipate future events requires the understanding of processes and how they interact with one another, especially when more than one type of material is involved – in this case both solid and fluid. Seeking an approach that considers multi-phase modelling with the ability to incorporate large volumes of sediment (rather than

purely hydraulic-driven equations) is required for this research. Traditional flood models are useful, but only if the event you are simulating has little sediment involved. When large sediment is input, these models lose accuracy and validity as the physical processes are different.

The complexity of advanced fluid dynamics and the interaction with sediment from mass wasting flows, such as landslides and debris flows, has led to the development of numerous physical based dynamic models. Traditional flood models have extended to include the conservation of momentum (Savage and Hunter, 1989) and the effect of pore fluid (Iverson and Denlinger), however only consist of a single phase approach. The use of a two-phase model is more suitable for the simulation of process chains and the interaction between processes moving downstream. For example this enables the simulation of lake outbursts and resultant flooding as well as debris flows. This requires the ability to model entrainment of basal material into the flow which dramatically alters the properties and dynamics of a river channel from a single phase model. Empirical laws for entrainment were first introduced by Rickenmann et al. (2003) and have continued to be recognised in updated multi-phase models to simulate mass wasting event (eg. Le and Pitman 2009). Erosion is however not the only process acting on a landscape during an extreme event and therefore numerical models have advanced to consider the exchange in momentum to enable the simulation of potential deposition. Pudasaini (2012) introduced a two-phase model to route mass wasting flows such as debris flows, from a predefined release area to a potential deposition area accounting for the interaction of processes and change in momentum over time. Landslides and debris flows induced by a typhoon present a challenge to model due to their

complexity and multi-hazard nature which is overcome by using this multi-phase approach.

Pudasaini (2012) reviewed pioneering mass flow models; such as the work of a single-phase model only accounting for the solid phase of sediment by Voellmy (1955) prior to advances by Grigorian et al. (1967), Takahashi (1991) and Pitman and Le (2005), in addition to many others. Mergili et al. (2017) updates this assessment by including additional models over time as modifications were made to earlier models through the inclusion of depth-averaged masses and momentum conservation by Savage and Hutter (1989). Adaptations of this model have since been created by many such as Mangeney-Castelnau et al. (2005) and McDougall and Hungr (2005). More recent versions of the model by Savage and Hutter (1989) have evolved further to encompass the effects of pore fluid as seen from Iverson and Denlinger (2001), Pastor et al. (2009) and Hutter and Schneider (2010).

Although appropriate for each respective investigation, these fail to fully consider the multi-phase nature of landslides and different mechanical controls acting downslope. Seeking an approach that has the ability to incorporate large volumes of sediment in conjunction with hydraulic-driven equations is required for this research. Therefore, r.avaflow has been selected for this research as is deemed appropriate for creating realistic simulations of changes in the river. It overcomes the incapacities of other multiphase models as is able to incorporate the fine-solid phase and has the ability to simulate a mass wasting event through the instantaneous release of sediment. Pudasaini (2012) introduced the multi-phase modelling approach which utilises Python for data management as well as pre- and post- processing tasks, however the core

program and algorithm is written in the programming language C. R is then used for both validation as well as visualisation purposes (Baggio et al., 2021). It allows for the modelling of how landslides influence changes in channel geomorphology as is able to account for sudden releases of sediment. In addition, it can simulate the different behavioural properties of landslide compared to runout sediment. r.avaflow considers both the solid and fluid components of the flows separately as well as the interactions between phases. The role of fluid is considered as a function of solid particles in suspension (von Boetticher et al., 2016) and dependent on the concentration defined may act with differing viscosities as the flow propagates downslope. r.avaflow allows for the input of these different phases and considers their behavioural properties as well as interactions over time.

.Modelling the transfer of momentum includes viscous drag, buoyancy and changes in mass based on the velocity of each phase. This computational model accounts for the deformation, mixing and separation between each phase, required due to their strong coupling. r.avaflow deploys a total variation diminishing non-oscillatory central differencing (TVD-NOC) (Wang et al. 2004) scheme whereby the cell averages of all variables are computed using a staggered grid across the study site over time. Gravitational forces are calculated based on the topographic input (DEM) in x, y and z directions which also defines the depths of sediment and direction of flow. Entrainment is considered as an additional function which is built on the user defined maximum entrainment values input. It is assumed that the entrainment initially increases the solid and fluid momentum and consequently the depth as well as velocity which indicates areas of erosion. Changes in velocities also affects the frictional forces acting on each phase and therefore the stopping approach must be

considered using a numerical scheme. Deposition can occur when the friction angle is greater than the modelled slope angle calculated separately for each cell. The resultant depths based on the erosion and deposition simulated through the exchange of momentum between phases over time are converted into raster heights for output. A schematic diagram of the modelling process can be seen in Figure 1.5. This method of modelling has since been utilised to best anticipate the impact areas, energy change and travel times of mass movements which allows for more complex real-world analysis. For example, *r.avaflow* can be used to simulate if a mass movement were to enter a lake or in the case of this investigation, a river network (Mergili et al., 2020). This model can be used to simulate the impact of an extreme weather event such as a rock avalanche (Zhang et al. 2023) or, as being investigated here, typhoon-induced landslides.

r.avaflow has been deemed the most appropriate model to simulate the effects of landslides on changes in channel geomorphology following a typhoon event. It models the required processes acting downslope during a mass wasting event including erosion, extraction of sediment, sediment transport and transfer as well as deposition. The additional in-built function enabling multiple model runs facilitates multi-parameter sensitivity to help validate the use of unknown input parameters. As this research is to be conducted remotely with limited data availability, multiple consecutive model runs will help to reduce the associated uncertainty of estimating input parameters.

Bennett et al. (submitted) applied *r.avaflow* to simulate landslide-flood interactions and channel width change in the North St Vrain catchment in Great Colorado Flood of 2013. This research builds on that of Rathburn et al. (2017)

to include the role of landslides coupled with flood dynamics to further understand the controls on variable channel widening following a major flood event. An area of interest was selected of dramatic increase in channel width as a result of erosion of the channel estimated using a DEM of difference. Across varying sections of the river studied, despite low stream power and channel confinement values calculated, large channel widening was observed. This indicated an alternate process driving change in channel geomorphology. An area of interest was identified downstream of two large landslides and a tributary river generating a greater sediment input. Field work was conducted by Bennett et al. (submitted) to calculate the ratio of field-measured to calculated runoff based peak discharge useful in testing sediment bulking and surging. By visiting the site, indirect measurements of flood peak discharge were taken using a differential GPS to collect pairs of highwater marks. Data estimations of peak discharge were made using ArcGIS and LiDAR then compared to previously estimated runoff based discharge values. Through the assessment of numerous sites downstream, it could be inferred that the post flood channel indicated a blocking of sediment suggesting the formation of a dam downstream of the two landslide locations. This then burst during the flood event due to increase discharge.

To simulate this, r.avaflow was selected to model the hypothesis of dam formation and burst during the flood event. Landslides were mapped as input for the solid phase and calculated values of runoff discharge were used for the fluid phase. As in field observations found landslide sediment to be coarse, the fine-solid phase was not included. Performed in two stages, the dam formation then the burst, topographic change simulated supported the hypothesis presented Figure 1.8). To validate this, analysis was conducted without the inclusion of

landslides, however limited erosion was simulated which supported the role of landslides in changes in geomorphology observed (Figure 1.6). This research used a combination of field practices and numerical modelling to understand the role of landslide sediment delivery on changes in channel geomorphology following an extreme weather event.

Subsequently, Panici et al (in review) applied r.avaflow to successfully simulate the geomorphic impacts of Typhoon Mangkhut (2018) in the upper Agno catchment in Itogon, Philippines. This paper aimed to quantify the role of landslides influencing geomorphic change by mapping landslides and channels before estimating changes in width and modelling channel interactions during a flood event. Changes in active channel width observed could not be fully explained by values of stream power calculated. Therefore, r.avaflow was employed to simulate the influence of increased sediment from landslides as is able to incorporate the complexity of mass wasting flows on the landscape. In addition, the model could account for the impact of mining within the region by simulating the influence of sediment delivery on the tailing dam identified within the study site (Figure 1.7). Panici et al. were successful in simulating the effects of Typhoon Mangkhut and improved the understanding of the role of sediment delivery during an extreme weather event.

Uncertainty however exists as a result of data availability and due to the fact this area of research is in its infancy. Therefore, as will be undertaken for this research, a sensitivity analysis was conducted to analyse the relevant influence of each parameter selected (Figure 1.8). Only slight variations could be observed and therefore the selection of parameters input was validated. Greatest variation existed between modelled outputs and observed channel width

when considering only the solid phase. This validates the use of r.avaflow as is a multi-phase model allowing the inclusion of both the solid and fine-solid phases with the fluid phase to best simulate the effect of landslide sediment input on changes in channel geomorphology.

This research aims to support the work of Bennett et al. (submitted) and more closely Panici et al. (in review) in a new area of the Philippines to further understand the role of typhoon-induced landslides and subsequent increases in sediment delivery on changes to channel geomorphology. The use of r.avaflow will aid in the purpose of this investigation to assess the suitability of using this model to effectively simulate the effects of typhoon induced landslides. . Model outputs generated will be used to better understand the processes driving the evolution of this landscape and the role that landslide sediment fluxes play in influencing these changes. This will provide a new conceptual framework as to the inclusion of landslide induced sediment fluxes when modelling changes in channel geomorphology following an extreme weather event.

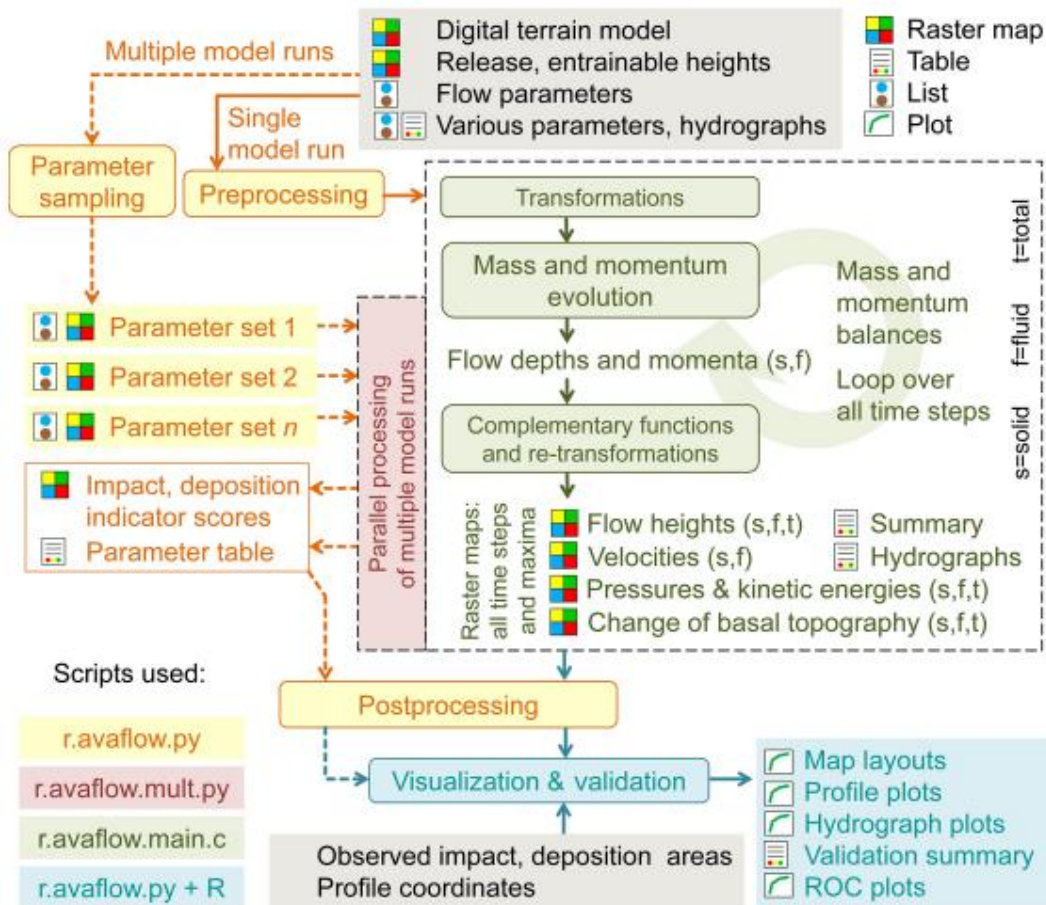


Figure 1.5: Schematic diagram of the framework of r.avafLOW produced by Mergili et al. (2017).

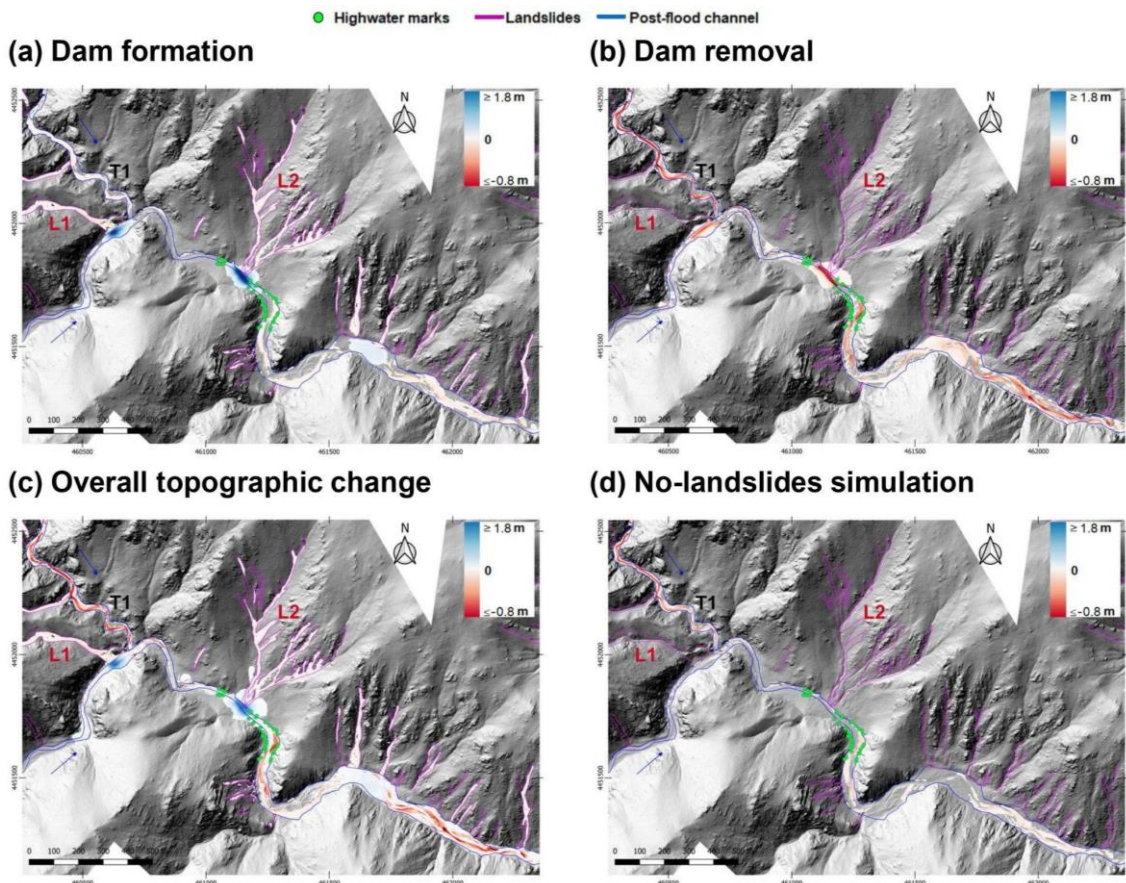


Figure 1.6: Results of simulations by Bennett et al. (submitted) using r.avaflow: (a) formation of the sediment dam, (b) dam removal with updated topography, (c) the resulting topographic change after both simulations, (d) the results of the simulations with no landslide sediment delivery, highlighting the importance of landslide sediment delivery for simulating observed channel widening.

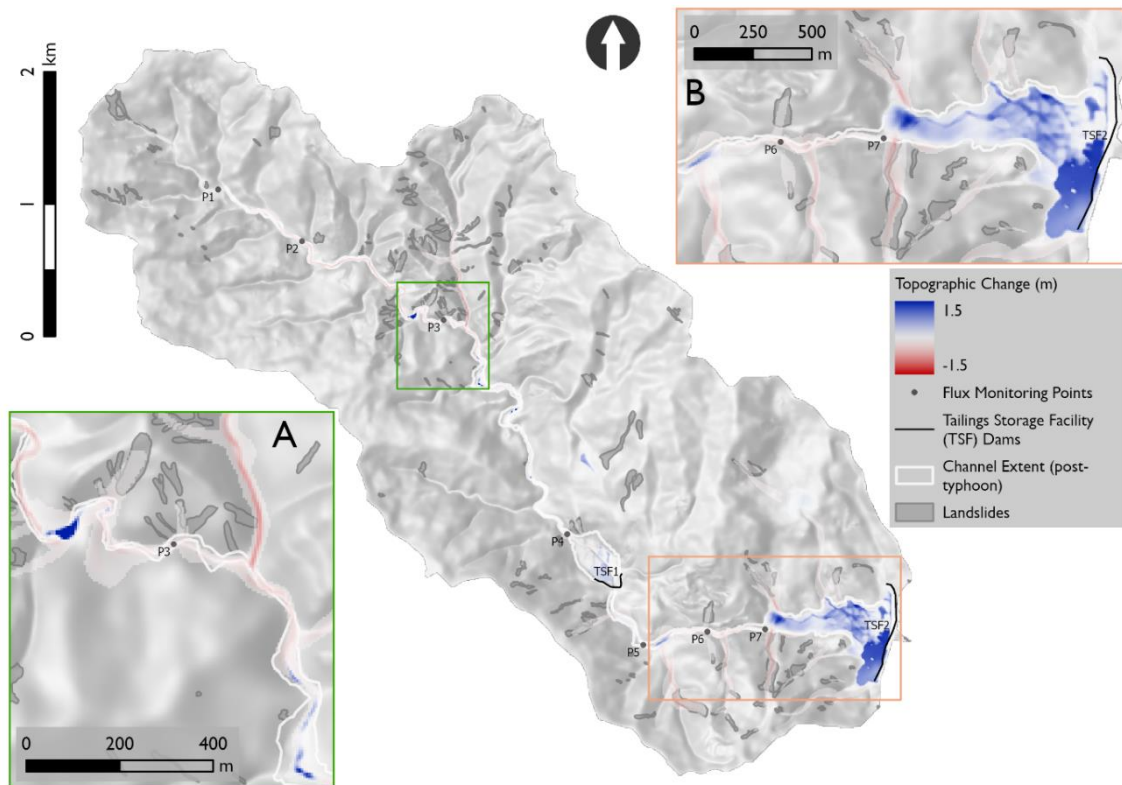


Figure 1.7: Model output results from Panici et al (in review) of topographic change of the Antamok River modelled by r.avaflow overlaid on the pre-event DEM and compared to the observed pattern of channel widening and landsliding. Predicted erosion and deposition are shared red and blue respectively. Two areas of interest (A and B) are shown in greater detail. Points of interest (labelled P1-P7) are indicated and used to analyse the temporal evolution of the simulated flows at flux monitoring points.

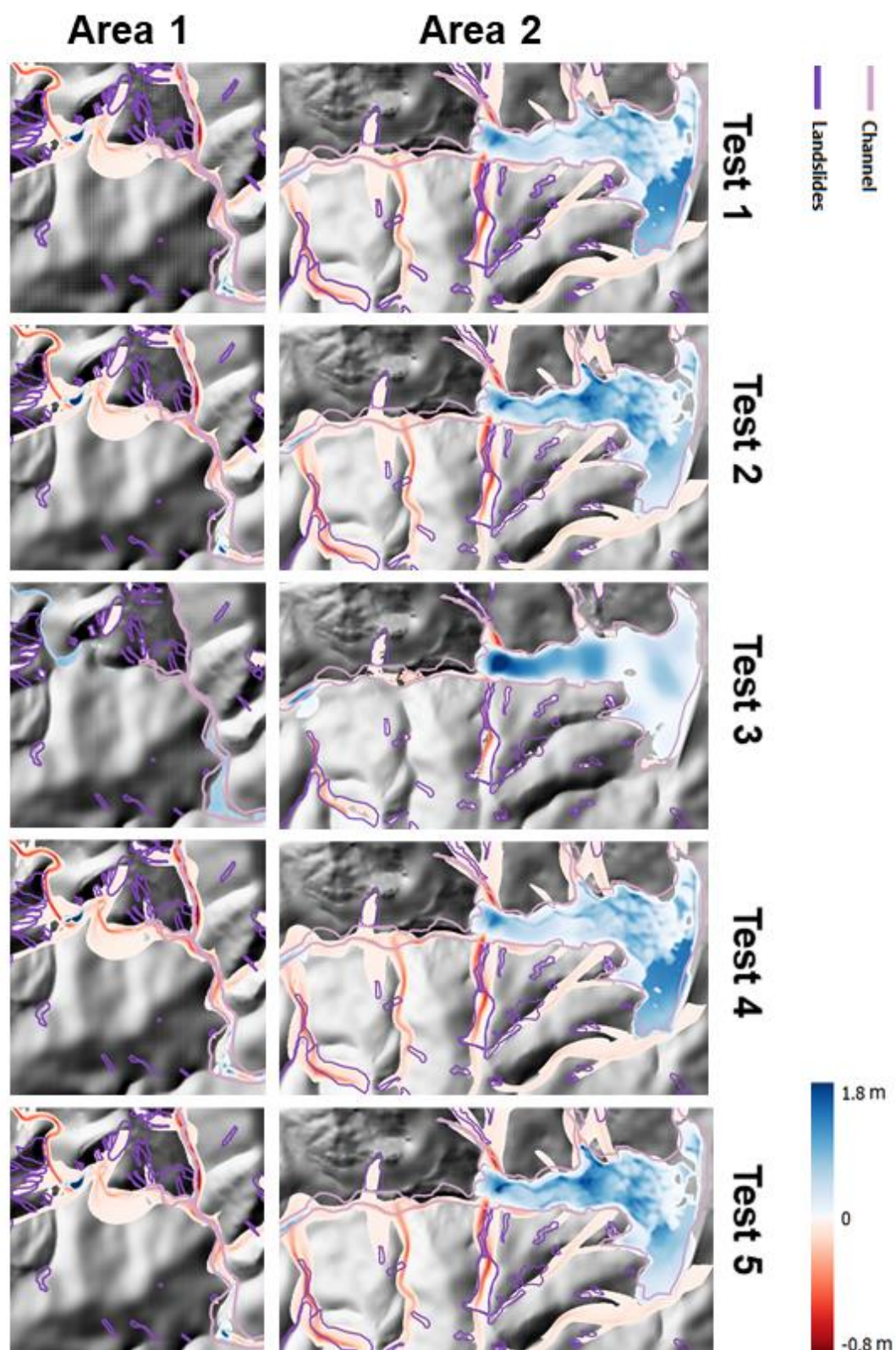


Figure 1.8: Simulations by Panici et al. (in review) at the two areas of interest testing different parameters. Tests refer to the baseline (Test 1) and one-at-a-time sensitivity analysis on linear drag (Test 2), single-phase (coarse) sediment (Test 3), angular friction reduction (Test 4) and entrainment increase (Test 5).

1.3 Aim, Research Questions and Objectives

1.3.1 Research Questions

1. What are the relative geomorphic impacts of Typhoons Kammuri and Lawin on the Abuan Catchment?
2. To what extent do landslides contribute to lateral channel widening during typhoons?
3. To what extent do multi-phase simulation models effectively simulate the effects of typhoon induced landslides on channel geomorphology?

1.3.2 Aim

The aim is to investigate the influence of landslide sediment delivery on channel geomorphic change during typhoon-driven flood events in the Philippines.

1.3.3 Objectives

1. To identify and map landslides following Typhoon Lawin (2016) to complement the existing landslide inventory (Jones et al., 2023) for Typhoon Kammuri (2019) in the Abuan catchment in Luzon, Philippines
2. To delineate and map the extent of river channels before and after each landslide event
3. To quantify changes in active channel width (ACW) across the study site
4. To quantify flood peak stream power throughout the channel network
5. To investigate the relationships between lateral channel widening, stream power and landslide sediment input
6. To identify possible interactions between landslides and lateral channel widening
7. To use a multi-phase mass simulation model to simulate landslide-channel interactions in at least one area of interest

1.4 Study Site

1.4.1 The Philippines

Despite a geographical bias of studies in Asia (Reichenbach et al., 2018), it is important to continue to study landslide occurrence in the Philippines as it experiences the most cyclones globally, suffering from ~20 typhoons annually (Evio and Bonito, 2017, Yonson et al., 2018). The likelihood of these storm events is expected to increase in intensity and frequency with climate change (Acosta et al., 2016). This in conjunction with high poverty rates among communities, due to the dependency on agriculture, validates the need to continue existing research focused on the Philippines, as landslides continue to pose a risk to its vulnerable communities. In addition, the pressures of urbanisation have seen the increase in development on hillslopes enhancing slope instability (Aleotti and Chowdhury, 1999), which provides further context as to the study site selected.

1.4.2 The Abuan River Watershed

The Abuan River catchment (494 km²) has been selected as the study site for this investigation located in the mid-west of the province of Isabela located in Luzon, Philippines (Figure 1.9). It has been chosen as it is found in the province that experiences the most tropical storms of all the Filipino islands (van der Meide and Pagaran, 2017). The Abuan River drains into the Pinacanauan de Ilagan River (catchment size: ~30004 km²) before joining the Cagayan River further downstream (Balderama, 2022). Based on the 2010 census, the Abuan catchment supports the livelihoods of ~2900 farming households with a population of ~14,360 people (Balderama et al., 2019). Filipino communities have a high dependency on agriculture for their livelihoods which is highly vulnerable to natural hazards, such as landslides. This investigation will help to

better inform mitigation efforts to reduce the vulnerability of communities (Pulhin et al., 2010).

The upper catchment is mainly comprised of forested land which is protected by the Northern Sierra Madre Natural Park. Despite this, large amounts of deforestation can be observed over time from satellite imagery (Araza et al., 2021) and reports have indicated illegal logging practices along the Abuan River channel (Barit et al., 2022). Contrastingly, the lower sub-catchments are made up of predominantly farmland, residual forest and brushland supporting agricultural practices of primarily maize production. Dingle et al. (2019) investigated channel change at the downstream confluences of the Abuan-Ilagan and Bintacan-Ilagan Rivers. This is a morphologically complicated zone and regarded as a dynamic confluence due to its high lateral channel migration. As yet, little work has been conducted on channel migration nor sediment transfer upstream of this confluence which I aim to address in this research. This may potentially contribute to the advanced understanding of channel change and dynamics further downstream.

Located nearby the eastern seaboard of the Philippines and with headwaters found in the Sierra Madre mountain range (Dingle et al., 2019) the catchment receives 2430 mm of rainfall on average per year distributed fairly evenly year-round (Araza et al., 2021). Luzon experiences low seasonality each year but, suffers from extreme typhoon events between October to January. This tends to be wettest in December in conjunction with monsoon season where lowland, built-up areas in the west are at risk of flooding (LiPad, 2018) whilst highland forested areas are more susceptible to landslide hazard (Balderama et al., 2016). As the Abuan catchment is prone to both landslide and flood events this

increases the vulnerability of its population, validating the need for investigation into this location.

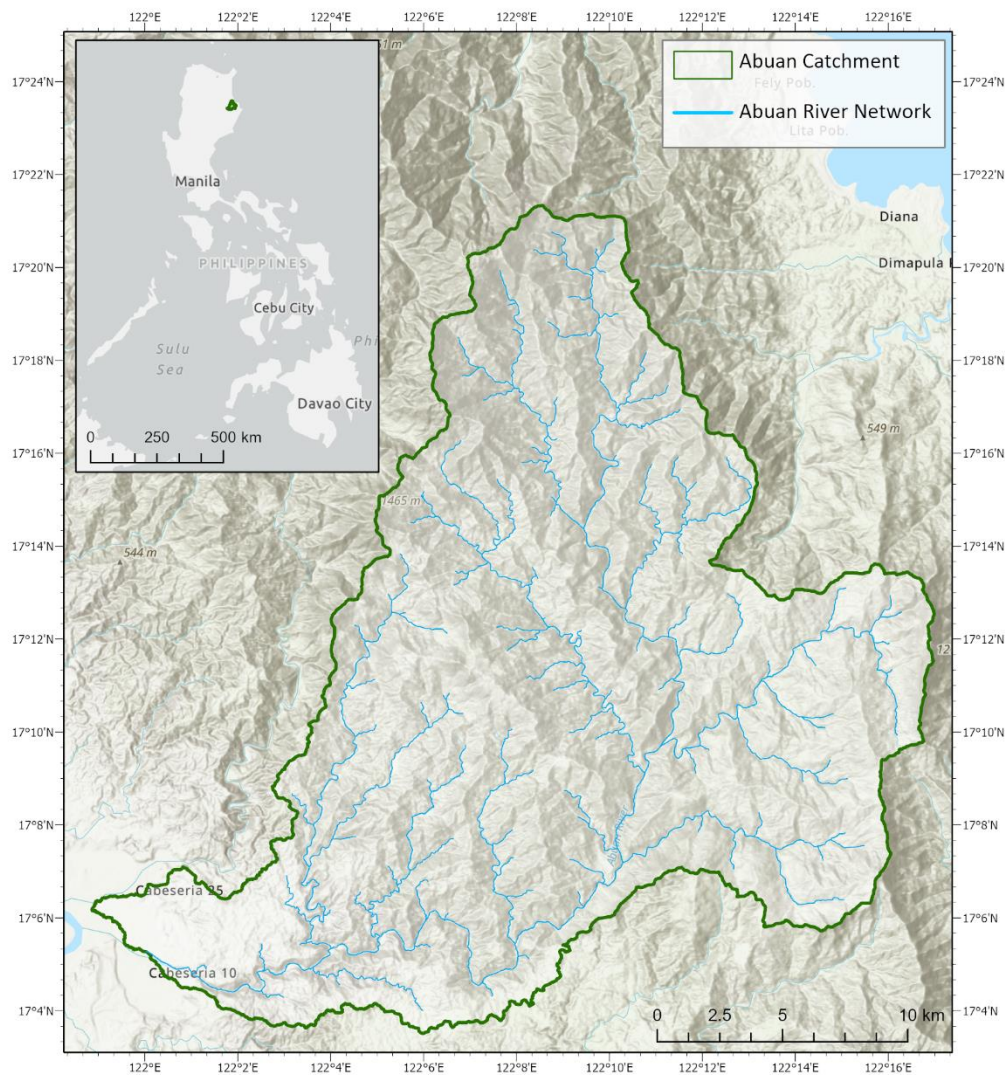


Figure 1.9: Map of the River Abuan network (blue) and catchment (green) with an insert map identifying the location within North Luzon, Philippines.

1.4.3 Geological Characteristics

Luzon island in which the Abuan watershed can be found is situated in a diverse geologic and tectonic setting causing spatial variations in morphological characteristics. The catchment is found in the Sierra Madre mountains which is geologically heterogenous in nature. It varies both geographically and

topographically, as the island is developed between the sialic continental basin of China and the basaltic Pacific Ocean basin (Durkee and Pederson, 1961). Upland areas are geologically exposed to metamorphosis as a result of previous pyroclastic and intermediate flows. This results from its geographical location bordered by mostly convergent plate boundaries (Fabregas et al., 2020). The region is characterised by intermediate (andesitic) igneous rock with Eocene to Oligocene meta-sediment and meta-volcanic deposits found nearer the margins of the Sierra Madre mountains (Dingle et al., 2019, Durkee and Pederson, 1961). Soils in low lying areas are mainly comprised of loam soil whilst sandy loam soils can be found in the upland areas (Balderama et al., 2019).

Geological data for the Abuan catchment was obtained from collaborators of the SCaRP project as seen in Figure 1.10. This included a lithology map, demonstrating a dominance of undifferentiated metavolcanics of metamorphosed spilites, shales and basalts. In addition, this digitises the spatial extent of different land uses ranging from built-up areas to open forest. Without the ability to conduct fieldwork at the study site, geologic data obtained is not as detailed as required. Therefore, for the purpose of modelling assumptions of soil type will be based on findings by Panici et al. (in review), investigating a region in Itogon, Philippines where fieldwork was conducted.

In addition to the geology type, relatively little is known about sediment grain size within the Abuan River network. A study by Dingle et al. (2019) collected surface sediment grain size distributions along the Ilagan, Bintacan and Abuan River channel in January 2018 on exposed gravel bars during low flow. Results demonstrated that samples taken from collection sites along the River Abuan

and Bintacan were relatively coarser than that found in the Ilagan channel. More coarse sediments found are direct inputs from the adjacent hillslopes as these rivers and their tributaries run through the Sierra Madre mountains. Sediments found in the Abuan River were the most variable in grain size and poorly sorted relative to the other rivers. Density of quartz and uncompacted sand were measured at 2650 kg/m^3 and 1600 kg/m^3 relatively which represents the widest possible range of values measured. This study was however conducted in the lowland region of these tropical rivers. Therefore there is a large amount of uncertainty attributed with the grain size distribution of sediment within the more upland areas of the Abuan River network where this research is to be conducted. Although variation in the sediment can be visually depicted from Google Earth imagery based on the size and differences in colour, the type and size of sediment cannot be determined from this remote source (Figure 1.11). Field observations and measurements by Dingle et al. (2019) will therefore help to inform estimations of grain size and sediment density as an input to model sediment cascade in the study site selected as fieldwork could not be conducted.

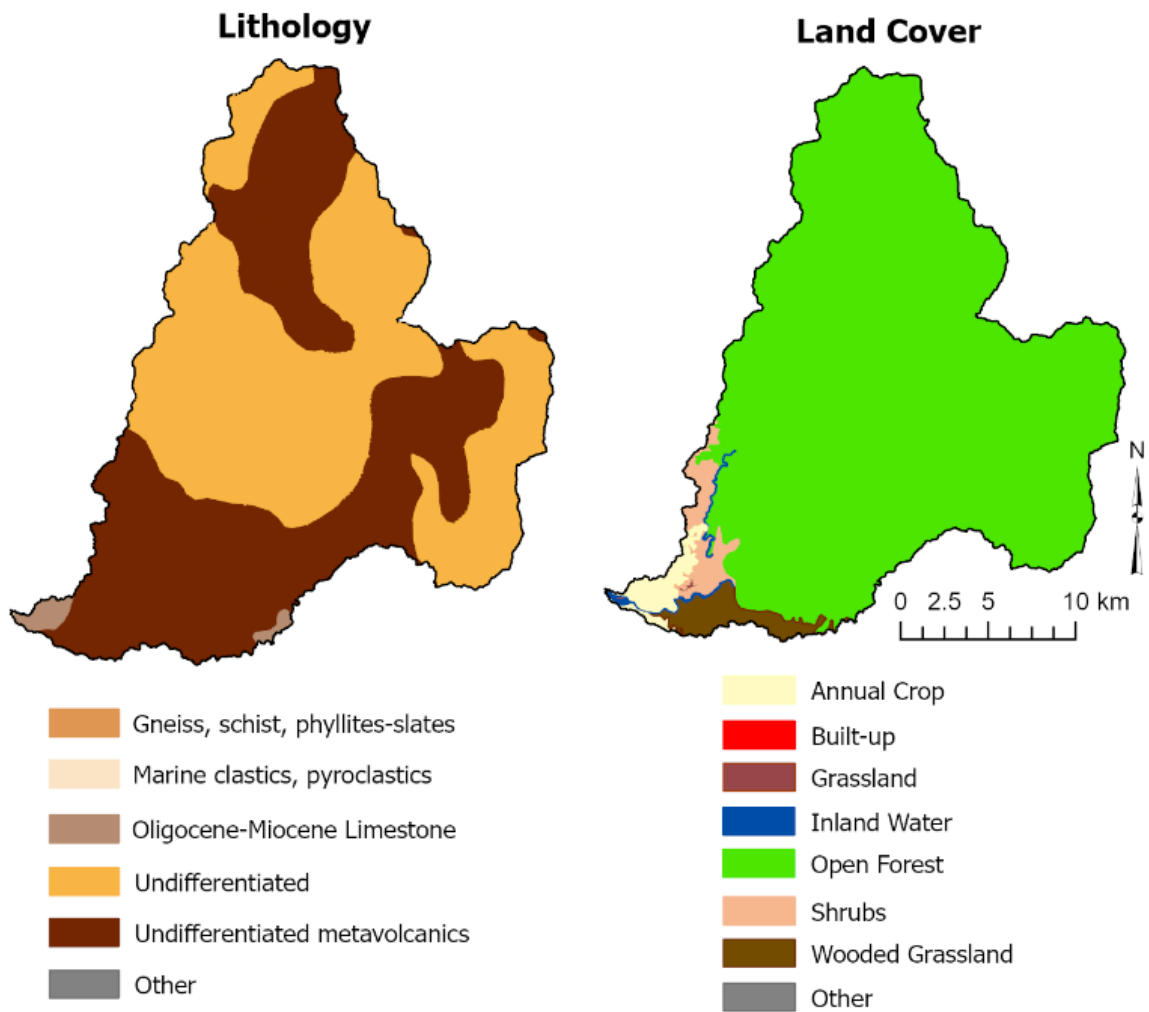


Figure 1.10: Maps of lithology (left) in 1976 provided by the Department of Environment and Natural Resources' Mines and Geosciences Bureau (DENR-MGB) and land use cover (right) provided by the National Mapping and Resource Information Authority of the Philippines (NAMRIA) of the Abuan River catchment from 2015.

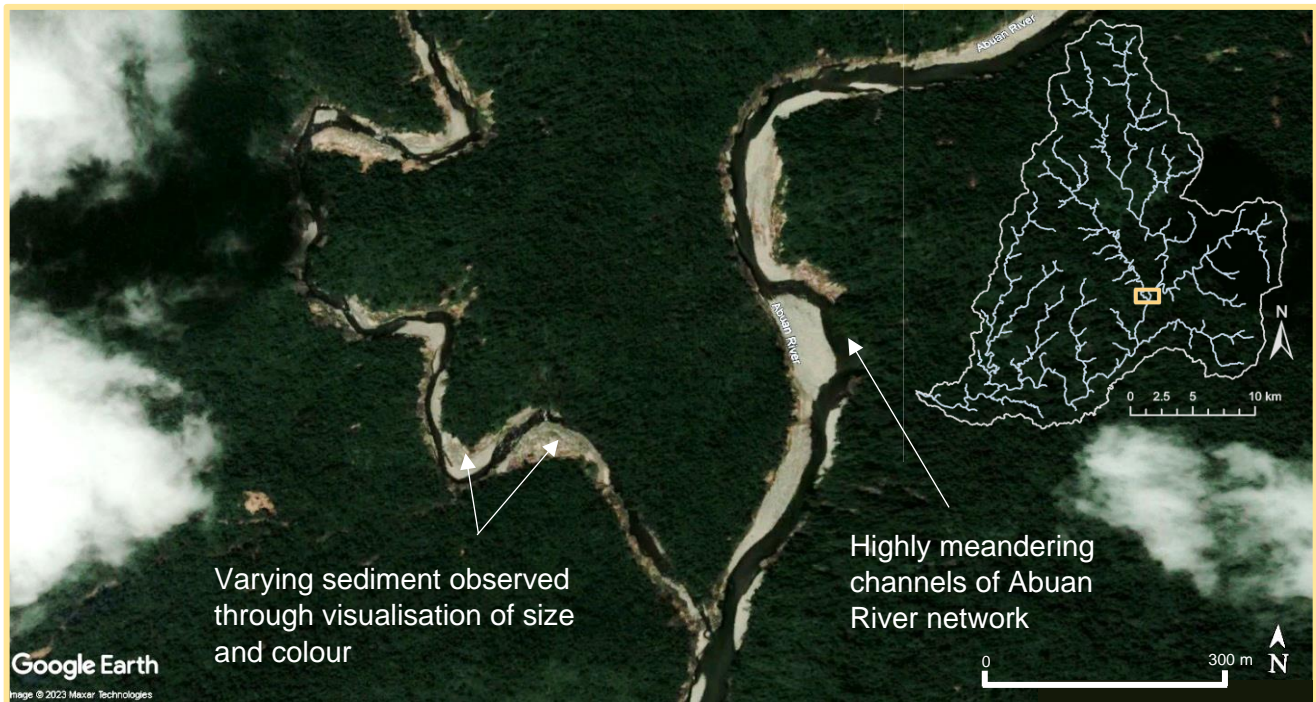


Figure 1.11: Close up of satellite Google Earth imagery (April 2017) of a confluence of the River Abuan found in the north of the catchment (orange box of insert map) highlighting the meandering of the channel and difficulty in visually identifying the sediment structure of channel change.

1.4.4 Sub-Area Modelled Site

Due to the power intensive nature of r.avaflow and high computational run times, a sub-section of the Abuan catchment had to be selected as an area of interest due to landslide-channel interactions. The area extends 3316.05 m by 1415.20 m situated in the north of the Abuan catchment as seen in Figure 1.12. It stretches along just over 4 km of a tributary river to the River Abuan northwest of the confluence.

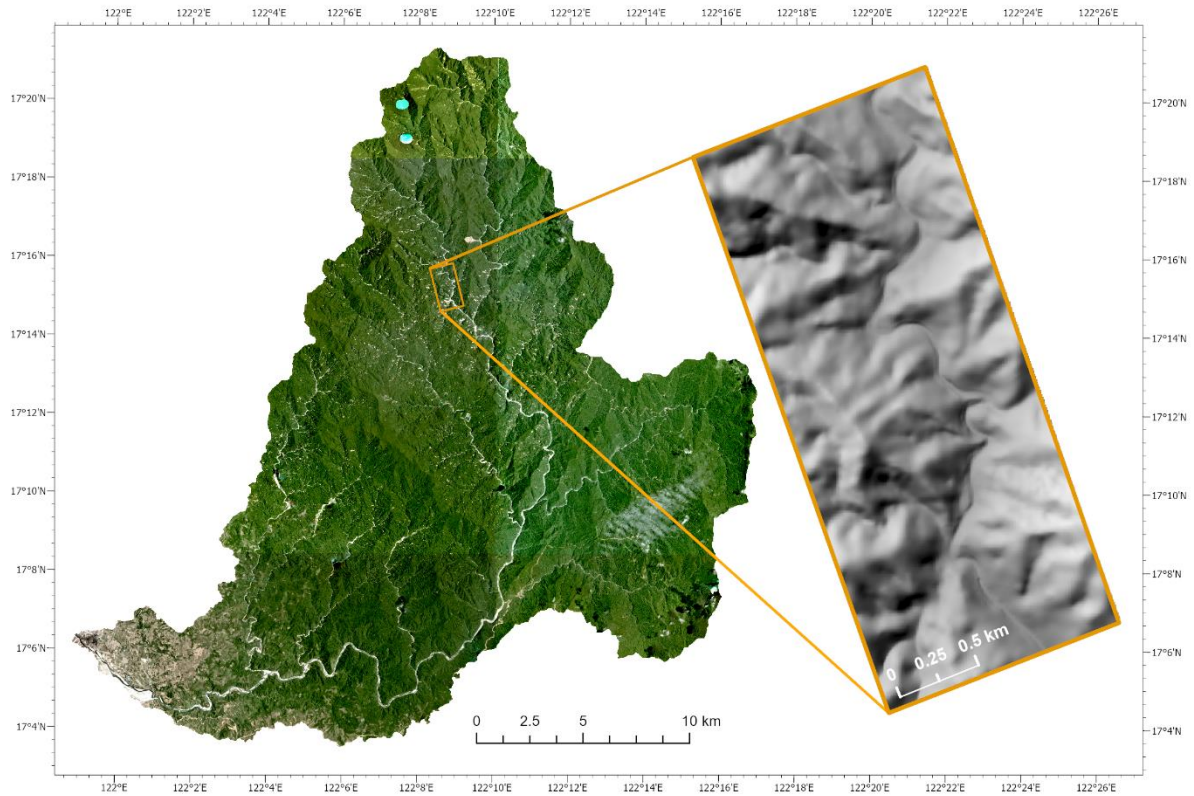


Figure 1.12: Map showing the River Abuan catchment with the study site selected to model magnified (orange).

1.5 Typhoon Events

The following typhoon events have been selected as they have triggered the most recent landslide events across the Abuan catchment and have sufficient data available for both events in order to conduct this research. Both typhoons identified occurred during the Northern Pacific monsoon season. However for the purpose of this research, the influence of rainfall prior to the events has not been considered it as goes beyond the requirements for this investigation. Nevertheless, it is important to investigate the effects of typhoons due to the vulnerability of populations and their dependency on the land for their livelihoods as it can induce significant economic losses.

1.5.1 Typhoon Lawin

Luzon experienced typhoons in 2015 and 2016 with only the latter event affecting the study area (Figure 1.12). Typhoon Haima as it is locally known, occurred in 2016, however is reported as Typhoon Lawin and will therefore be referred to as throughout this paper (NDRRMC, 2016). Starting as a tropical storm in the sea, Typhoon Lawin entered the Philippine Area of Responsibility (PAR) on the 17th October 2016 experiencing sustained winds of 175 kmph and gustiness of 215 kmph with moderate to heavy rains across its 600 km diameter (NDRRMC, 2016). Once making landfall over the Cagayan-Isabela area (in which the Abuan watershed is located) this tropical cyclone intensified into a super typhoon. It reached maximum winds of 225 kmph with a diameter stretching 200 km on 19th October 2016 (van der Meide and Pagaran, 2017), raising the highest warning signals across numerous north-eastern provinces, including Isabela and Cagayan. Within the first 24 hours, northeast Luzon suffered 250 mm of rainfall, ~20-30 mm per hour concentrated most heavily in the surrounding eye (southwestern section) of the tropical cyclone (Observatory, 2016).

By the 25th October the NDRRMC (2016) confirmed 14 deaths as a result of Typhoon Lawin with four people injured as a direct consequence of landslides. The casualties of this event were comparatively smaller than typhoons reported to be of a similar size, such as Typhoon Haiyan in 2013 causing over 6000 deaths (Go, 2017, NDRRMC, 2014). Despite this, the widespread impact on the Cagayan and Isabela provinces was significant (van der Meide and Pagaran, 2017) with 118 barangays flooded (Ramos and Nees, 2017). Over 75,000 houses were damaged with power cut off to 160 municipalities, leading to the evacuation of over 90,000 people (NDRRMC, 2016). In addition, roads and

bridges were obstructed by debris, uprooted trees and floodwater, hindering the ability to effectively deploy aid to those most vulnerable in rural settings (Sargeant et al., 2020). Most significant damage was experienced through the loss of crops (e.g. rice and corn regarded as high value crops) and damage to farmland. This further highlights the vulnerability of local communities due to their high dependency on agriculture for their livelihoods (Pulhin et al., 2010). To mitigate these impacts and help reduce the vulnerability to Filipino communities, it is paramount to learn from past events to best inform future mitigation strategies.

1.5.2 Typhoon Kammuri

In 2019, Luzon suffered from Typhoon Kammuri, locally known as Typhoon Tisoy (Sevieri and Galasso, 2020), which started as a tropical depression on the 25th November 2019 and intensified into a tropical storm. This strengthened into a typhoon when it entered the PAR one day later (NDRRMC, 2020), first making landfall on the southeast tip of Luzon in the morning of the 2nd December (NASA, 2019) with sustained winds of 150 kmph and a gustiness of 185 kmph (NDRRMC, 2020). The typhoon continued westward weakening to a Severe Tropical Storm on the 4th December 2019 before exiting via the South China Sea. Heaviest rainfall was experienced in the northern half of the island where the study site can be found with total rainfall reported between 100-150 mm more than the average rainfall of that period of 150 mm (NASA, 2019).

Although the heaviest rainfall and winds were associated offshore, Typhoon Kammuri damaged an estimated 561,000 buildings with 17 people found dead, slightly more than that of Typhoon Lawin (LeComte, 2020). This affected over ~820,000 families of which approximately a third of these people had to take

temporary shelter in evacuation centres (NDRRMC, 2020). A total of 196 areas were reported to be flooded either as a direct result of the typhoon or linked to a secondary hazard, with most floodwaters subsiding within a month of the event date. This is considerably higher at nearly four times the number of areas following Typhoon Lawin, likely resultant of the increased rainfall intensity. Typhoon Kammuri induced rainfall had a significant immediate effect on Luzon, however due to the intensity had a long-lasting effect on communities. For example, the suspension of school attendance and employment due to the loss of infrastructure; cost to livelihoods following evacuations and damage to farmland. As a result, this caused over 250 cities/ municipalities to declare a State of Calamity in order to seek help required (NDRRMC, 2020). As the frequency and intensity of tropical cyclone events is predicted to rise in line with climate change (Gariano and Guzzetti, 2016, Kubota and Chan, 2009), it is important to continue investigations into the impact of typhoons on landscape and channel dynamics to inform future mitigation efforts.

2. Methodology

2.1 Data Collection

Previous to this study, similar studies have been conducted in Colorado, America and Itogon, Philippines (Bennett et al. submitted; Panici et al., in review). These used a combination of both remotely sensed sources and data collected in the field to inform model inputs. Due to the remote location of the study site and difficulty in travelling due to the global pandemic, no fieldwork was conducted. This research differs from previous studies as it aims to use only remotely sensed data and empirical formulas alone. As a variety of different data types were required for this investigation, they have been collected from a range of different sources, including reliable online resources with more specialised data having been sourced from collaborators of the SCaRP project. The use of satellite imagery, however, presents its own challenges as images may have a high percentage of cloud cover. Also the ability to attribute landslides to a specific events is dependent on the time intervals of image availability. In choosing which satellite imagery data use, attention must be paid to the date captured as well as percentage cloud cover to ensure it is fit for purpose and must also ensure it comes from a reliable data source.

2.1.1 Digital Elevation Model

DEMs are datasets that have been geo-spatially referenced to digitise and visualise the topography of a landscape (Hutchinson and Gallant, 2000). DEMs are required as input into the r.avafLOW model (Section 4.2.7), and to quantify depths of landslides triggered by the studied typhoon events and validate model outputs (e.g. Bennett et al. submitted). A DEM was sourced from collaborators

of the SCaRP project who provided a nationwide DEM of 5 m spatial resolution. It was created using airborne IfSAR technology with a vertical accuracy of 1 m root mean square error (Grafil and Castro, 2014) for 2013, prior to Typhoon Lawin and Typhoon Kammuri. This DEM forms the input into r.avaflow modelling.

In order to quantify geomorphic change during typhoon events and quantify landslide depths for input into r.avaflow, a post-typhoon DEM was needed. Pleiades stereo satellite imagery was requested and sourced for the SCaRP project from the CEOS landslide pilot (Kirschbaum, 2016), partially covering the extent of the study site with 0.5 m resolution obtained via the constellation of two satellites for multispectral and panchromatic observations of the surface of the Earth (Bagnardi et al., 2016). This is the first of its kind to obtain three synchronous images of the same area, however the creation of a DEM is made difficult by the lack of associated ground control points (GCP). Initially an attempt was made to create a DEM from the Pleiades imagery in Erdas Imagine using similar methodology to Stumpf et al. (2014) which eliminates the need for GCP.

Following this, a more accurate technique was deployed using an online service provided by Terradue and the University of Strasbourg. CNRS EOST has developed methodologies to generate and correct orthoimages, such as Pleiades. This uses their Digital Surface Models from OPTical stereoscopies high resolution imagery (DSM-OPT) algorithms to create a DEM from Pleiades imagery available using the parameters set out in Appendix A. With a lack of GCP's, the DEM created from this method needed to be georeferenced to be able to be used for analysis within this investigation.

2.1.2 DEM Co-Registration

Due to the lack of GCP, the DEM created from 2020 Pleiades imagery needed to be co-registered with the existing 2013 DEM to compensate and remove bias creating an accurate DEM from Pleiades data acquired (Palaseanu-Lovejoy et al., 2019). It is important that when comparing two different DEMs, that they are not shifted relative to each other. By comparing the differences in slope and elevations across the catchment, differences can be accounted for and removed thereby quantifying the differences more accurately between the two DEMs (Nuth and Kääb, 2011). This is an area of contemporary methodology as most frequently GCP are available and therefore numerous methods were trialled.

Initially, the two DEMs were run through a routine written in Jupyter-Notebook based on the co-registration algorithm outlined by Nuth and Kääb (2011).

Firstly, this removes shifts between the DEMs before checking and correcting for elevation and sensor specific biases. This is a more simplistic approach which was found to be unsuitable when altered to incorporate the DEMs sourced for 2013 and 2020. Datasets were obtained from different satellite imagery sources and therefore contained biases that were not accounted for using this code.

Finally, Least Squares 3D Surface Matching (LS3D) was experimented with which is a point cloud and surface co-registration software that uses the Generalised Gauss-Markov model (4dexplorer, n.d.). This allows the matching of different oriented 3D surfaces without the need for GCP and can be used to test the accuracy of existing DEMs. However, due to the large spatial extent of the Abuan catchment being investigated and the extremely time intensive nature of

this software, the use of LS3D to co-register the DEMs was not plausible for this investigation.

Unfortunately, after trialling different methods to co-register the DEMs, approaches used were found to be unsuitable for the data acquired for this research. In addition, Pleiades imagery covered only a small proportion of the study site in the southwest of the catchment, where only a small proportion of total landslides for each event occurred. Without a post-typhoon event DEM, I explored other ways of estimating landslide depths from areas (section 4.2.4) validating the geomorphic change simulated by *r.avaflow* (section 4.2.7).

2.1.3 Satellite Imagery

Due to the lack of a post-typhoon DEM with which to do geomorphic change detection analysis of landslides and channel geomorphic change (Rathburn et al., 2017), geomorphic change was mapped visually from satellite imagery. The value of using remotely sensed satellite imagery has been well established (De Beurs and Henebry, 2005) and globally there is a wealth of imagery available across numerous time series. Satellite data is appropriate for providing repeatable and consistent temporal images across different spatial scales useful in capturing processes driving change (Verbesselt et al., 2010). The ability to detect and interpret channel change and driving factors is however dependent on the spatial and temporal quality of data (Ziliani and Surian, 2012).

The time period between each satellite image source must be considered due to the high vegetation growth and recovery rates in the Philippines. The ability of a forest to recover following an abrupt change, such as a typhoon event, involves a combination of the recruitment, release and regrowth of vegetation following mortality (Everham and Brokaw, 1996). Following a typhoon, Yap et

al. (2016) found relatively low mortality and fast recovery rates in the Palanan forest, similar to that found across the Abuan River catchment. Therefore, it can be inferred that upland forested regions of the Philippines possess a resilience and resistance to abrupt disturbances caused by typhoon events. Whether a forest can tolerate the predicted increase in typhoons is not yet fully understood, and although has been projected under different scenarios (Knutson et al., 2010, Solomon et al., 2007), presents an area for further research. With high recovery rates of vegetation following a typhoon event, the smaller the time frame between the occurrence of the event and the date of the imagery obtained, the smaller the associated uncertainty. To improve accuracy and reduce the associated uncertainty of quantifying changes in ACW, data should be dated soon after the event.

Therefore, a combination of imagery has been used in order to cross reference the features identified, validating the results as seen in Table 2.1. For landslide inventory creation imagery was first analysed in Google Earth from the 19th April 2017, using imagery from the 10th of April 2016 as a guide to ensure that only landslides that occurred as a direct result of Typhoon Lawin were mapped as opposed to relic landslides from historic events. Ideally a smaller time frame would have been selected, however due to data availability in this region this was not possible using Google Earth satellite imagery. Therefore, data was requested and sourced from PlanetLabs Scope imagery on the 22nd of October 2016 with a 3m spatial and 8 band spectral resolution. Acquisition of this imagery enabled existing mapping to be validated and landslides missed to due to high cloud cover to be delineated.

A combination of Google Earth and PlanetLabs Scope imagery was obtained pre- and post- each typhoon event to map changes in active channel width. Previous imagery used in the mapping of landslides for Typhoon Lawin was also used to identify existing channels within the Abuan River network from April 2016 and 2017 as above. Across the Abuan catchment, Google Earth imagery was then only available from the 6th of July 2020 after Typhoon Kammuri and with a large amount of cloud cover, consequently additional imagery was required from an alternative data source to assess the impact of the event. Therefore, PlanetLabs Scope satellite imagery was used as the dominant data source to supplement previously obtained imagery. Images have less than 30% cloud cover and cover the extent of the study area deeming imagery appropriate for this investigation to manually identify channel network extent and landslides. Throughout analysis of changes in ACW and the magnitude of landslides, an uncertainty associated with the spatial resolution of the data source must be considered (± 5 m).

Imagery sourced for Typhoon Lawin has a small time frame of within a month of the day it made landfall. Therefore a high confidence can be associated with mapped and calculated changes in ACW. In contrast, Google Earth imagery was obtained in April 2017, over five months after Typhoon Lawin where riparian vegetation regrowth on the bank can clearly be observed, supporting the findings of Yap et al. (2016). Channels digitised using satellite imagery with a time frame smaller than six months therefore have a lesser associated uncertainty. As for Typhoon Kammuri, images obtained were from March and July 2020, with the latter over six months after the extreme weather event resulting in a greater associated uncertainty. Changes in ACW quantified may not truly reflect the impact of Typhoon Kammuri as riparian vegetation may

have regrown due to high recovery rates across the catchment. Therefore, to investigate the effects of sediment cascades on geomorphic change, this research focuses on the effects of Typhoon Lawin. Data obtained demonstrates a greater associated certainty in observed geomorphological changes from satellite imagery, compared to that presented following Typhoon Kammuri.

Table 2.1: Table of satellite imagery data used.

Source	Date	Notes
Google Earth	10/04/2016	Collection of satellite imagery obtain from different companies mosaiced to display one continuous image (Earth, 2023)
	19/04/2017	
	06/07/2020	
PlanetLabs Scope Imagery	28/09/2016	3 m spatial and 8 band spectral resolution, requested and sourced from collaborators of the SCaRP project
	22/10/2016	
	29/10/2019	
	31/03/2020	

2.1.4 Rainfall Data

Rainfall data was requested and obtained by collaborators of the SCaRP project and utilises remotely sensed Integrated Multi-satellite Retrievals for Global Precipitation Measurement (GPM IMERG) data using NASA’s international network of satellites (NASA, 2019). This has been selected due to the lack of gauge data availability in the region during the event. The dataset provides annual rainfall data in mmhr^{-1} given in 30 minute intervals of mean rainfall intensity with a spatial resolution of 0.1° . Despite data being available throughout the duration of the typhoon event, rainfall data at each rainfall cell location has been extracted for the day the typhoon made landfall to calculate

the total and intensity of rainfall (Appendix B). This is because rainfall has been identified as a triggering factor to these landslide events.

2.2 Data Analysis

All analysis was completed in the projected coordinate system WGS 1984 UTM Zone 51N as is the projection that best represents the Philippines. As remote sensing techniques have been adopted, associated uncertainty within the datasets must be considered throughout this investigation (Salvatici et al., 2018).

2.2.1 Creating a landslide inventory

To model landslide sediment hazard and cascade, first landslide inventories for each typhoon event identified in 2016 and 2019 had to be created. To create the inventory following Typhoon Lawin, landslides were mapped as polygons using ArcGIS Pro. Landslides following Typhoon Lawin were identified from different satellite imagery sources, including Google Earth Pro and PlanetLabs (Table 2.1). These could be visually identified as debris flows cause the mass movement of colluvium which leaves visible scours in the landscape, often removing vegetation in the forested region. Therefore, landslides could be easily distinguished as areas of visible bare soil in areas from densely vegetated land. Comparison across different sources of imagery reduces the associated uncertainty of the spatial accuracy of landslides, validating the inventories created which reduces the potential human error associated with visually mapping landslides. The use of multiple data sources aids in overcoming the challenges of cloud cover. In addition, this enables the delineation of landslides from within a sensible time window to ensure landslides are solely attributed to the event studied as opposed to before or

after. The landslide inventory following Typhoon Kammuri in 2019 was obtained from collaborators of the SCaRP project (Jones et al., 2023 and Abancó et al., 2021). Methodology used in the landslide inventory created for Typhoon Lawin mirrors that used for Typhoon Kammuri to ensure consistency when comparing datasets.

Runout areas have been delineated to identify inundation areas and help to assess the potential effects of how landslide sediment influences changes in channel geomorphology (McDougall, 2017). These areas represent a proportion of sediment that is mobilised, transported and deposited downslope of scars which are known as debris tails (Page et al., 1999) or runouts as they have been referred to in this investigation. These have been mapped following Typhoon Lawin which has been identified as the more catastrophic event of the two typhoons studied. The distance each runout extends depends on the volume of the landslide as opposed to the fall height and valley slope (Legros, 2002). Runout areas have been mapped with high confidence, however a greater uncertainty is associated with the amount of sediment mobilised as a result of using the empirical formula to calculate their depth. To understand the impact of sediment cascades, runouts have been separately delineated from landslide scars for input into r.avaflow. This accounts for the differences in mechanical processes driving sediment transport and deposition as well as the viscosity of sediment transport.

2.2.2 Mapping active river channels

River channels were manually digitised and the channel margin was defined to be on the border of continuous riparian vegetation and the riverbank. Methods of mapping channel widths used are based on that presented by Panici et al. (in

review), such that active channel was manually digitised in ArcGIS Pro using satellite imagery acquired to cover the extent of the wetted river channel and edge of distinguishable alluvial deposits. Challenges arose in visually interpreting the channel width due to areas of high cloud cover and as a result of the spatial resolution of the data (Figure 2.1). This was overcome by using both Planet and Google Earth imagery to cross check and validate the mapped channel extents. To further reduce the associated uncertainty, only I myself mapped each river channel pre- and post- each typhoon across all four datasets of satellite imagery acquired rather than by multiple people (Donovan et al., 2019, Nelson et al., 2013, Rowland et al., 2016).

In addition, to assess the change in active channel width, each river polygon (vector data) was first separated into 1 km segments before being converted into regular grid cell product with 1 m spatial resolution (raster data). This enabled the accurate quantification of the area of river channels and thereby allowed the assessment of relative channel change using the raster calculator function as before. ACW has been calculated using $\frac{ACW_{pre} - ACW_{post}}{ACW_{pre}}$, where ACW_{pre} and ACW_{post} are pre- and post- typhoon active channel width (m) respectively. This was achieved by first calculating the area and then dividing by 1 km with changes compared pre- and post- each of the typhoon events to analyse the geomorphic change of channels within the Abuan River network. Due to the presence of high cloud and dense vegetation cover, a lower confidence is associated with channels mapped following Typhoon Kammuri compared to Typhoon Lawin.

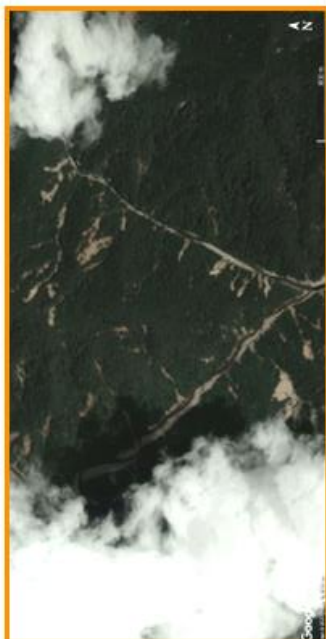
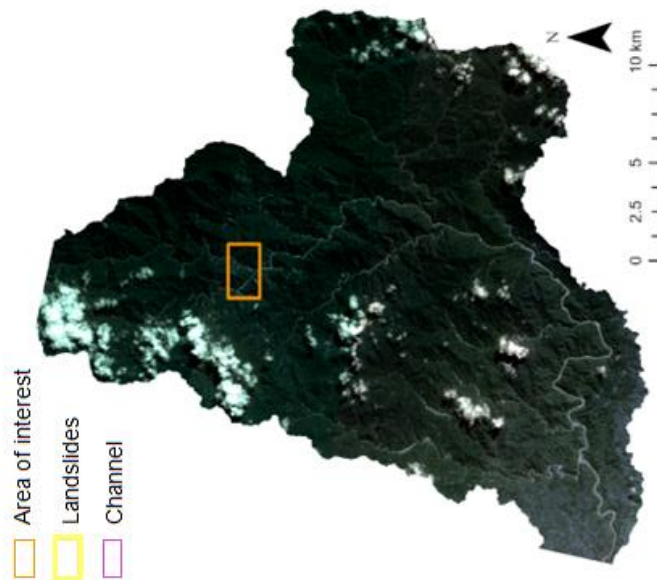
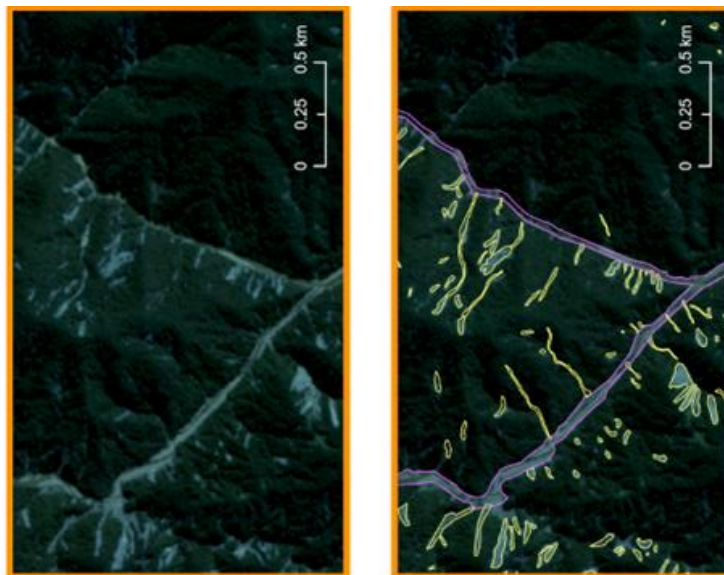


Figure 2.1 – map showing area of interest in the Abuan River catchment (orange) with magnified views of Google Earth (19/04/2017, left) and Planet Labs (22/10/2016, right) satellite imagery used to delineate landslides (yellow) and channel extents (purple).

Equation 2.1: Equation to calculate active channel width (ACW) by comparing the river channel pre- and post- each typhoon event

$$\Delta ACW = ACW_{\text{post}} - ACW_{\text{pre}}$$

2.2.3 Uncertainty associated with human error

Human error has also been considered when manually delineating both landslides and channel change following each typhoon event. Hence, a combination of both PlanetScope and Google Earth Imagery were analysed to cross-check and validate the size and magnitude of landslides as well as the extent of the channel network. This method additionally limited potential human error thereby reducing the associated uncertainty for each landslide inventory and delineated channel network. Although each landslide inventory was mapped by different researchers, criteria in mapping landslides was predetermined and followed whilst creating the landslide inventories as there are no universal guidelines (Karsli et al., 2009). In addition, both landslide inventories were analysed by collaborators of the SCaRP project to validate the frequency of landslides mapped following each event, further reducing the associated uncertainty. As for each channel network mapped before and after the landslide event studied, delineation was conducted by the same person throughout to ensure continuity and reduce associated human error.

2.2.4 Topographic analysis

Topographic properties were calculated using the 5 m resolution DEM to acquire slope, aspect and elevation data. This was achieved by first resampling the dataset to a 10 m spatial resolution using the TopoToolbox in MatLab using resources and methods provided by a collaborator of the SCaRP project, Richard Boothroyd (Schwanghart and Scherler, 2014). Rasters produced have

then been analysed in ArcGIS Pro to extract and analyse topographic statistics used to calculate stream power during each typhoon event.

2.2.5 Landslide depth estimation

As the volume of landslides is unattainable from geomorphic change detection given the lack of a post typhoon DEM, an alternative method was acquired using the volume-area scaling exponent set out by Larsen et al. (2010). The volume and magnitude of landslides is significantly more difficult to obtain compared to the frequency as requires information of the surface as well as sub-surface geology of the failed slopes (Guzzetti et al., 2009). Larsen demonstrates how the volume of landslides can instead be estimated without the need for field measurements. Instead the analysis of satellite imagery and topographic maps is sufficient to accurately estimate volume measurement (Guzzetti et al., 2009, Larsen et al., 2010).

This method adopts an empirical relationship linking volume of individual landslides to their area depending on a scaling exponent γ and an intercept α as seen in Equation 2.2. To obtain γ , the geology of the Abuan catchment was compared to an existing global compilation of landslide geometry measurements. Landslides found in the Abuan River catchment have been identified to have been soil-based which limits the amount of material that can be eroded. On investigation, there was no directly comparable research area as the Abuan catchment is a mountainous region comprised of heterogenous geology which is densely forested. In areas of most similar geology, such as in British Columbia (Guthrie and Evans, 2004) or Uganda (Knapen et al., 2006), the area was either glaciated or deforested. These landslide events were also of

a lower frequency and induced by differing triggers to the typhoons experienced in the Philippines.

Sensitivity analysis of the influence of different inputs into the r.avaflow by Panici et al. (in review) demonstrated that changes in the volume of landslides input had a relatively small impact on the overall model results (Figure 1.8). Therefore a worldwide scaling exponent based on a global inventory of soil landslides has been used of $y = 1.145 \pm 0.008$ and $\log \alpha = -0.44 \pm 0.02$ (Larsen et al., 2010). Shallow landslides characteristic of the Abuan catchment are estimated by a γ exponent of between 1.1-1.3 (Larsen et al., 2010), which validates the scaling exponent used to calculate landslide volume. In addition, 1.145 lies between the values used for landscapes of similar geology to the Abuan catchment (Table 2.). Landslide areas were obtained from the landslide inventories created for both typhoon events using the 'Calculate Geometry' function in ArcGIS Pro, before being input into Equation 2.2 in Excel to estimate the volume of each individual landslide.

Equation 2.2: Scaling relationship of volume (V) dependent on landslide area (A), scaling exponent (γ) and intercept (α).

$$V = \alpha \cdot A^\gamma$$

Table 2.2: Landslide datasets and parameters used for the scaling relationship $V = \alpha \cdot A^\gamma$ where γ = scaling exponent, α = intercept, R^2 = statistical goodness of fit and n = no. of landslides.

Data Set	γ	$\log \alpha$	R^2	n
Soil landslides	1.145±0.008	-0.44±002	0.9	2136
Uganda	1.22±0.12	-0.4±0.12	0.91	93
British Columbia	1.09	-0.81	0.95	124

2.2.6 Rainfall-runoff analysis

Rainfall-runoff analysis has been conducted as is later required to derive stream power across the channel network. It is assumed that soils are fully saturated by the day that the typhoon made landfall. Daily rainfall was extracted based on the timings of the event when Typhoon Lawin made landfall on the 19th October 2016 from 00:00 to 23:30 (UTC) in accordance with reports by the NDRRMC (2016). This is all considered to contribute to runoff based on the assumption of saturated soils. To analyse the impact of rainfall across the catchment, data was first manipulated in Excel to find both the rainfall total and intensity during the event. For visual interpretation and further analysis, rainfall data was extracted as point data for each cell location in ArcGIS Pro before being interpolated across the study site using a regularised spline (weight = 0.1; $n = 20$). This created a raster of 24-hour rainfall totals and mean average intensities of 100 m spatial resolution which indicates the spatial distribution of rainfall across the catchment (Figure 2.2).

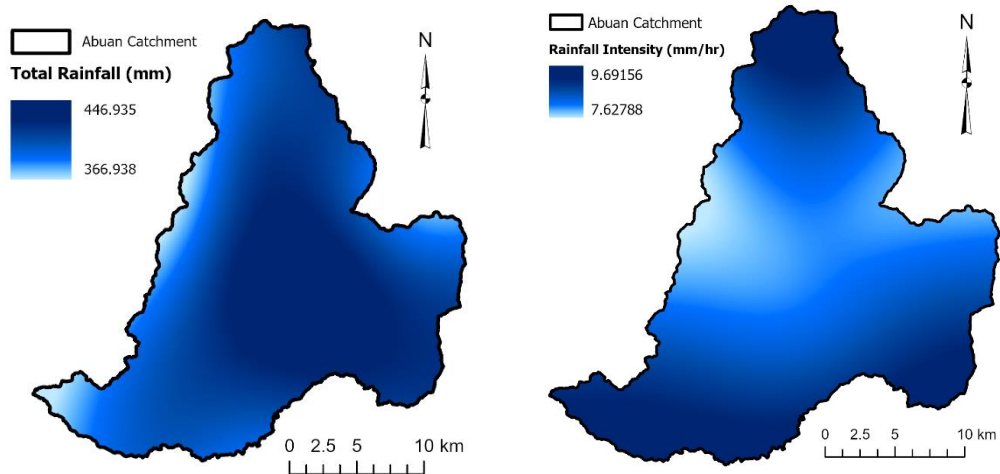


Figure 2.2: Total event rainfall (left) and peak rainfall intensity (right) during Typhoon Lawin when it first made landfall on 19th October 2016 over 24 hour period.

2.2.7 Discharge and stream power analysis

As an indicator of a river's capacity to mobilise and transport sediment, stream power is often calculated (Bizzi and Lerner, 2015). These initial estimates have been used to assess channel stability and understand controls acting within the landscape on the geomorphic change of the river network. Script has been written in MatLab using Topotoolbox V2 by Bennett et al. (2016) and adapted by Panici et al. (in review). Inputs to the numerical model include the 2013 DEM and the total rainfall raster for the day of the event. When running the model, first topographic analysis is conducted whereby the Abuan catchment is clipped and defined as the study area. Slope gradient derived using this code has been calculated with a 50 m moving window using the first order Savitzky-Golay filter. This is used to reduce the noise with the DEM by reproducing elevations near confluences and the junctions of tributaries ensuring the raster is hydrologically correct (Bennett et al., 2016). In addition, imposing a minimum value of 0.001 m/m avoids spurious errors in the smaller slope values. The position of the

delineated stream network was comparable to that mapped and deemed appropriate for analysis.

Next stream properties of the Abuan River network are calculated. First, rainfall data was converted from mm to mean depth per second expressed as a percentage, required to calculate discharge. A single flow direction algorithm was applied for flow accumulation, used to calculate gridded instantaneous discharge across the Abuan River network converted from drainage area values calculated. Discharge has been calculated through assuming no infiltration and steady uniform runoff based on the assumption the ground is fully saturated from heavy typhoon induced rainfall. Therefore antecedent rainfall has not be considered which presents an area for further research. The total stream power for the River Abuan and its contributing tributaries has been calculated using Equation 2.3 using parametrisation from Craddock et al. (2007) and Bookhagen and Strecker (2012) which varies as a function of rock type. As little is known about the geology of the region, an estimation is used based on the width and discharge calculated similar to Bennett et al. (submitted).

Outputs include distance from channel head, elevation, slope gradient, discharge, stream power and specific stream power averaged over 50 m segments of river channel. With gauge data unavailable in this region and in similar environments, it is difficult to indicate the potential overestimation of discharge and consequently stream power. Outputs generated extend across a 200 m, 100 m and 50 m spatial distance. Therefore, the smallest distance has been selected to allow for the most detailed analysis. In addition, this aids in smoothing out potential noise and error associated with the DEM, as extends across a greater spatial distance than its 5 m resolution.

For the purpose of this investigation total stream power will be assessed at the catchment scale to identify patterns across the channel network. To allow for a more detailed analysis, unit stream power will be assessed along the main channel as well as the area of interest to allow for a more detailed analysis. This is calculated by dividing total stream power by the active width of each segment following the typhoon event.

Equation 2.3: Total stream power (Ω , Wm^{-1}) calculated as the product of discharge (Q , m^3s^{-1}), smoothed channel slope (S , mm^{-1}) and unit weight of water (γ , $kg m^3$).

$$\Omega = \gamma QS$$

2.2.8 Sediment input from landslides analysis

Landslide sediment flux has been estimated from the volume of sediment calculated using the aforementioned empirical formula by Larsen et al. (2010) along 1 km sections of the River Abuan and study site selected. Landslides have been included within a 500 m² radius of the river channel, selected based on the density of landslides and runout lengths across the catchment. Sediment from landslides within this radius are anticipated to transport sediment to the river channel during an following the typhoon event.

2.2.9 Modelling the sediment cascade

Finally, to simulate the observed patterns of erosion and deposition, a model will be run using r.avaflow. r.avaflow is a raster module of GRASS GIS 7 as outlined by Mergili and Pudasaini (2019) who provided the a user manual for the open source code of which the steps undertaken are outlined below. The

model is used to simulate and anticipate the motion of sediment once it has been released as well as its interaction with channel flows (e.g. fluid flow). It accounts for different processes acting within the river channel, such as entrainment, erosion and deposition, therefore can simulate the triggering of landslides and debris flows. Landslides are represented as a sudden release of volume that can move freely along the hillslopes. The movement of this sediment is controlled by the transfer of momentum and energy between solid phases as well as at the interface between the solid mass and the bedrock. To simulate real-world heights, pores are assumed to be filled with fluid as opposed to air, a fair assumption following a heavy rainfall induced typhoon event. As r.avaflow is a multi-phase model it accounts for the properties of both solid and liquid states of sediment transfer following a landslide and the changes in energy as well as momentum between these phases downslope. Differences in their behavioural properties are accounted for in the volume and velocity of sediment modelling altering the ability to erode or deposit within the channel, resulting in the changes in geomorphology simulated.

Inputs

Table 2.3 summarises the large number of parameters and inputs required to investigate and calibrate results to best fit the observed changes in erosion and deposition. The essential inputs into r.avaflow are the DEM, solid, fine-solid and fluid release heights, a flood hydrograph to set out the initial upstream boundary conditions and values to set out the flow rheology. Input parameters also include rainfall distribution derived from satellite data, discharge and velocity defined by applying a single flow direction algorithm as well as entrainment values calculated from landslide inventories. Additionally, there are optional

complementary parameters that can be employed and altered in r.avaflow. These include conversion of release heights to depths, diffusion control, surface control and special parameters, however are not required for this research. Therefore, parameters have been set to default as defined in the manual by Mergili (2014-2023), other than those defined in Table 2.2. Model boundary conditions of water and sediment influx have been defined upstream by hydrgraph input. Downstream the water moves freely outside of the study area such that water and sediment leave based on the flow rate calculated at the downstream terminal. Therefore, boundary conditions vary across all the domain boundaries as are individually defined. Ready for input into r.avaflow, data collected had to be extracted to the study site selected as seen in Figure 1.12 shown in the table of inputs (Table 2). The 2013 DEM used to derive catchment elevation was clipped using the 'Extract by Mask' tool within the ArcGIS Pro Spatial Analyst toolbox which defines the baseline topography used within model simulations (DEM). Next, the depth of released sediment was analysed by taking the derived volumes using the scaling relationship outlined previously by Larsen et al. (2010) and dividing this by the area of the landslide calculated. Each cell has its own area defined from input raster files with cell size of 5 m. This technique has been applied to both landslides and runouts identified to account ready for input into the model. The release heights have been input as rasters to represent the depths of each phase across landslides, runouts and the river channel channel (Table 2 - HRelease 1, 2, 3). As a fluid component is not included for entrainment, only landslides and runouts have been input within depths of maximum entrainment hence why there are only two input rasters (Entrainment 1, 2). All landslides and runouts are simulated to be

triggered simultaneously at the start of each model run by releasing the defined depth of sediment.

Without the ability to conduct fieldwork, ratios between phases is based on research by Panici et al. (in review) with a heavier weighting of solid compared to fine-solid material (45:55 respectively), included to account for their differences in behaviour. Additionally, the depth of fluid was also based from Panici et al. (in review) of 0.2 m found to be the depth of water saturation in the area at the start of the simulation (Hrelease3). Without a DoD, maximum entrainable area has been attained by creating a raster file of landslides, runout areas and channel width following the landslide event using the same ratio of solid to fine:solid as before (Entrainment1 and Entrainment2). Depth of landslides and runouts were attained using the empirical formula as before. As for the channel, initial starting entrainment depths were estimated based on numerous model outputs, ranging between 3 m to 5 m, as could not be accurately obtained due to the lack of DEM following the event. Additionally, flood hydrographs were created, made into a tab delineated text file for input into r.avaflow. Hydrographs defined the water discharge released into the catchment and flow velocity every 200 m along the Abuan River and tributary rivers at the start of the simulation. Discharge has been calculated from the stream power analysis code aforementioned of which flow rate has been derived by dividing discharge by channel area every 50 m downstream. Hydrographs define the flow rate and also define the upstream boundary conditions. There is a high amount of associated uncertainty due to the spatial resolution of delineated channel extents (± 5 m) and derived discharge values (50 m).

Finally, observation points have been identified along the length of the main channel modelled, identified to further understand the role of sediment at areas of different levels of modelled topographic change, shown in Figure 2.3.

Table 2.3: Table of input parameters for r.avaflow

Parameter	Computational Meaning
Phases	Combination of phases to be considered, default and used here is a multi-phase model with solid (P1), fine-solid (P2) and fluid (P3) material
Elevation	Defined input elevation raster map considered as the area of interest
Hrelease(1)(2)(3)	Separate input raster maps which refer to each phase of the model representing spatial distribution of P1, P2 and P3 release heights found in landslide and runout areas. Includes the release height of each phase of landslides, runouts and flow of river channel.
Entrainment(1)(2)	Input raster maps of the maximum entrainable height useful in modelling to constrain entrainment areas, found in areas of landslides and runouts as well as along the river channel.
Friction	Internal and basal friction parameters attributed to each phase
Density	Define the grain density of each phase whereby P1- is the greater than P2 which is greater than P3 set to 2700, 1800, 1000 respectively
Hydrographs	Flood hydrographs of river discharge and velocity calculated to allow the continuous input of flow material along the given profile at given points along the channel (hydrocoords)
Time	Defined time interval for output results and end time
Ctrlpoints	Coordinates of control points/ points of interest along the channel for main model outputs to be written as a text file for analysis

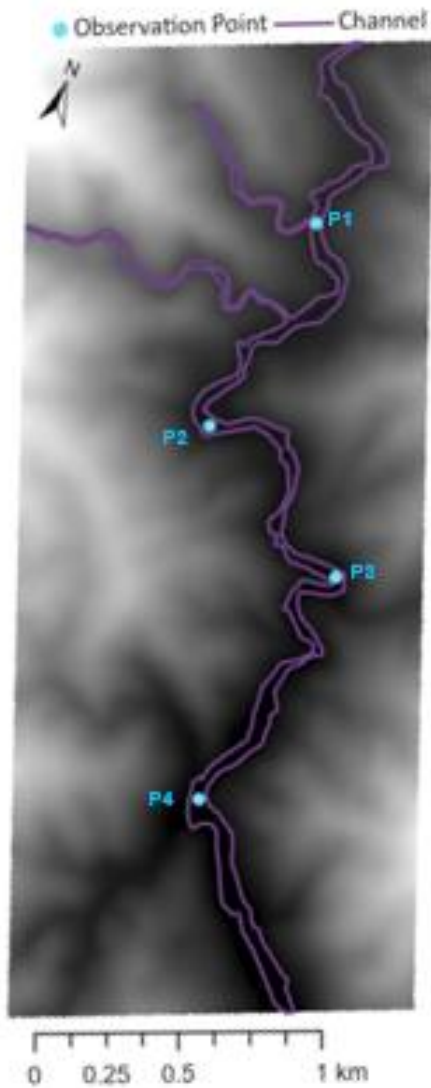


Figure 2.3: Location of observation points (P1-4) along the channel modelled which overlays the pre-event DEM.

Process

The steps required to model changes in geomorphology over time have been based on Panici et al. (in review) who also provided a virtual workshop to myself and collaborators of the ScaRP project.

Step 1 - Download and install r.avaflow, GrassGIS and Python 3 on Linux.

Although r.avaflow 2.4 can be run on Windows through a virtual machine, for

optimum performance the software is best run on a Linux system, where the code is native.

Step 2 – Download all relevant input files (rasters and text files) afformentioned in Table 2 into a Linux working directory.

Step 3. 1 – Launch GrassGIS in the Linux terminal command window, creating a new project folder in which to run the model and collate results generated.

Step 3.2 – Input all saved files, defining the area in which to model, boundary conditions and which projected coordinate system to use.

Step 3.3 – Alter default settings using a combination of sourced information and educated estimates for relevant parameters as well as inputs.

Step 3.4 – Run the model to simulate the consequences of the release of landslide and runout sediment input on changes in channel geomorphology during an extreme weather event. Initially, the model releases the depths of sediment defined in each phase, simulating the flow of sediment and water over time. By considering the exchange in momentum between phases, the differences in sediment volume and velocity simulated over time determine overall channel change by either erosion or deposition.

Step 4.1 – Analyse simulated results in ArcGIS Pro by obtaining relevant files of basechange and flow height for solid and fine-solid phases before combining these rasters to derive overall modelled topographic change (see outputs section below)

Step 4.2 – Compare simulated channel change to that observed, if large differences occur revert back to Step 3.3. Use results to re-run the model with altered parameters and inputs to find the best fit with the observed changes.

Step 5 – When modelled and observed results are comparable, with only minor deviations, use the fully calibrated model output raster and text files to generate figures ready for analysis.

Step 6 – Test the validity of parameters and inputs used by conducting a sensitivity analysis. Run with baseline inputs of the calibrated model and change only one key parameter with each sensitivity run (Table 2.4). In addition, to validate the impact of landslides on channel geomorphology, a run should be simulated omitting landslides (Test 0) to observe the role of landslide sediment input in simulation of channel geomorphic change. Here, maximum entrainable depth was only delineated in the main and tributary channels.

Table 2.4: Table summarising changes in parameters tested in sensitivity analysis

Test	Internal Friction	Solid: fine-solid ratio	Phases Modelled	Entrainment Depth
1 (Baseline)	Default – 35° and 0° for solid and fine-solid phases respectively	45:55	Multi-phase (1,2,3)	Baseline
2	Default – 35° and 0° for solid and fine-solid phases respectively	55:45	Multi-phase (1,2,3)	Baseline
3	Default – 35° and 0° for solid and fine-solid phases respectively	45:55	Solid phase only (1)	Baseline
4	25° and 20° for solid and fine-solid phases respectively	45:55	Multi-phase (1,2,3)	Baseline
5	Default – 35° and 0° for solid and fine-solid phases respectively	45:55	Multi-phase (1,2,3)	+50%

Outputs

Once a model run has been completed, r.avaflow automatically saves output files (into ascii, text and plot folders) of which those required are to be extracted. Animated GIFs of channel change are created to enable quick visual depiction of modelled results to check if the simulation has been successful. To be able to present modelled results and calculate the extent of modelled channel change, first raster files of final base change (basechange 1 and 2) and flow height (hflow 1 and 2) are extracted for each phase from the ascii files generated. Adding these using the 'Raster Calculator' tool in ArcGIS Pro results in a raster of overall topographic change across the study site. From this, the modelled channel can be digitised by visually identifying the change in topography downstream compared to the existing pre-event DEM. Negative topographic change indicates areas of erosion and positive represents areas of deposition. Modelled channel widths can be extracted using the measuring tool in ArcGIS from the digitised modelled channel. These can be compared to the existing pre-event channel widths to calculate simulated channel change. In addition, the depth and velocity of pre-defined observation points can be extracted from the text files generated. Within the summary file, maximum depth and velocity at each observation point is given across the length of the simulation at time intervals specified. This is input to Excel to calculate total change over time for both depth and velocity, then presented in graphs ready for analysis.

3. Results

All results have been presented and rounded to a maximum of one decimal place (excluding values of slope) for continuity, to avoid spurious accuracy and ensure numbers are easy to interpret.

3.1 Landslide Inventory

3.1.1 Typhoon Lawin

Following Typhoon Lawin a total of 3357 landslides were manually mapped, predominantly found in the northwest of the River Abuan catchment (Figure 3.1a). Table 3.1 of descriptive statistics for this inventory indicates that landslides following Typhoon Lawin ranged from the smallest of $6.4 \text{ m}^2 (\pm 5 \text{ m}^2)$ to the largest of $34837.1 \text{ m}^2 (\pm 5 \text{ m}^2)$. Landslides had an average magnitude of $688.8 \text{ m}^2 (\pm 5 \text{ m}^2)$ covering a total extent of $2578024 \text{ m}^2 (\pm 5 \text{ m}^2)$. Volumes have been calculated using Equation 2.2, resulting in a range from 12.1 m^3 to 980.8 m^3 with a cumulative volume of 8369749.9 m^3 .

As the 2016 Typhoon Lawin event was selected to investigate geomorphic channel change, landslides and landslide runouts were mapped separately as required for r.avaflow input. Of the ~3000 landslides mapped, 220 generated runouts that have been mapped which connect with the river network (Figure 3.1b). The largest landslide had a total volume of $10385 \text{ m}^3 (\pm 5 \text{ m}^3)$ found near one of the confluences of the Abuan River in the north of the catchment (Figure 3.1). This varies considerably from the smallest landslide with a magnitude 10379 m^2 smaller of $6 \text{ m}^2 (\pm 5 \text{ m}^2)$. Landslides have been delineated in areas where the removal of vegetation and sediment has left visible scours across the landscape at differing magnitudes. The use of multiple satellite imagery sources overcomes the presence of cloud cover, this can be seen in the magnified view

of the Google Earth imagery (Figure 3.1c) where landslides in this area have been identified from PlanetLabs imagery (Figure 3.1d). In addition, this figure indicates both landslides and runouts which have both been manually mapped with high confidence.

3.1.2 Typhoon Kammuri

In comparison, fewer landslides occurred as a result of Typhoon Kammuri with a landslide inventory comprising of 1963 landslides. Again, these were predominantly found north of the catchment, but further east than those mapped for Typhoon Lawin. Landslides were however of a greater magnitude with an average area of landslides of $3494.9 \text{ m}^2 (\pm 5 \text{ m}^2)$ which is 2806.1 m^2 greater than in Typhoon Lawin. Landslides ranged in area between $40.2 \text{ m}^2 (\pm 5 \text{ m}^2)$ and $82177.5 \text{ m}^2 (5 \text{ m}^2)$. Results of landslide areas calculated are greater than the $\pm 5 \text{ m}^2$ uncertainty associated with the resolution of the satellite imagery used. Therefore results are within the bounds of acceptability and are deemed appropriate for analysis.

3.1.3 Landslide magnitude-frequency

The exceedance probability distribution of both landslide events follow a characteristic power law tail, Figure 3.2. Figure 3.2a shows the power law magnitude frequency distribution of landslides as a result of Typhoon Lawin has a power tail exponent of 2.96 and a landslide threshold size of 2.3 km^2 . In comparison, following Typhoon Kammuri there is a significantly greater landslide threshold size of 6.8 km^2 with a slightly lower a power law tail of 2.70 as seen in Figure 3.2b.

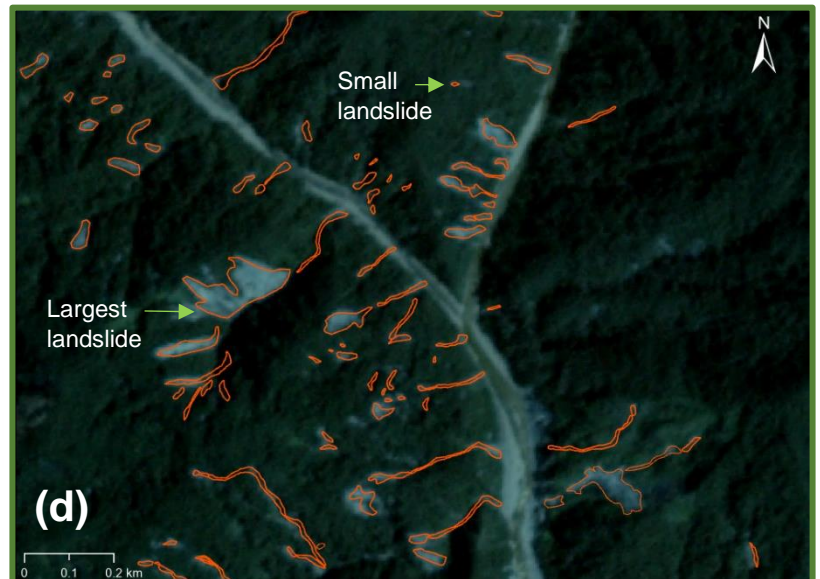
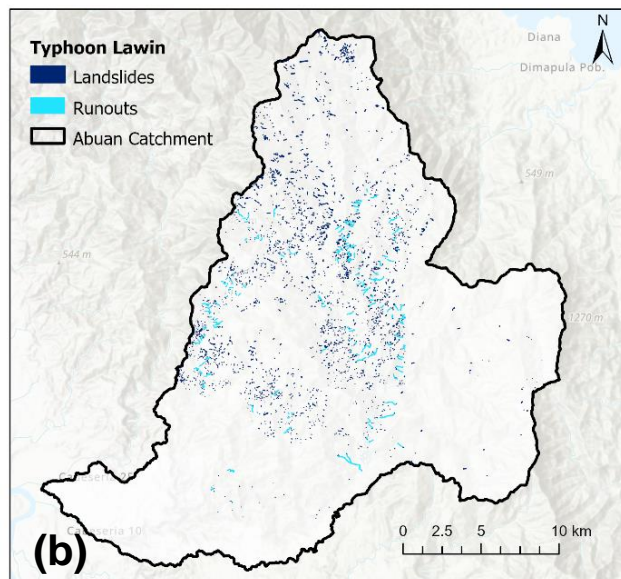
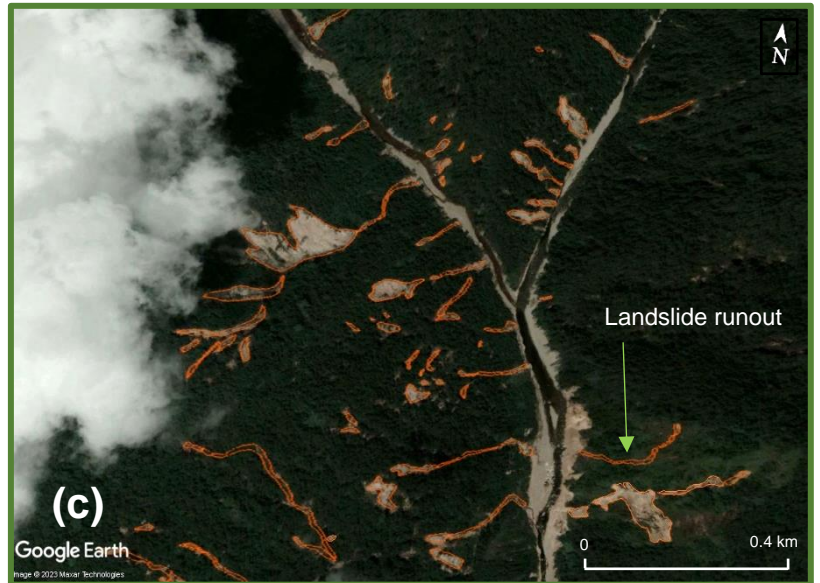
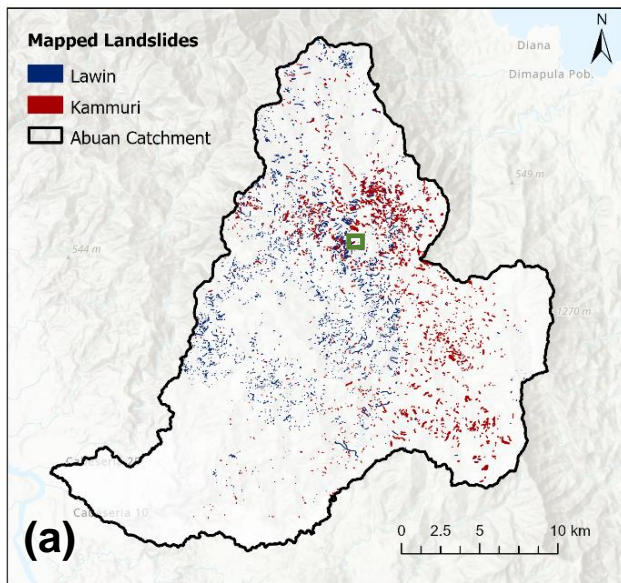


Figure 3.1: Map of the Abuan River catchment showing (a) mapped landslides following Typhoon Lawin (dark blue) and Typhoon Kammuri (red), and (b) with addition of mapped runouts (light blue). Area of interest to show the largest landslide has been outlined via the green box with magnified view of landslide mapping using PlanetLabs (c) and Google Earth (d) satellite imagery acquired on 19/04/2017 and 22/10/2016 respectively.

Table 3.1: Descriptive statistics of landslide inventories following Typhoon

Lawin and Typhoon Kammuri.

	Area (m ² , ±5 m ²)				
	Minimum	Maximum	Mean	Standard Deviation	Total
Lawin	6.4	34837.1	688.8	1276.1	2578024.0
Kammuri	40.2	82177.5	3494.9	6243.1	6863936.0
	Volume (m ³ , ±5 m ³)				
	Minimum	Maximum	Mean	Standard Deviation	Total
Lawin	12.1	223976.0	2240.3	7508.2	8369749.9
Kammuri	58.4	638129.8	16540.1	41929.1	32484791.1

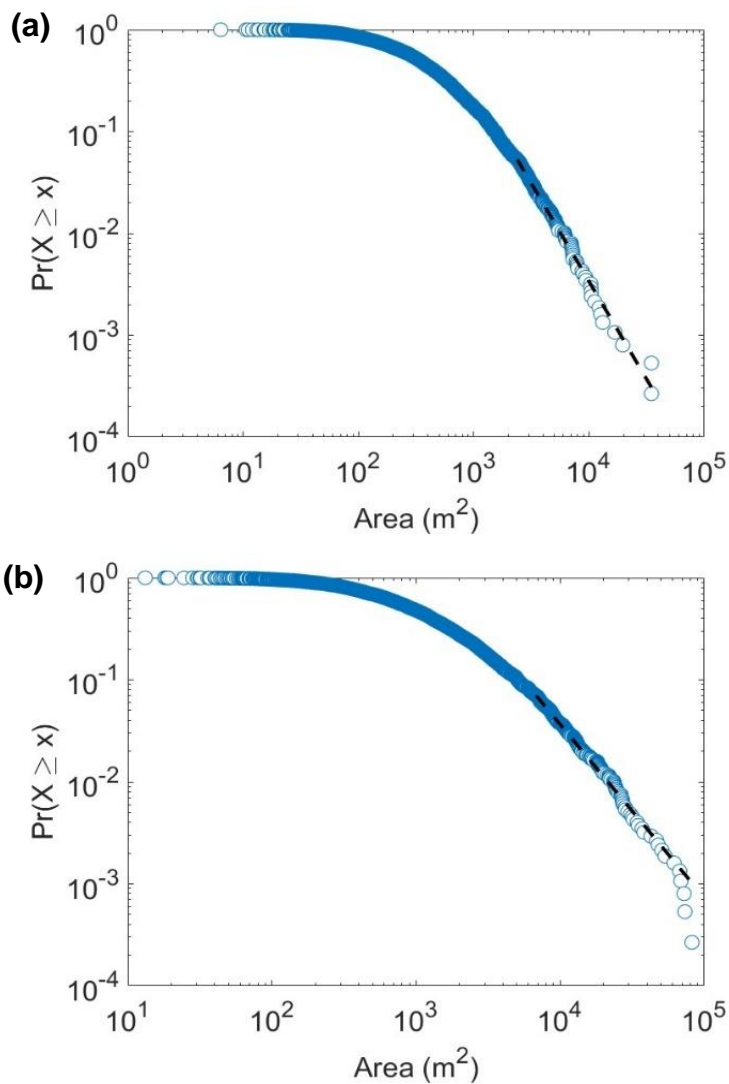


Figure 3.2: Power law magnitude frequency distribution for landslide inventories of (a) Typhoon Lawin and (b) Tropical Storm Kammuri, fit with the theoretical power law model using the maximum likelihood method.

3.1.4 Landslide density

Both typhoon events observed had profound geomorphic effects on the River Abuan catchment as shown in Figure 3.3 indicating the density of landslides. Following Typhoon Lawin there is a high density of landslides in the headwaters of the catchment with the greatest density of landslides occurring in the upper course of the River Abuan of 145 landslides per 500 m radius. In addition, in the western periphery of the catchment there is a high density of landslides surrounding tributary rivers of the River Abuan of up to 130 landslides per 500 m². The number of landslides per 500 m² of the catchment is considerably higher in 2016 than in 2019 when Typhoon Kammuri hit with the greatest density of 61.9 landslides per 500 m² found more easterly. Similarly, across both inventories, a high density of landslides occurred upstream of the River Abuan and near the headwaters as well as confluences of its tributary rivers .

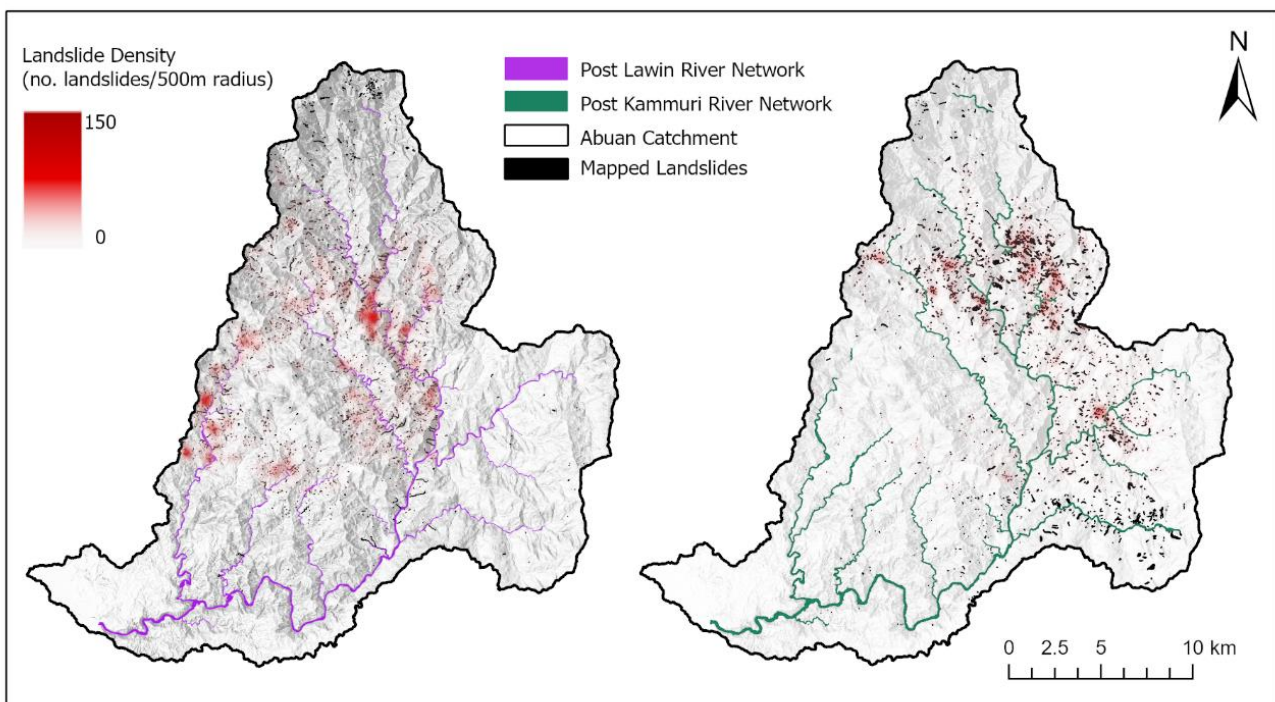


Figure 3.3: Landslide density maps showing the geomorphic effect based on the landslide inventories mapped following Typhoon Lawin (left) and Typhoon Kammuri (right) calculated as the number of landslides per 500 m² radius (red).

3.2 Geomorphic change in Abuan River network

Channel change is variable across the study area following both Typhoon Lawin and Typhoon Kammuri which also vary considerably in magnitude. To quantify channel change, first channels across the Abuan River network have been mapped pre- and post- each typhoon event (Figure 3.4), delineated using primarily PlanetLabs imagery (Table 2.1). To validate channels mapped, polygons were cross-checked with Google Earth satellite imagery. Areas of interest (AOI) where dramatic changes in the channel have been identified to provide further detail of mapped channels (Figure 3.5). Changes following Typhoon Lawin have been presented, as this has been identified as the more catastrophic event, therefore analysis will focus on this extreme weather event. Areas have been magnified to demonstrate the detailed mapping of channels comparing the delineated pre- and post- typhoon channels along the edge of riparian vegetation using both PlanetLabs (Figure 3.6) and Google Earth satellite imagery layout maps corresponding to each AOI location (Figure 3.7). Channel widening along the channel can be visually identified as a result of the removal of vegetation exposing sediment along river embankments. Whether geomorphic channel change is attributed to the exposure of bedrock due to high rates of fluvial erosion or the deposition of sediment from debris transported and deposited remains uncertain due to the resolution of imagery. In some areas, visual delineation of the channel network was difficult and not always possible due to high cloud cover over sections of the river network especially along small tributary rivers (Figure 3.7, AOI 3 pre-typhoon channel). Areas of low confidence have therefore been delineated with a dashed line (Figure 3.4). The mapping of landslides and runouts has also been presented overlaying Google

Earth imagery to provide greater detail and further validate inventory mapping (Figure 3.7).

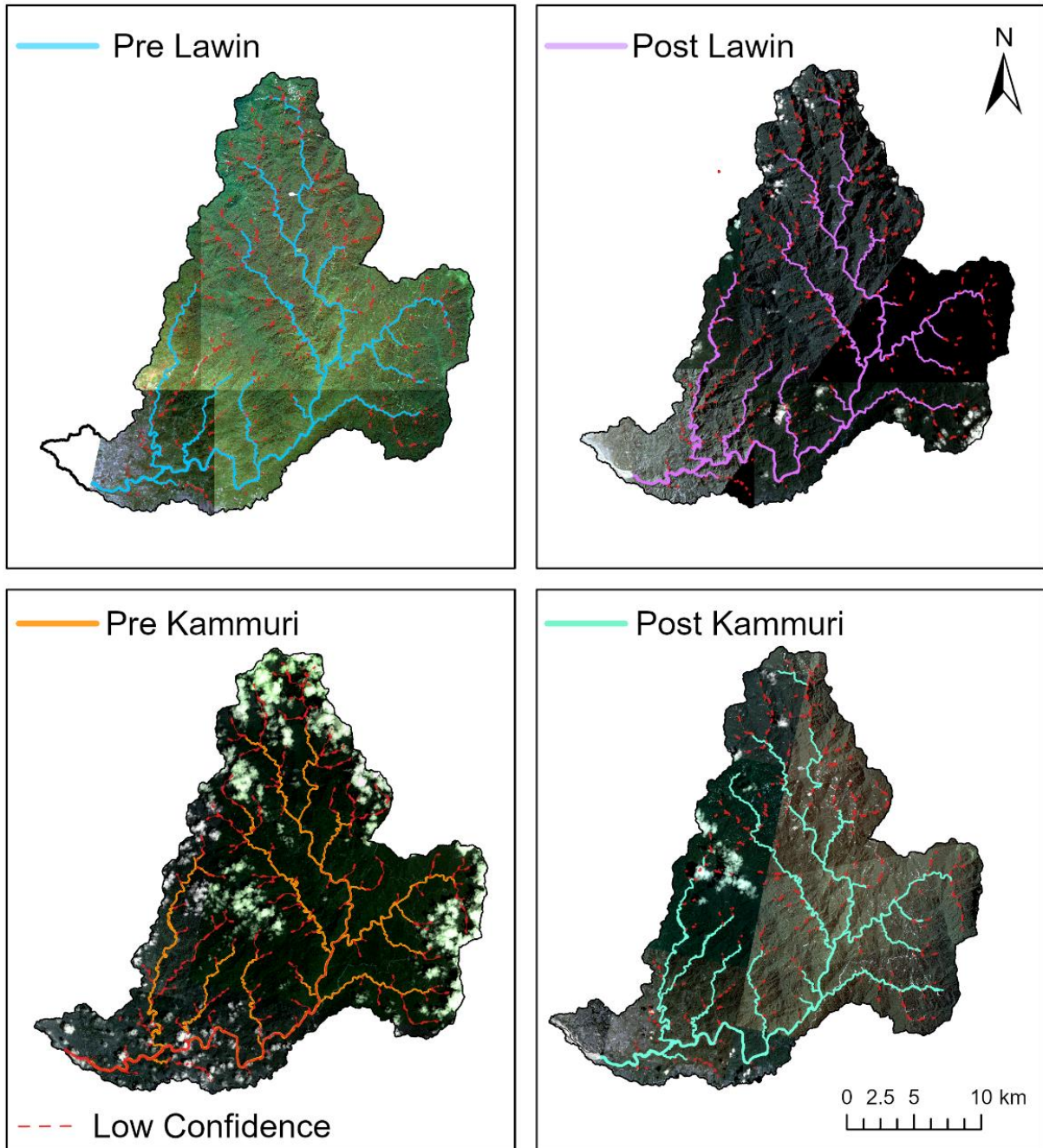


Figure 3.4: Maps showing mapped channel networks in the River Abuan catchment pre (blue) and post (purple) Typhoon Lawin in 2016 and pre (orange) and post (turquoise) Typhoon Kammuri in 2019 with segments of low confidence indicated (red dashed). Channels overlay PlanetLabs Scope satellite imagery (Table 2.1).

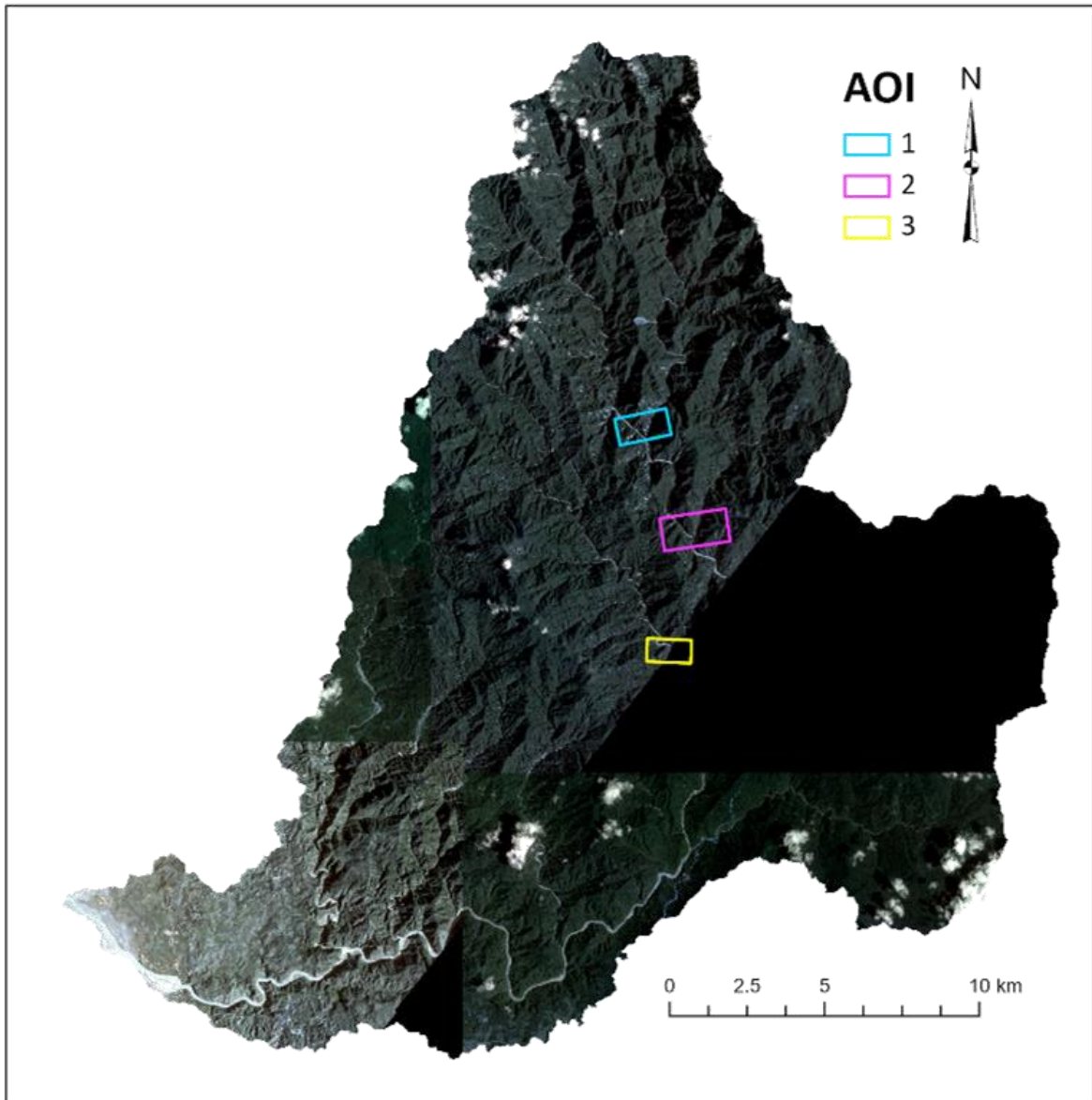


Figure 3.5: Areas of interest (AOI) identified of dramatic channel change following Typhoon Lawin overlaying PlanetLabs satellite imagery sourced (Table 2.1).

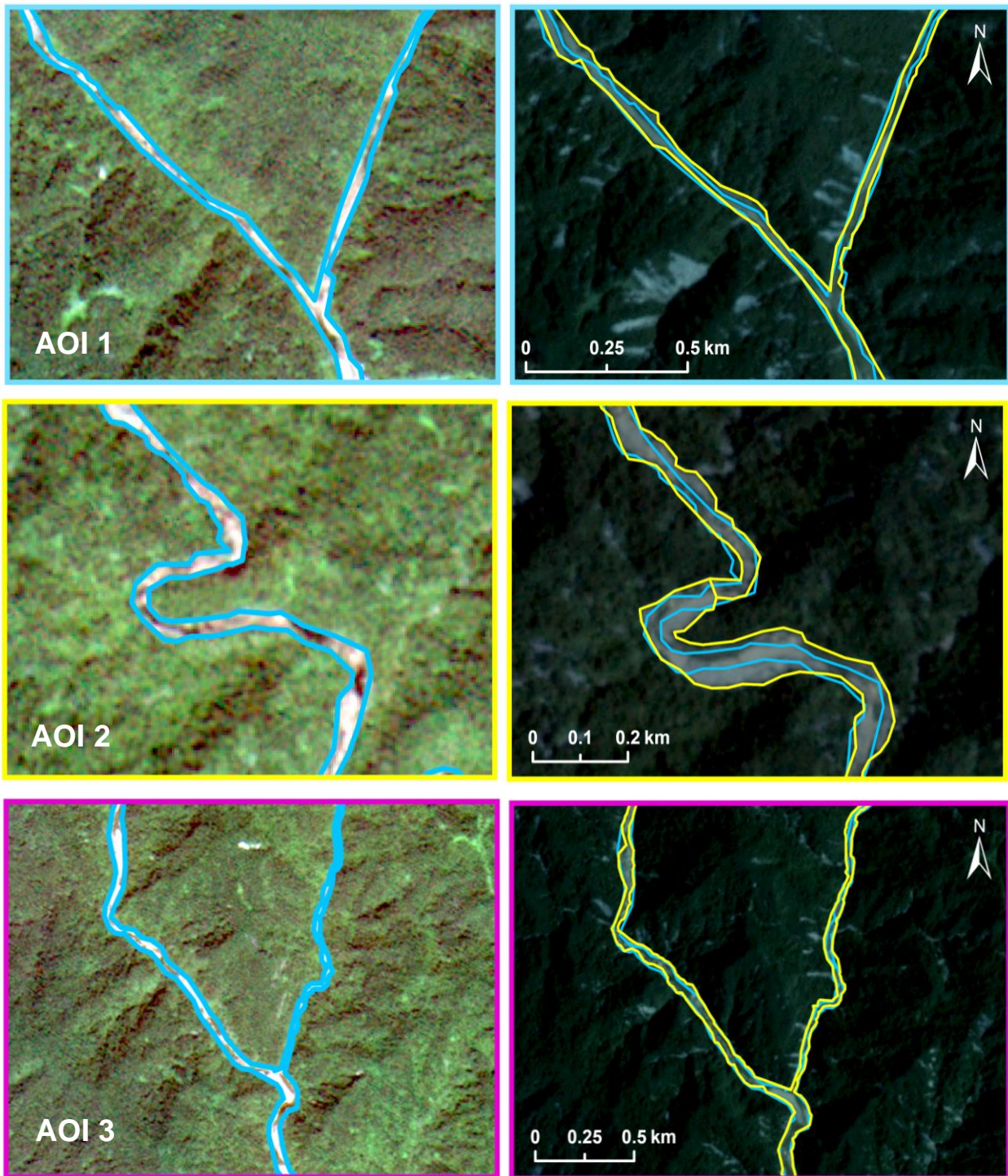


Figure 3.6: AOI numbers 1-3 showing magnified sections of the River Abuan channel network in June 2016 (left) and December 2016 (right) from PlanetLabs satellite imagery (Table 2.1). Channel extents mapped have been shown before (blue) and following (yellow) Typhoon Lawin.

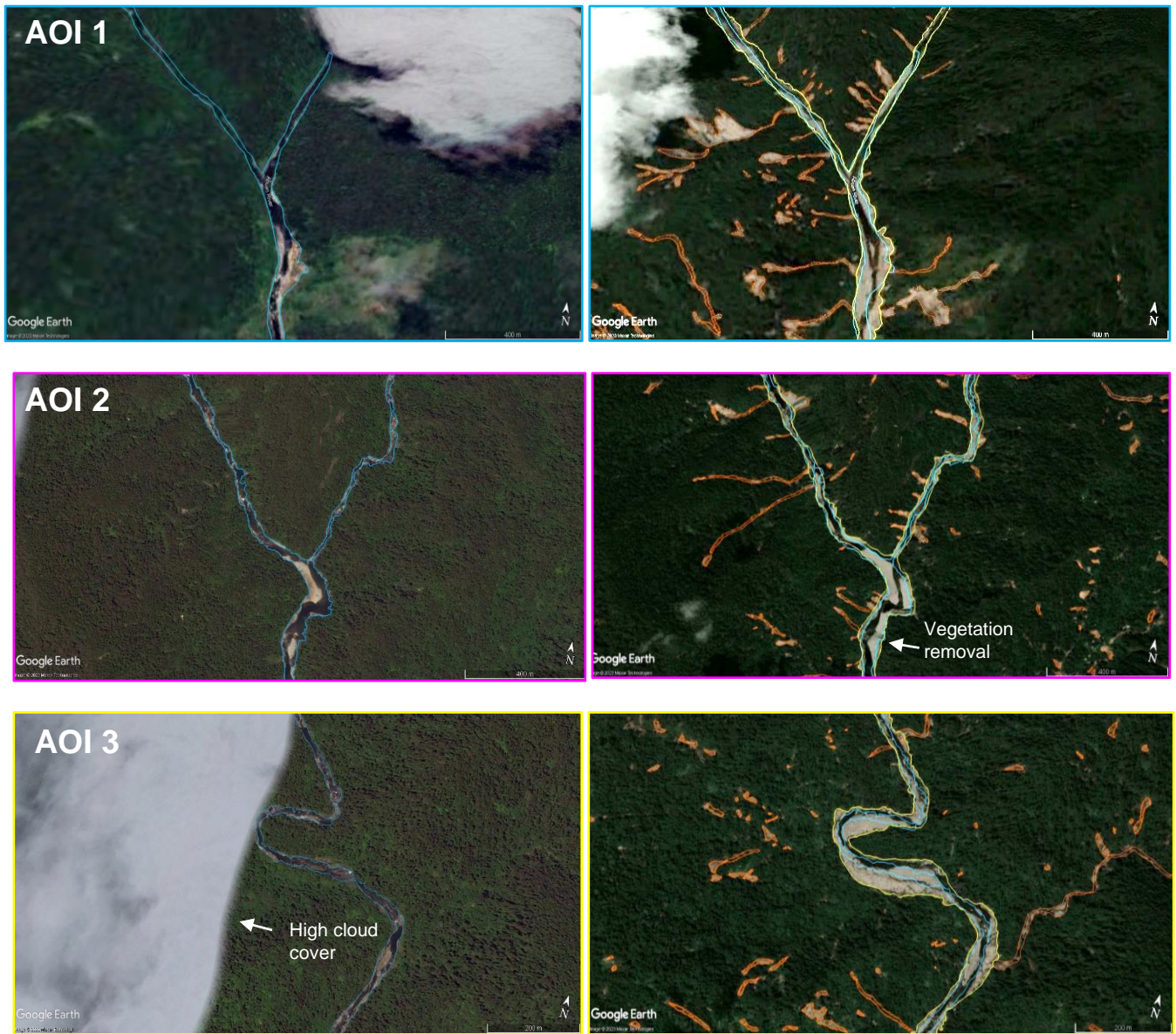


Figure 3.7: AOI numbers 1-3 showing magnified sections of the River Abuan channel network in April 2016 (left) and April 2017 (right) from Google Earth Pro. Landslides and runouts have been delineated in orange with pre-typhoon channel in blue and post-typhoon channel in yellow.

3.2.1 Active Channel Width (ACW)

To assess changes in ACW associated with each landslide event, channels before and after each event have been assessed across the entire catchment in lengths of ~1 km (Figure 3.8). When quantifying ACW, sections of low confidence identified whilst mapping the Abuan River network have not been included (shown by the dashed red lines). The results can be observed in Figure 3.8 and are stated in Table 3.2, with some stretches of the Abuan River network experiencing greater than 100% widening following each typhoon event. Along the River Abuan prior to Typhoon Lawin, ACW ranged from between 17.5-139.7 m (± 5 m) increasing to between 26.0-164 m (± 5 m) after the event. Comparatively, prior to Typhoon Kammuri ACW ranged from 17.8-127.4 m (± 5 m) once again increasing to between 20.4- 164.5 m (± 5 m) post the event.

Following both typhoon events channel widening was comparable with the percentage of ACW widening higher by 1.8% after Typhoon Kammuri compared to Typhoon Lawin (Table 3.1). On average channels following Typhoon Lawin widened by 7.6 m (± 5 m) compared to 9.5 m (± 5 m) following Typhoon Kammuri. When channel change exceeds 100%, pre- and post- Typhoon Kammuri increase by 9.2% compared to only 3.4% following Typhoon Lawin, demonstrating the greatest difference in change between the two events.

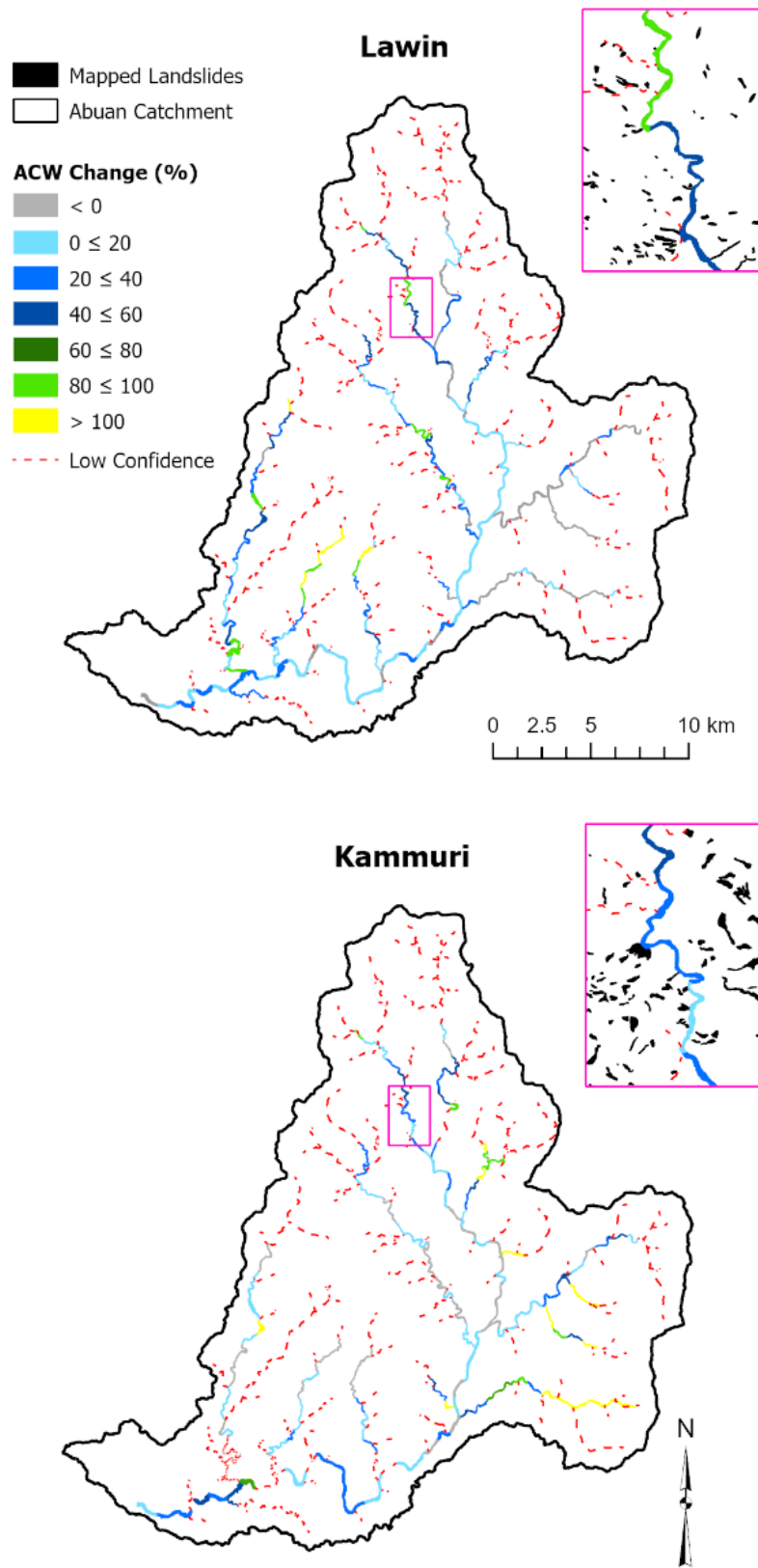


Figure 3.8: Map showing changes in ACW across the Abuan catchment over ~1 km segments of river segments using imagery pre and post each typhoon event with the study site selected for modelling magnified (red).

Table 3.2: Statistics of ACW change in the Abuan River network following Typhoon Lawin and Kammuri

ACW Change %	Lawin		Kammuri	
	Km	%	Km	%
<0	37	21.1	35	22.9
0≤20	56	32	50	32.7
20≤40	38	20	29	16.6
40≤60	20	11.4	15	9.8
60≤80	6	3.4	3	2
80≤100	12	6.9	7	4.6
>100	6	3.4	14	9.2

3.2.2 River Abuan

To further quantify changes in ACW, analysis has been conducted along the Abuan River comparing the digitised channel from before and after each Typhoon event being investigated. For Typhoon Lawin a total of 56 km of the main channel was analysed (Figure 3.9) compared to 49 km for Typhoon Kammuri (Figure 3.10) due to the high cloud cover observed in the satellite imagery over the upper sections of the river (Appendix C). Following Typhoon Lawin, 80.4% of the main channel experienced an increase in ACW with the greatest increase observed in the upper course of the river widening by 46.9 m (± 5 m). Following Typhoon Kammuri widening of the channel was of a higher magnitude with a maximum increase of 26.9 m (± 5 m) resulting in a 77.6% increase in ACW from pre to post the event in 2019.

After Typhoon Lawin, the majority of the river widened by between 0-10% stretching across a total of 18 km of the channel, predominantly along the middle of the Abuan River (Figure 3.9 and Table 3.3). Similar can be said following Typhoon Kammuri, with widening of between 0-10% experienced along 10 km of the river. However, a large proportion of the river narrowed accounting for 12 km, 24.5% of the Abuan River quantified (Figure 3.10 and Table 3.3). Only following Typhoon Kammuri did widening exceed 50% ACW increase, with results demonstrating that increases in percentage change of ACW are experienced at an increasing rate downstream along the Abuan River channel. Therefore, widening following each of the typhoon events was comparable with similar results observed of greater total widening than narrowing, however most commonly of a low percentage increase (Appendix C).

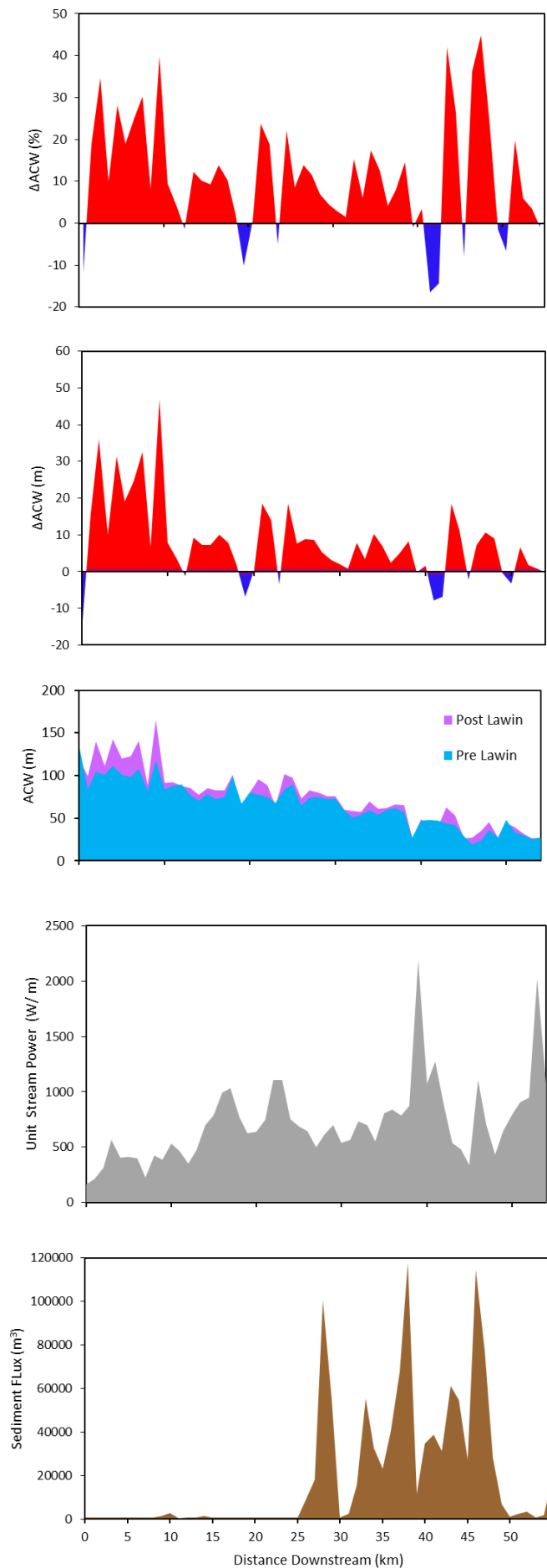


Figure 3.9: Longitudinal patterns of changes in the ACW of the River Abuan downstream comparing digitised channels pre and post Typhoon Lawin, stream power, specific stream power and landslide sediment flux.

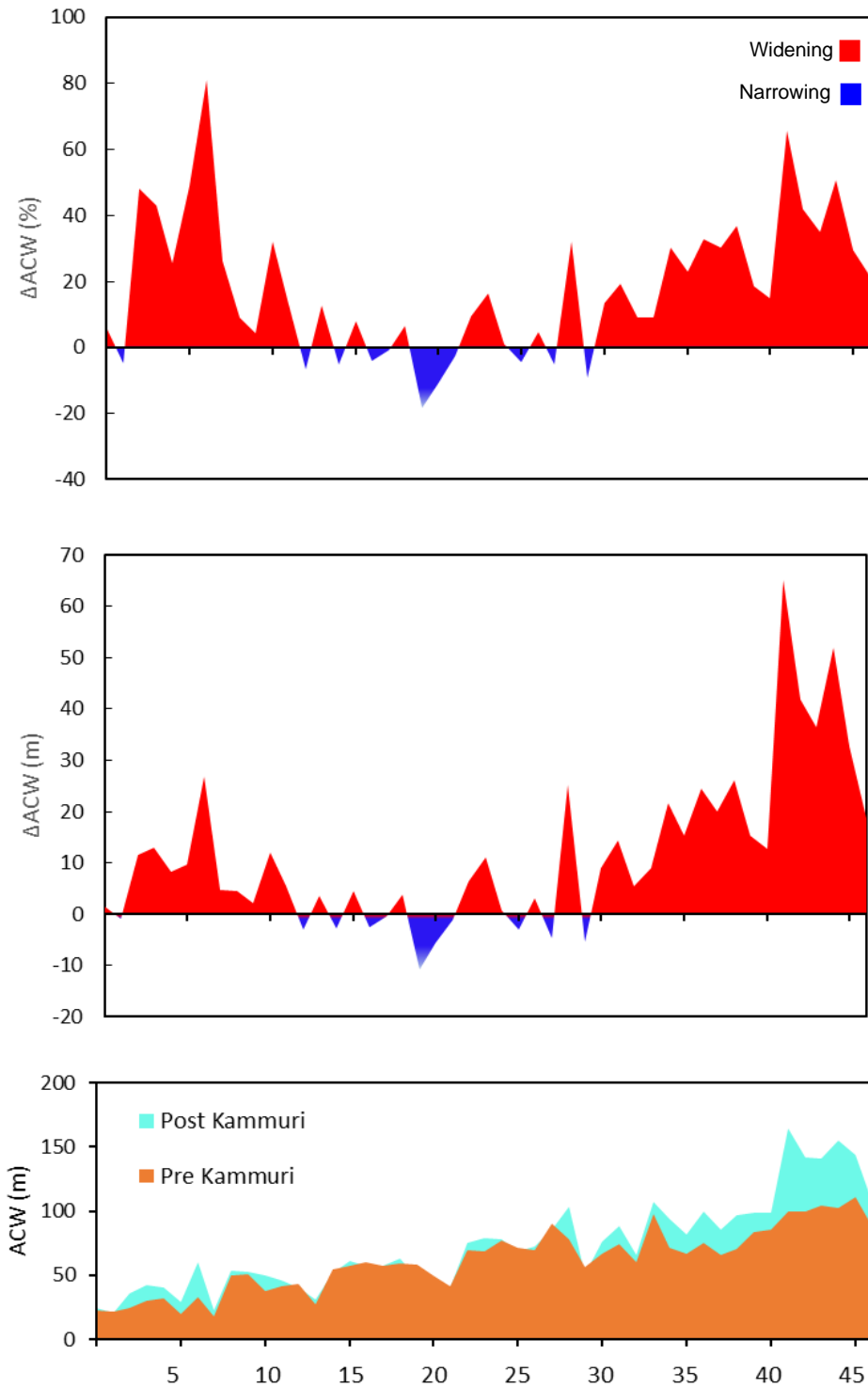


Figure 3.10: Longitudinal patterns of changes in the ACW of the River Abuan downstream comparing digitised channels pre and post Typhoon Kammuri.

Table 3.3: Statistics of changes in ACW along the River Abuan after Typhoon

Lawin and Typhoon Kammuri

ACW Change %	Lawin		Kammuri	
	Km	%	Km	%
<0	11	19.6	12	24.5
0≤10	18	32.1	10	20.4
10≤20	15	26.8	8	16.3
20≤30	6	10.7	5	10.2
30≤40	4	7.1	7	14.3
40≤50	2	3.6	4	8.2
50≤60	0	0.0	1	2.0
60≤70	0	0.0	1	2.0
70≤80	0	0.0	0	0.0
80≤90	0	0.0	1	2.0
90≤100	0	0.0	0	0.0

3.2.3 Sub-catchment identified for modelling

More significant channel widening can be visually observed along tributary rivers, such as in the study site selected for modelling (Figures 3.6 and 3.7, AOI 1), along a main tributary of the upper Abuan River where a large amount of channel widening can be observed following both events. Divided into four 1 km segments, after Typhoon Lawin the channel widened by 19.8 m, 16.1 m, 12.3 m and 13.9 m (upstream to downstream, ± 5 m) giving a percentage increase of 99.9%, 69.9% 53.3% and 58.3% respectively. Following Typhoon Kammuri the

channel widened by lesser percentage of 50.5%, 26.8%, 38.5% and 5.5% from increases in width of 13.1 m, 9.5 m, 10.0 m and 1.8 m (± 5 m) respectively.

3.2.4 Rainfall, discharge and topographic factors

Discharge, elevation and slope gradient have been visualised in Figure 3.11 and statistics have been summarised along the 56km of the River Abuan analysed in Table 3.4. Discharge has been calculated from rainfall totals ranging from between 367 to 447 mm across the catchment during Typhoon Lawin, presented in Figure 2.2. Discharge increases approximately linearly in the downstream direction as the frequency of tributaries increases along the course of the River Abuan. Discharge ranges from 4.6 to 2383.6 m³/s with a mean value of 272.1 m³/s. Moving onto patterns in topography, elevation decreases downstream ranging between 1041.5 m in the headwaters to 41.8 m at the end of the river quantified with a mean value of 344.7 m. Slope gradient varies considerably along the profile of the river reaching a peak of 0.4 m/m compared to downstream where the slope is flat (0.0001 m/m), however is generally steep.

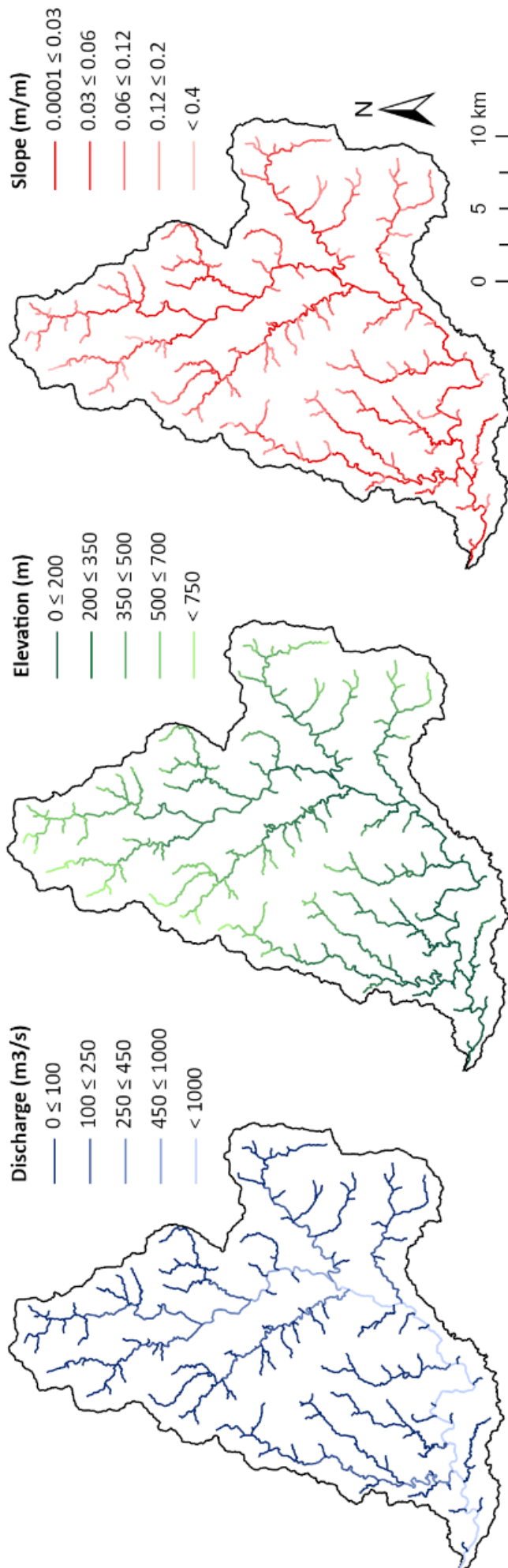


Figure 3.11: Map showing values of discharge (left, blue), elevation (middle, green) and slope gradient (right, red) across the River Abuan channel network.

Table 3.4: Derived topographic, discharge and slope statistics across the River Abuan network

	Mean	Standard Deviation	Minimum	Maximum	Range
Discharge (m ³ /s)	272.1	565.6	4.6	2383.6	2793
Elevation (m)	344.7	197.9	41.8	1041.5	999.7
Slope Gradient (m/m)	0.059	0.057	0.0001	0.39	0.3899

3.3 Stream Power

Total stream power has been calculated following Typhoon Lawin and has been compared against changes in ACW calculated from the same extreme weather event for analysis (Figure 3.9). Total stream power varies considerably across the Abuan River catchment ranging from 10.0 W/m to 194,449.0 W/m (Figure 3.12). The minimum amount of energy required to cause channel widening has a stream power of 9.7 W/m where a 123.0% increase in ACW was observed found along a tributary of the River Abuan. In some areas only a small amount of energy is required to cause channel widening. This varies spatially as ~20 km along the River Abuan, following Typhoon Lawin this section of channel experiences a decrease in ACW of 14.3% despite stream power reaching 73348.3 W/m.

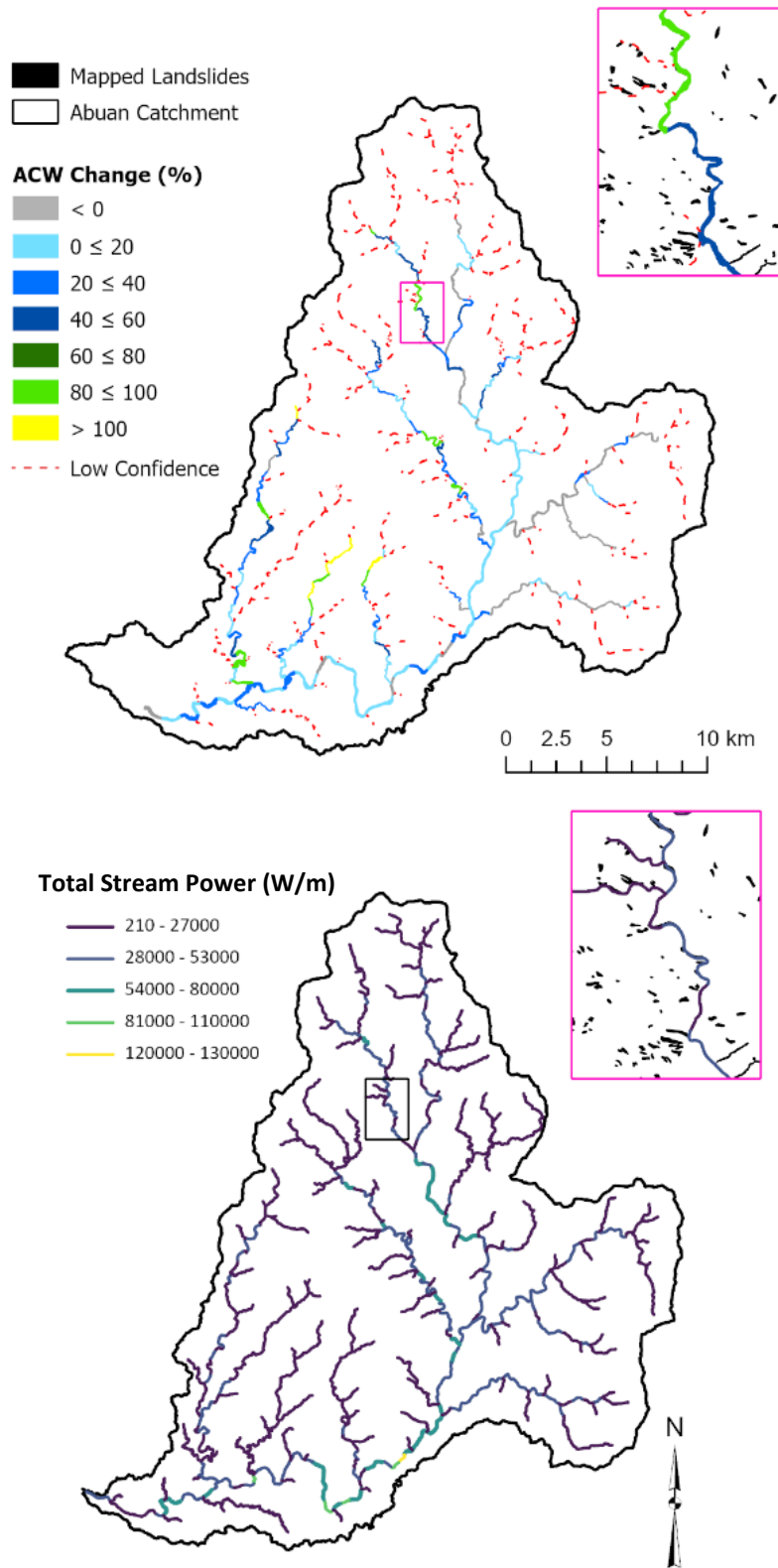


Figure 3.12: Comparison of change in ACW and total stream power calculated every 1 km and 100 m respectively across the River Abuan watershed.

3.3.1 River Abuan

To analyse the impact of stream power further, total stream power has been converted to unit stream power along the Abuan River. Figure 3.90 demonstrates that unit stream power along the River Abuan ranged from 163.9W/m to 2189.4 W/m, visualised in Figure 3.12. Unit stream power is highly variable downstream along the course of the Abuan River and has a mean average of 718.4 W/m. Trends observed in results demonstrate unit stream power starts high upstream and fluctuates downstream demonstrating an overall increase along the course of the river. Attributed to a 18.8% increase in ACW experiencing an increase in ACW of 18.8%, unit stream power peaks 33 km downstream. Despite the highest value of stream power calculated, channel widening experienced here is 26% lower than the greatest calculated along the River Abuan.

3.3.2 Study area

Focusing on the area selected for modelling, following Typhoon Lawin despite relatively high increases in ACW, stream power is comparably low (Figures 3.12 and 3.13). Moving downstream as aforementioned ACW increases by 99.9%, 69.9% 53.3% and 58.3%. However, unit stream is comparatively lower along the section of river selected starting at 819.2 W/m, increasing to a maximum of 1070.8. Along all of the channel selected for modelling stream power remains below 15,000 W/m. Therefore, despite large increase in ACW, this section of river experiences comparably low stream power compared to the rest of the Abuan River network and therefore stream power cannot explain channel widening experienced.

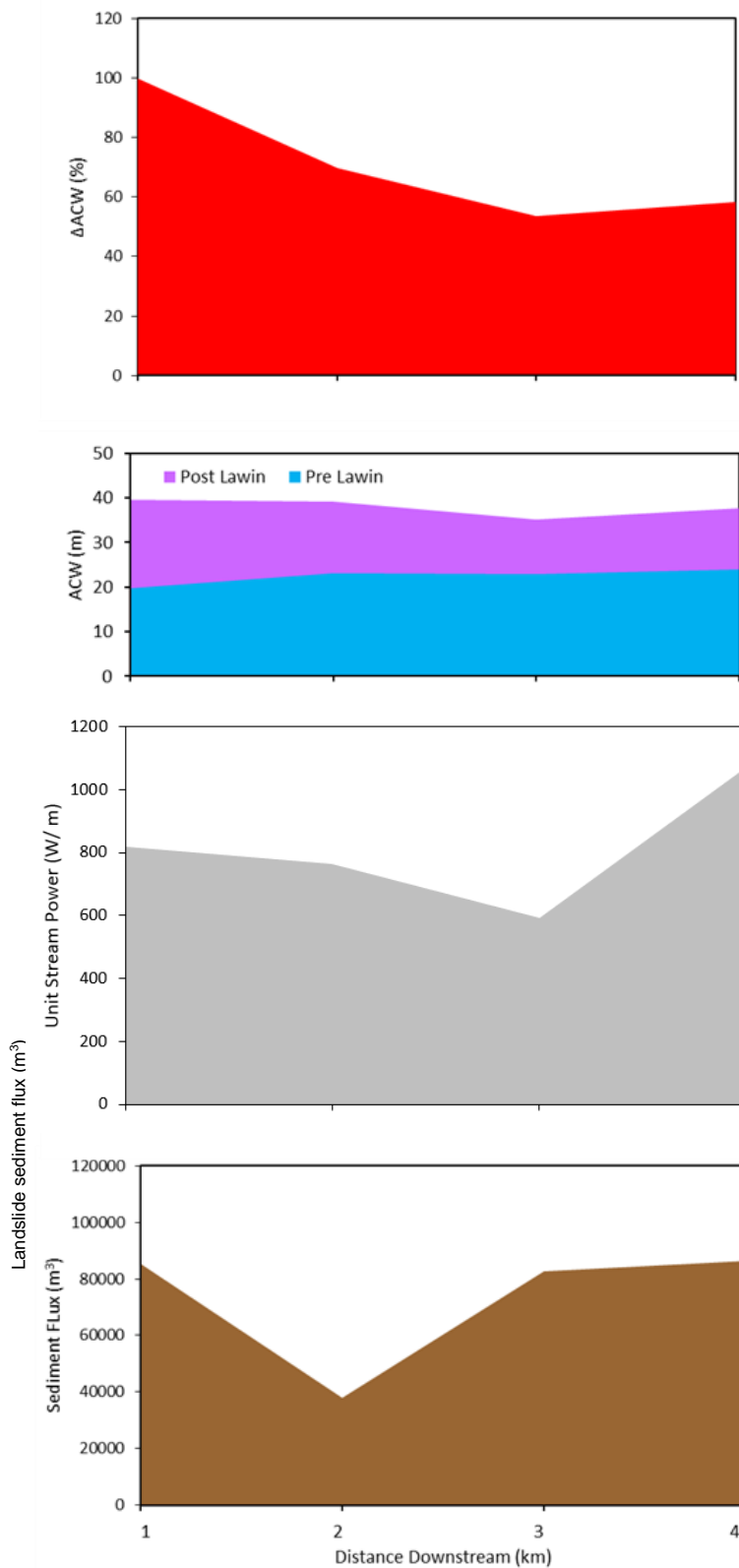


Figure 3.13: Longitudinal patterns of changes in the ACW downstream along the study site selected comparing digitised channels pre and post Typhoon Lawin, stream power and landslide sediment flux

3.3.3 Comparison of ACW, unit stream power and sediment input from landslides

River Abuan

Changes in ACW demonstrate that the mean channel width was 7.8 m greater after Typhoon Lawin and also experienced a wider range of width values, difference of 117 m compared to 138.5 m before and after the event respectively (Figure 3.9). Despite increases in channel width statistics following the typhoon event, sections of the channel also narrow by a maximum of 15.8 m attributed to a 16.8% decrease in ACW.. Despite this, on average the channel increased by 7.8 m causing an 11.1% increase in ACW. Topographic and ACW statistics have been assessed alongside changes in landslide sediment flux and stream power to better understand the influence of sediment cascades on changes in channel geomorphology (Figure 3.9, 3.11 and Table 3.4). Along numerous sections of the River Abuan there is no contribution of landslide sediment flux, however where landslide density is greatest the river experiences peak landslide sediment flux of 117762 m³, receiving an average of 18980 m³. As for unit stream power, this varies considerably downstream reaching a peak of 2189.4 W/m with a range of 2025.5 W/m across the River Abuan.

To spatially assess the influence of sediment cascades on channel geomorphology, changes in ACW, unit stream power and landslide sediment flux along the River Abuan have been graphically presented together for comparison in Figure 3.9 and Table 3.5. Greatest channel widening following Typhoon Lawin of 45.0% is experienced 8 km downstream. Along this section, the River Abuan experiences both high unit stream power of 708 W/m and high sediment input from landslides of 77,448.2 m³. Large changes in ACW are

however not always attributed to combination of both high stream power and sediment input. Along the midcourse of the river no landslides occur within a 500 m² radius and therefore channel widening is solely attributed to high stream power ranging from 623.6 W/m to 1035.4 W/m. Although stream power remains high along the course of the river, when sediment input contribution is at its highest peaking at 114475.8 m³, stream power is comparatively low. Overall the relationship between changes in ACW, stream power and sediment input from landslides cannot be clearly defined from results presented in Figure 3.9. Therefore modelling of the selected study site will inform a better understanding of the role of stream power and sediment input from landslides in driving changes in channel geomorphology following a typhoon event.

Table 3.5: Derived stream power, sediment contribution and active channel statistics along the River Abuan

	Mean	Std Dev	Min	Max	Range
Unit Stream Power (W/m)					
Landslide sediment flux (m ³)	18980.0	30188.2	0.0	117762.0	117762.0
ACW _{pre} (m)	67.0	26.7	19.7	136.7	117.0
ACW _{post} (m)	74.8	32.8	26.0	164.6	138.5
Δ ACW (m)	7.8	11.0	-15.8	46.9	62.7
Δ ACW (%)	11.1	13.9	-16.5	44.9	61.4

Study Site for modelling with r.avaflow

To better understand the drivers of changes channel geomorphology following a typhoon event, the longitudinal patterns of unit stream power and landslide

sediment flux have been presented alongside changes in ACW (Figure 3.13).

The graphs illustrate that unit stream power is low along the length of the channel selected compared to the rest of the Abuan River network, increasing only marginally across the final kilometre. On the contrary, sediment input to the channel relatively high compared to the rest of the River Abuan. This is due to the density of landslides experienced within 500 m of the channel selected, which fluctuates only slightly downstream.

The greatest channel widening is calculated across the first kilometre channel, nearly doubling in width with an increase in ACW of 99.9%. Moving downstream, the second kilometre of the river experienced the lowest volume of landslide sediment flux decreasing to 37961.3 m³. Despite this the channel widened by 16.1 m widening attributed to a 69.9% increase in ACW, with unit stream power decreasing slightly to 765.6 W/m. Moving further downstream landslide sediment flux increases to a value similar to the upstream channel of 82743.2 m³ attributed to a 53.5% increase in ACW, whilst unit stream power decreased to 593.3 W/m. Along the final kilometre of river channel selected, landslide sediment flux further increased to 86208.6 m³, the greatest volume experienced across the study site selected. In addition, unit stream power also increased to the greatest value of 1070.8 W/m leading to an increase in ACW of 58.3%

Overall, the study site along one of the main tributary rivers to the River Abuan indicates an area of high channel widening with comparatively low unit stream power. This suggests there is an additional factor driving changes in ACW. A high frequency and magnitude of landslides can be found in close proximity to the river across this study site (Figure 3.8) and therefore this area experiences

comparatively high landslide sediment flux input. The patterns are however spatially variable and no clear relationship between landslide sediment input, unit stream power and ACW can be identified. This justifies the use of a multi-phase model to better understand the relationship between landslide sediment input and observed widening.

3.4 r.avaflow model outputs

3.4.1 Topographic changes in channel geomorphology modelled following Typhoon Lawin

This section will focus on the modelled outputs run using r.avaflow, including changes in the topography and sediment delivery to the channel simulated in response to Typhoon Lawin. Figure 3.14 depicts topographic change after completion of the simulation run for 1000 s with baseline parameters (Table 2.4). Erosion occurs widely across the study area with greatest depths found predominately in landslide scours and runouts as well as incisions along the channel. Visual depiction indicates a greater proportion of erosion (in scales of red) compared to deposition (in scales of blue) upstream of the channel selected with high levels of erosion along the first two tributaries to the main channel. Erosion, reaching depths up to -2.4 m, tends to occur on the outside of meanders and follows a decreasing trend moving downstream. Contrastingly, from ~2 km downstream deposition acts as the dominant process reaching depths of up to 19.2 m at the downstream confluence. Contrastingly to the upstream tributaries, a high amount of deposition is modelled along the final tributary of the study site. Deposition tends to coincide with a higher density of contributing landslides and therefore sediment input as well as with the inside of meanders.

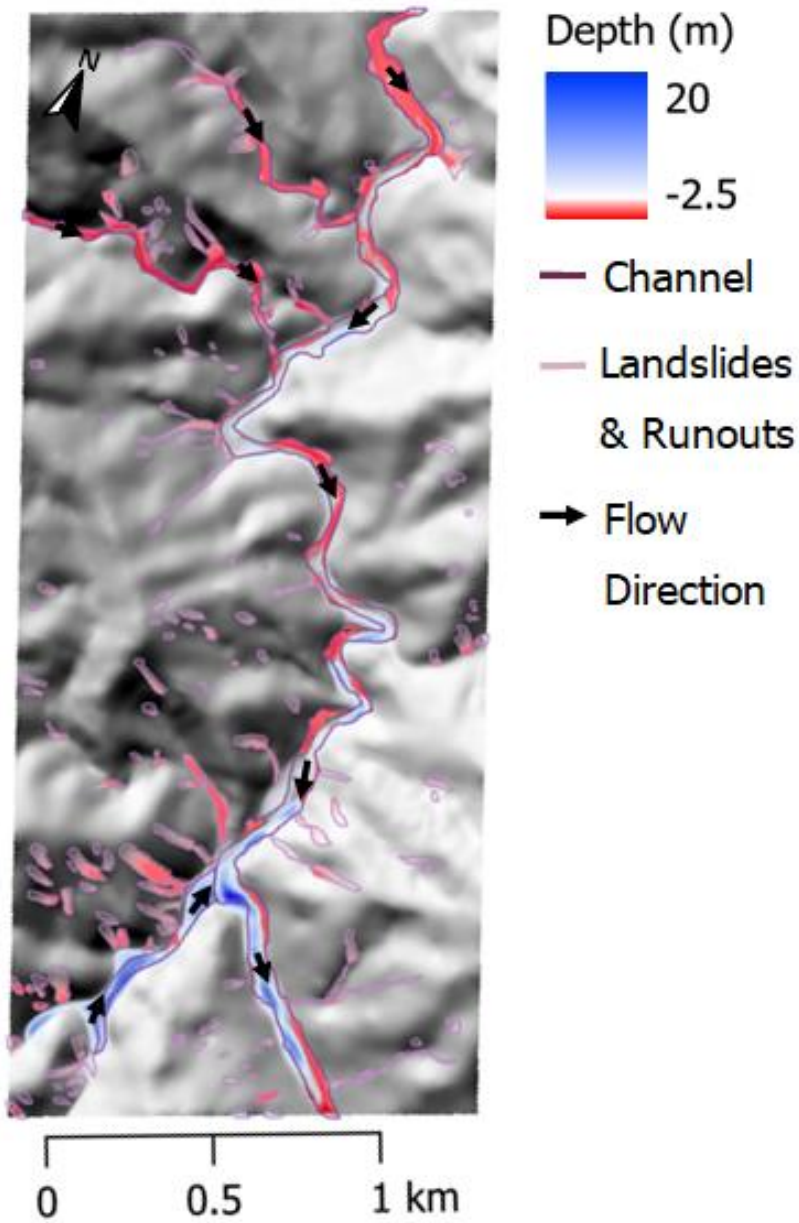


Figure 3.14: Topographic change of the study site following Typhoon Lawin modelled using *r.avaflow* using baseline parameters (Test 1) projected onto the pre-event 2013 DEM.

3.4.2 Comparison of modelled to observed changes in ACW

To compare lateral channel changes modelled compared to observed, transect lines have been delineated every ~150 m along the main channel as seen in Figure 3.15. Observed channel widths ranged from between 28.1 m to 73.6 m compared to 28.6 m to 80.5 m for the modelled channel (Figure 3.16). The greatest difference exists ~3300 m downstream at the greatest observed channel widening where the modelled channel is 6.9 m wider. On average across all transect sites, the modelled channel is 1.7 m wider than the delineated channel from satellite imagery following Typhoon Lawin. Differences between the modelled and observed channel widths vary from by 12.17 m with underestimation greatest ~2850 m downstream at -3.6 m. The modelled channel is shown to predominately overestimate the width of the channel, with only a third of the widths found to be narrower than the observed channel.

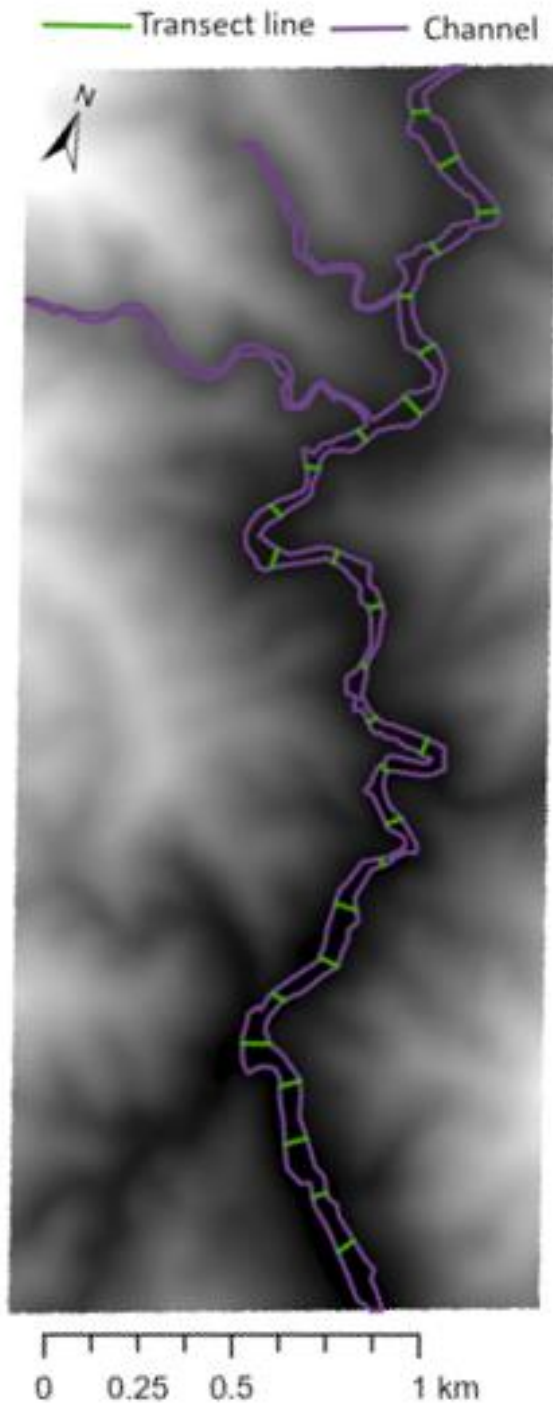


Figure 3.15: Location of transect lines (green) located every ~150 m downstream along the main channel modelled (purple) which overlays the pre-event DEM.

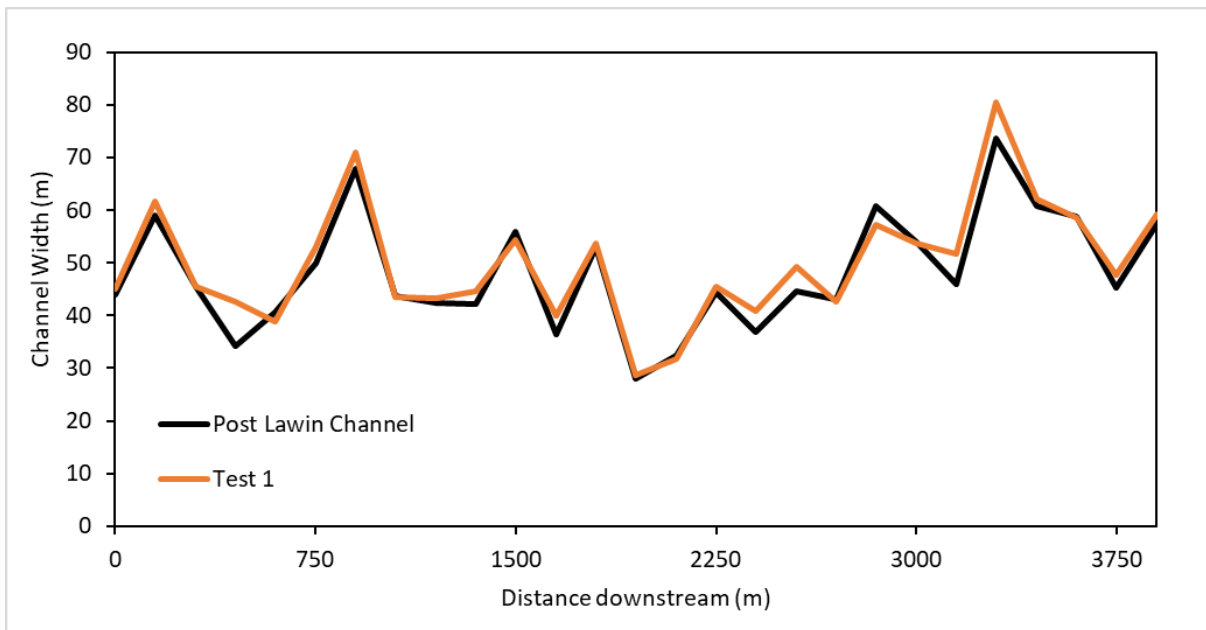


Figure 3.16: Modelled changes in channel width measured along specified transects downstream for the baseline scenario (Test 1) compared to observed changes in the channel following Typhoon Lawin.

3.4.3 Changes in sediment depth and velocity between different phases over time

The contribution of solid and fine-solid sediment varies from both each other and over time, shown in Figure 3.17. Focusing on solid sediment, contributions are found to increase over time with greatest depths observed at P4 found furthest downstream, reaching a maximum depth of 49 m. Initial depths of solid sediment contribution are next greatest at P1, 0.7 m 70 s into the simulation. This however changes 100 s later where solid contributions at P3 increase at a greater rate and therefore surpass contributions made at P1. Throughout the simulation solid sediment contributions are lowest at P2 which reach a maximum by the end of the simulation of 0.5 m, whereby peak velocity is shifted rightwards and later in the simulation compared to other observation points.

The pattern of fine-solid sediment contribution is more varied over time and are of a greater magnitude compared to solid sediment (Figure 3.17). Initial contributions across the first three observation points start low and remain relatively stable for the first 300 s, after which patterns vary from one another over time. Contributions at P3 increase the most reaching its first peak of 4.9 m 420 s into the simulation, before decreasing and increasing again to a maximum depth of 5 m by the end. Contrastingly, at both P1 and P2 depth contributions remain comparatively low and more stable reaching peaks of 1.0 m and 1.2 m respectively. The starkest difference can be observed at P4 which experiences a sharp increase to 6.0 m from 80-160 s in fine-solid sediment depth after a smaller initial peak. Sediment contributions at P4 are considerably higher than the other observation points, reaching a final peak of 13.7 m after 900 s before falling to similar depth as P3 by the end of the simulation. Total depth over time trends follow a similar pattern to fine-solid contributions, but with an increased depth as a result of the increased solid sediment contributions. Therefore, total depth reaches a maximum of 1.6 m, 1.8 m, 6.2 m and 17.4 m for P1-4 respectively at different time intervals across the simulation.

Figure 3.17 shows the solid depth (left) and average velocity (right) for solid, fine-solid and total solid phases. The plotting effectively represents the amount of sediment (its depth and its velocity) at given points of interest P1-P4 along the channel of river (Figure 2.3). The pattern of changes in velocity over the simulated time period of each sediment contribution phase varies significantly compared to sediment depth. For both solid and fine-solid sediment, and consequently total sediment, velocity is initially high, but fluctuates over the first 200 s. For P1, the pattern of sediment contribution is comparable for both solid and fine-solid, however peak average velocity occurring after 20 s is 2.3 ms^{-1}

higher for fine-solid compared to solid. Similarly, to P1, at P4 initial patterns of changes in average velocity are similar for both phases. In contrast, peak solid phase velocity is greater than fine-solid phase velocity by 2.3 ms^{-1} only 10 s into the simulation. In addition, further differences can be observed after a fall in velocity after 60 s. Solid phase average velocity remains low despite slight fluctuations, whereas average fine-solid phase velocity increases slightly before rapidly increasing to 2.7 ms^{-1} by the end, surpassing all other observation points.

Initial observations made for P1 can also be attributed to P3, with multiple spikes peaking at 2.7m and 4.2 m for solid and fine-solid phases. As time progresses, trends then follow a more similar pattern to P4 as average solid phase velocity remains low and stable over time whereas for the fine-solid phase, values fluctuate demonstrating further increases and decreases over time. It can be observed that when sediment decreases, velocity also decreases. Finally, at P2 little variation can be observed in the pattern of average velocity between the two phases over time. This being said, peak velocity occurs sooner after 30 s at 6.9 ms^{-1} for fine-solid compared to 5.3 ms^{-1} 680 s later for the solid phase. When considering the overall sediment contribution, P4 experiences the highest average velocity just 10 s into the simulation of 18.5 ms^{-1} . This is closely followed by P1 with an average velocity 18 ms^{-1} 10 s later. As P1 is upstream of P4 and its peak occurs afterwards, this suggests that peak velocity observed is independent of each other.

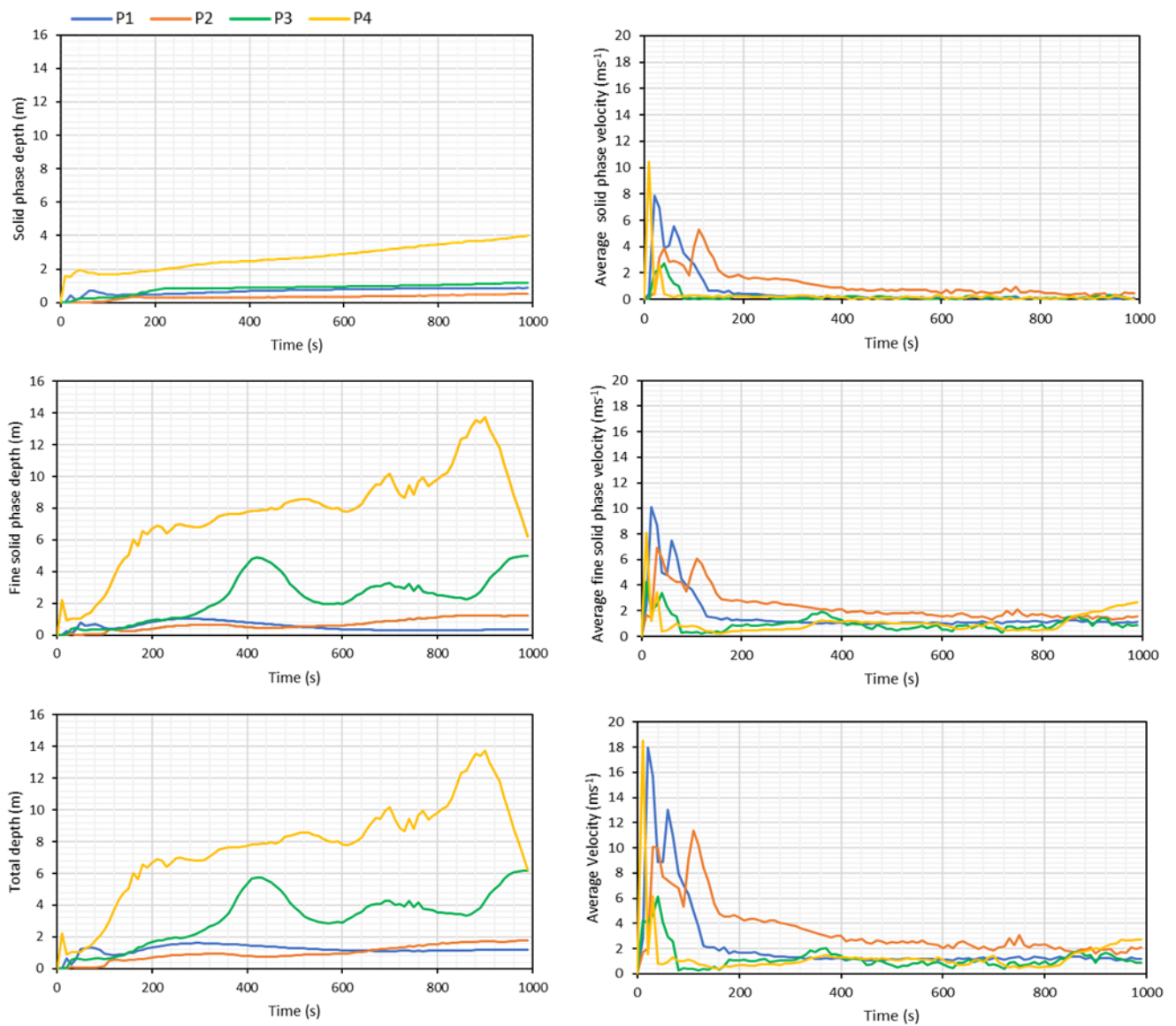


Figure 3.17: Elevation and average velocity of solid, fine-solid and total sediment contributions at observed points along channel modelled.

3.4.4 Assessment of the inclusion of landslides

Test 0 has been run with no sediment input from landslides. Figure 3.18 visualises topographic changes across the study area which contrast results presented with landslide sediment input (Test 1). The depth of erosion peaks at -1.7 m which is 0.7 m lower compared to Test 1 and varies more considerably for deposition which is 17.0 m shallower at 2.3 m. Overall, topographic channel change is of a lesser magnitude for Test 0 compared to Test 1 and extends over a smaller area of the study site.

As well as differences in the topographic changes, discrepancies exist in changes in lateral channel change compared to Test 1 and observed channel can be seen in Figure 3.190. Channel width ranges from 15.8 m to 67 m demonstrating that the changes in lateral migration of modelled channel without landslides are smaller than that observed. Contrastingly to Test 1, Test 0 largely underestimates the width of the channel, with just over 25% of the transects overestimating lateral channel migration. Greatest difference is observed upstream of the main channel, with a modelled with 35.9 m narrower than that observed. Overall, without the inclusion of landslides, modelled changes in channel poorly reflect the observed channel due to large over and underestimations.

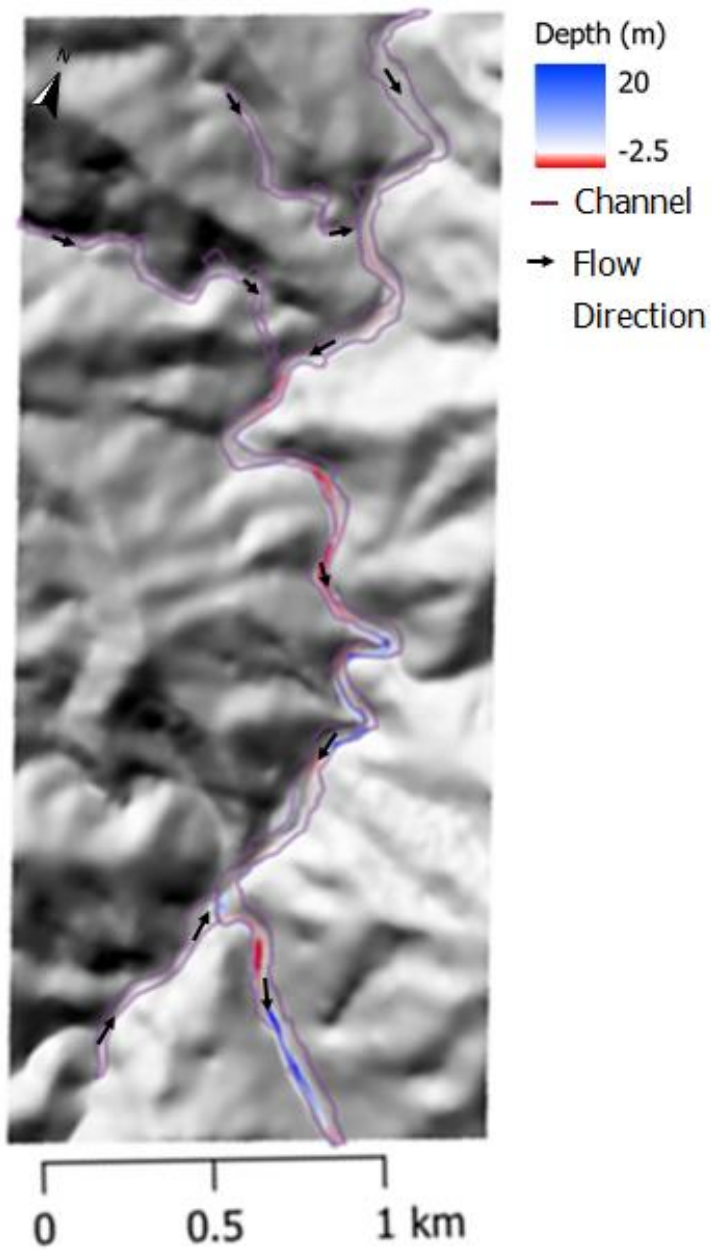


Figure 3.18: Topographic change of the study site following modelled using r.avaflow without the input of landslides and runouts (Test 0) projected onto the pre-event 2013 DEM.

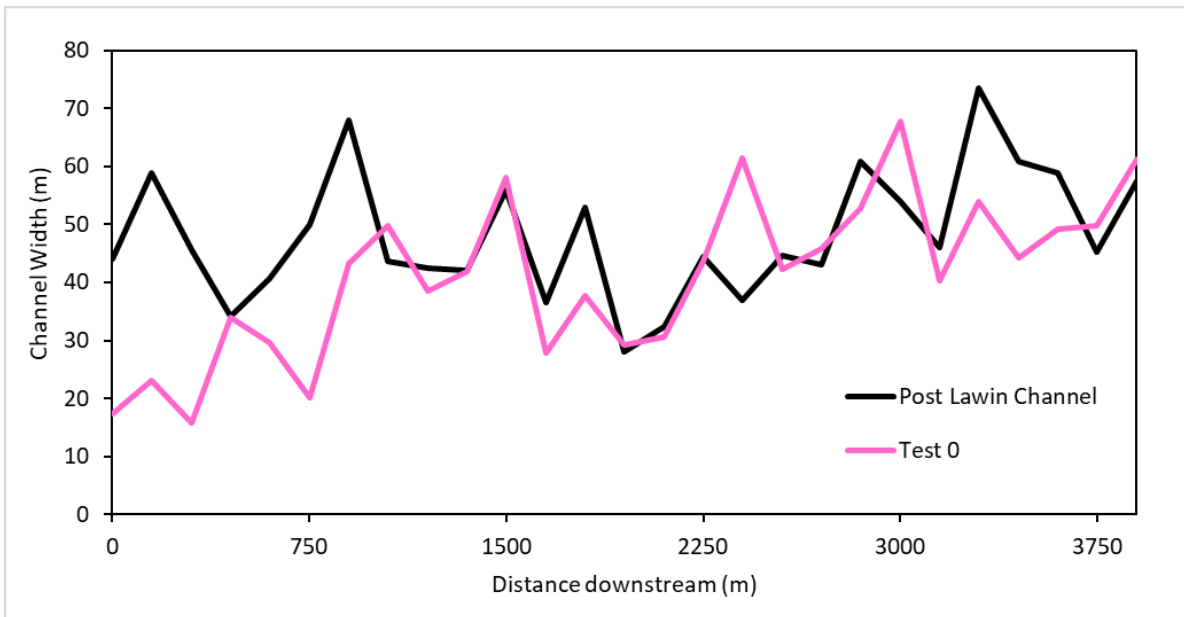


Figure 3.19: Modelled changes in channel width measured along specified transects downstream for Test 0 compared to measurements of observed channel change following Typhoon Lawin.

3.4.5 Sensitivity Analysis

To assess the impact of adjustments made from different model inputs, a sensitivity analysis has been conducted (Table 2.4). Model outputs are presented and compared to Test 1 in Figure 3.20 and Table 3.6 (Appendix D). Test 2 analyses a greater weighting of solid to fine-solid sediment (55:45) input to assess the suitability of adopting the ratio used by Panici et al. (in review) on a different region of the Philippines. Test 2 results in similar topographic changes to Test 1, however depths of deposition are lower along the downstream tributary. Erosion peaks at the same value of -2.4 m and deposition is slightly higher at 19.3 m found once again at the downstream confluence. Greater differences can be observed in the ACW of this modelled channel as the channel varies in width between 31.2 m and 77.1 m, a range 8.1 m smaller than Test 1 (Figure 3.21). Changes in the ratio of solid to fine-solid sediment also predominately overestimate channel widening, reaching a maximum

difference of 13.4 m compared to the observed channel. The Test 2 model simulation also underestimates the channel by a greater amount than Test 1. For example, 3900 m downstream the modelled channel is 16.8 m narrower than that observed compared to a difference of 1.9 m for Test 1 at the same transect location.

Next, the model was run only including the solid phase (Test 3) to assess the importance of using a multi-phase model (Test 1). Differences can be visually interpreted from Figure 3.20, with erosion on the outside of meanders decreasing in the upper and middle course of the section of channel selected. In addition, the height of deposition decreases to a maximum of 10.4 m whilst the depth of erosion also decreases by 0.3 m compared to Test 1. As with Test 2, greater differences can be observed in the modelled changes in lateral channel migration with widths ranging from 30.9 m to 78.5 m (Figure 3.21). Test 3 on average overestimates the channel width by 5.8 which is the greatest overestimation of all sensitivity test scenarios indicating a more erosive channel when run including only the solid phase.

Additionally, the friction coefficient was changed in Test 4 to investigate the suitability of using default internal friction as also assessed by Panici et al. (in review). This caused a slight increase in the depth of deposition compared to Test 1 with a maximum value of 19.6 m compared to a smaller amount of erosion at -2.1 m (Figure 3.20). The spatial distribution of areas of high deposition and erosion however remain similar to Test 1, with most change occurring downstream. Once again greater differences are observed in the modelled changes in ACW with greatest underestimation of -16 m and overestimation of 37.8 m, 3900 m and 1950 m downstream respectively.

Despite a similar range compared to other tests of width between 30.8 m to 79.5 m, Test 4 presents an average overestimation of 5.2 m when compared to Test 1.

Finally, Test 5 assessed the impact of changes in depth of entrainment by increasing the maximum entrainable depth of both the solid and fine-solid component by 50% to evaluate the suitability of using the empirical formula used to derive depth measurements. This caused both the maximum erosion and deposition experienced along the channel to decrease by 0.3 m and 8.9 m respectively compared to Test 1 (Figure 3.20). The spatial pattern of channel change also varies with less erosion on the meandering sections of channel and decreased depths of deposition moving downstream and along the final tributary. Changes in ACW along the transects demonstrate a similar range to all other test runs of between 30.8 m and 79.2 m (Figure 3.21). Similar to other sensitivity tests, a change in the model parameters here once again causes a greater difference between the width of the modelled and observed channel compared to Test 1. The channel is underestimated by a maximum of -16.8 m and overestimated by 22.0 m, averaging 4.6 m.

It can be concluded that changes in different model input parameters (Test 2-5), cause only slight changes in the amount and spatial variation of erosion and deposition modelled compared to baseline parameters (Test 1). Greatest differences can be observed when only the solid phase was included in the model (Test 3) followed by when changing the friction coefficient. Despite differences between the modelled widths, differences are small ranging between 2.9% and 5.3% (Table 3.6) and trends observed along the transects quantified follow a similar pattern to that of the observed channel (Figure 3.21).

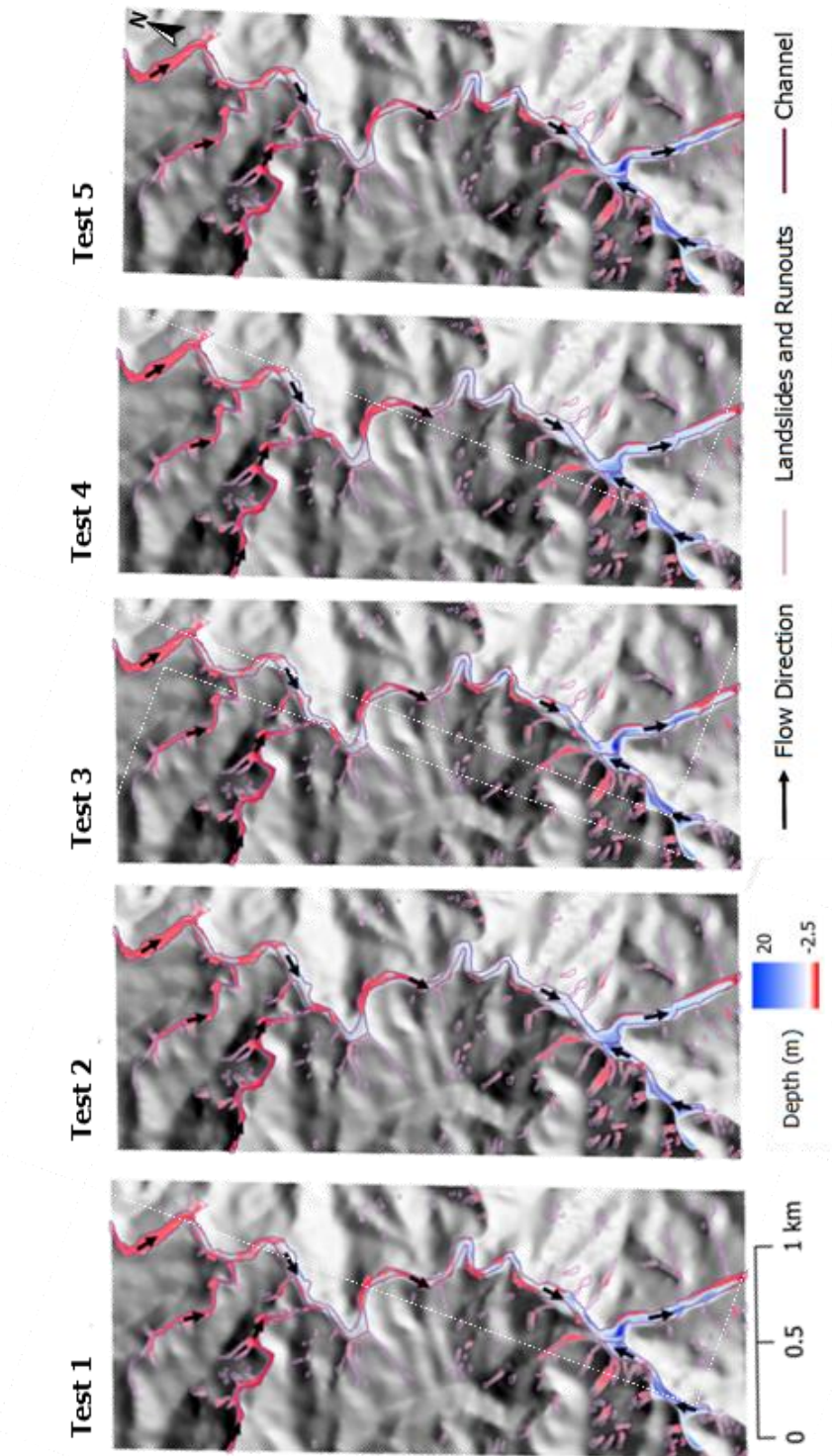


Figure 3.20: Sensitivity analysis of topographic change to alterations in model input parameters projected onto pre-event 2013 DEM: modelled change with base parameters (Test 1), change in ratio of solid: fine-solid sediment (Test 2), inclusion of solid phase only (Test 3), change in friction coefficient (Test 4) and 50% increase in depth of entrainment (Test 5).

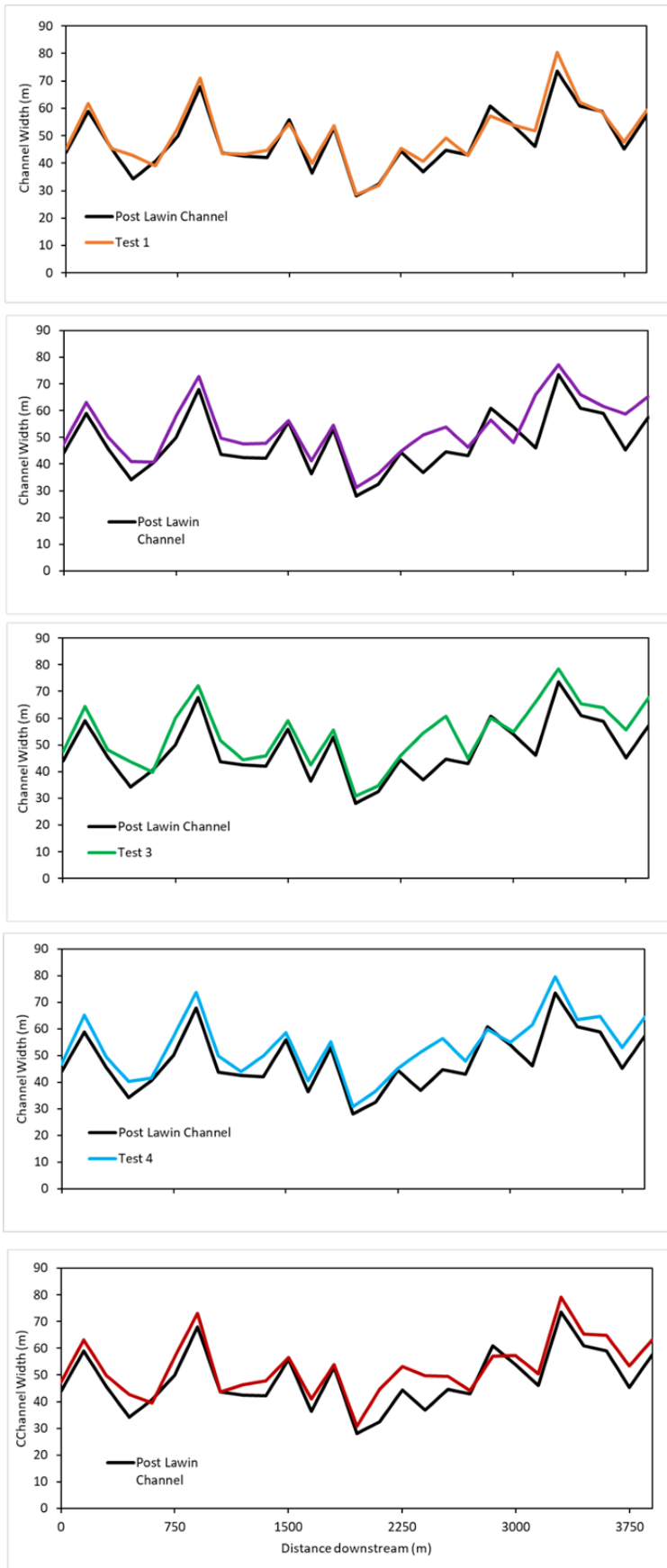


Figure 3.21: Modelled changes in channel width measured along specified transects downstream for comparing the baseline scenario (Test 1) to sensitivity analysis runs (Test 2-5) compared to measurements of observed channel change following Typhoon Lawin.

Table 3.6: Table of statistics comparing the changes in ACW between simulated channel change in Tests 1-5 to the observed channel change.

Compared to observed channel	Test 1	Test 2	Test 3	Test 4	Test 5
Δ ACW (m)	2.2	3.8	5.1	4.4	4.6
Δ ACW (%)	104.0	106.9	109.3	108.0	108.3

4. Discussion

4.1 Relative geomorphic impacts of Typhoons Lawin and Kammuri on Abuan catchment

4.1.1 Differences in landslide characteristics between typhoon events

Landslide inventories were created following each of the typhoon events identified enabling analysis of the size and magnitude of landslides (Lee and Evangelista, 2005). The ability to effectively quantify and assess the distribution of sediment helps to inform the relative influence of landslides on changes in channel geomorphology. Although landslides of a large magnitude are perceived to be more hazardous, landslides smaller in size occur more frequently. Understanding the relationship between frequency and size is an important factor in the analysis of overall landslide hazard imposed on the landscape (Malamud et al., 2004). Landslide occurrence and the ability to generate, transport and deposit sediment in response to a rainfall event varies between catchments (Glade, 2003). Therefore, a typhoon event inducing landslides of a greater magnitude may not always have as large an impact as small landslides of a higher frequency.

Although both landslide events studied were triggered by extreme rainfall, differences exist in the frequency and magnitude of landslides attributed to each event (Figure 3.1a). Landslides following Typhoon Lawin were considerably more frequent, with a greater landslide density of close to double that triggered by Typhoon Kammuri (Figure 3.3). In contrast, landslides were of a greater magnitude following Typhoon Kammuri (Figure 3.1a and Table 3.1). As a result, the volume of landslides calculated attributed to Typhoon Lawin is less, with individual landslides averaging 1499.8 m³ smaller in volume than landslides

following Typhoon Kammuri (Table 3.1). Greater contrast can be observed between the total volume of landslides between each typhoon event, with Typhoon Kammuri mobilising ~24,000,000 m³ more sediment from hillslopes. From reports provided during and shortly following each typhoon event studied (Larsen et al., 2010, NDRRMC, 2016, NDRRMC, 2017, NDRRMC, 2020), despite greater geomorphic change following Typhoon Kammuri, effects of Typhoon Lawin caused more devastating human consequences. This is due to the fact, Typhoon Lawin, also made landfall in Hong Kong as well as Macau as a tropical depression (NDRRMC, 2020), therefore affected other nations as well as the Philippines. This suspended international flights and further delayed international aid which was late in being requested. In addition, roads and bridges were obstructed by debris, uprooted trees and floodwater, further hindering the transport of aid to those affected (Sargeant et al., 2020).

When comparing the power law magnitude frequency distribution (Figure 3.2), the likelihood of a large hazardous landslide increases between these typhoon events. This is due to the power law exponent decreasing slightly by 0.26 between events, with an exponent of 2.96 in Typhoon Lawin and 2.7 in Typhoon Kammuri. Following both events, the exponent is however higher than reported in the literature. An assessment of debris flows across numerous locations found the power law exponent to be between 1.93 (Malamud et al., 2004) and 2.44 (Stark and Hovius, 2001). It is however more consistent with Abancó et al. (2020) who reported on landslides triggered by the 2018 Typhoon Mangkhut in the Philippines with a power-law exponent of 2.65. This indicates that deep and large failures are less common in the Philippines compared to other geographic locations. The higher exponent can be explained by geology and soil type which indicates a soft geology in the Abuan River catchment prone to less frequent

large landslides compared to areas of harder geology reported. This validates the investigation into shallow debris flows which are characteristic of the Philippines and study area selected. To improve estimations of the frequency and magnitude of potential future landslides, further mapping across larger extents would help to refine distributions and power law exponents for the Philippines.

4.2 Landslide contribution to lateral channel change during typhoon events

Patterns of change in ACW across the Abuan River network (Figure 3.8 and Tables 3.2- 3.3), demonstrate that geomorphic changes are not spatially uniform and are in fact highly variable moving downstream (Figures 3.90 and 3.10). In various places, active channel width has narrowed in the years following Typhoon Lawin due to revegetation of the floodplain. It is difficult to distinguish whether channel narrowing is actual or apparent. Uncertainty must however be considered of ± 5 m and the narrowing between events may be apparent, attributed instead to the coarse resolution of satellite imagery or human error. Narrowing observed may also be actual due to physical processes acting across the channel network. One of the causes of channel narrowing is land use change. For example Liebault and Piegay (2000) investigated the cause of channel narrowing on the Piedmont Rivers, France during two distinct periods of channel narrowing. Geomorphological change was in response to recovery processes following widespread flooding in the area causing the destabilisation of channel margins. These were amplified by the afforestation of the floodplain and implementation of flood defences which reduced sediment delivery and encouraged vegetation growth on the embankments. As a result channel narrowing increased across the river channel network. Channels that were previously destabilised by the flood were re-established by human

accelerated vegetation growth. The River Abuan however did not experience such human-induced fluvial adjustment and therefore it is unlikely that this is the cause of narrowing observed in sections of the river network. The Abuan River catchment is however forested and experiences high recovery rates (Yap et al., 2016). Therefore despite the lack of human influence, the fast recovery and growth rates may have led to the re-establishment of vegetation along the embankments. This will aid in restabilising and narrowing channels following the disturbance of the typhoon event.

In addition, as these are bedrock reaches it may be due to incision of the channel. With increased flow and shear stress exceeding the critical erosion threshold, downcutting may initiate in the thalweg which creates a narrower channel (Whittaker et al., 2007). This process enhances maximum stream power, increasing rates of incision to maximise the erosional potential. This reduces changes in lateral channel migration often creating a narrower and less meandering channel (Huang et al., 2014). Human induced change, such as the building of levees to constrain and direct the channel, can also lead to further incising and therefore the narrowing of the channel. In the Abuan River catchment these have not been imposed. Based on that modelled and high levels of deposition simulated, as opposed to erosion theorised here, it cannot be confirmed that this process has resulted in the narrowing observed. Further investigation is required as to whether the narrowing observed is actual or apparent and the conduction of fieldwork to understand the geology would aid in this.

4.2.1 Stream power and changes in ACW

In previous research, when investigating changes in geomorphology following an extreme weather event, ACW has been used as a quantifiable and evolving parameter to gain a better understanding of processes acting along the river at large scales (Wobus et al., 2006). This is most commonly compared to changes in stream power downstream as indicates the ability of a river to mobilise and transport sediment. Stream power is used to assess channel stability and indicates the rivers capacity to drive processes causing geomorphic change (Bagnold, 1960, Bizzi and Lerner, 2015). As Typhoon Kammuri has a lower associated confidence in ACW due to higher cloud cover in satellite images available, stream power analysis was only conducted for Typhoon Lawin (Figure 3.12).

Greater change in ACW following Typhoon Lawin compared to Typhoon Kammuri may be attributed to differences in the reported rainfall with Typhoon Lawin receiving a greater total and higher intensity compared to Typhoon Kammuri (NASA, 2019, Observatory, 2016). This being said, as these are both extreme weather events, associated rainfall is high across all of the catchment compared to prior conditions (Figure 2.1). This results in high fluvial erosional power (ie stream power) across the River Abuan channel network, a contributing driving force of differences in lateral channel change observed. Greater widening occurred in the west of the catchment following Typhoon Lawin (Figure 3.8), despite low total stream power and slightly lower discharge compared to the rest of the river network (Figures 3.11 and 3.12). This may be attributed to differences in typhoon trajectories, however this goes beyond the scope of this research and without further investigation cannot be directly

inferred. Instead, the resulting research focused on exploring the connection between landslides and channel widening in Typhoon Lawin.

Across the River Abuan network, total stream power calculated fluctuates, however is overall high averaging at 46824.3 W/m (Table 3.5). Therefore, to understand processes driving channel geomorphology in the catchment, the River Abuan has been analysed in greater detail. Assessment has been conducted to compare the changes in ACW compared to calculated patterns of unit stream power as opposed to total stream power to allow for a more detailed analysis. Figure 3.9 demonstrates that upstream, despite a high percentage increase in ACW, unit stream power is relatively low compared to higher values observed in the mid-course of the river, peaking a further 25 km downstream. Widening of ACW may therefore not be attributed to peaks of high unit stream power suggesting there is an alternate factor driving changes in channel geomorphology.

4.2.2 Influence of landslides on changes in ACW

Patterns of landslide density observed follow a similar spatial pattern (Figure 3.3) to the sections of greater change in ACW attributed to each typhoon event. Processes driving change in ACW may therefore be attributed to the occurrence of landslides and consequent landslide sediment fluxes following a typhoon event. Over time geomorphologists have begun to understand the concept of sediment connectivity linking sediment source areas to sinks which contributes to changes in channel geomorphology across catchments (Brierley, 2010, Croke et al., 2005, Fryirs et al., 2007, Wainwright et al., 2011). To explore this, the input landslide sediment fluxes from within a 500m radius of the River Abuan channel have also been compared alongside changes in ACW and unit

stream power in Figure 3.9. When greatest ACW widening occurs, as aforementioned unit stream power is relatively low, however landslide sediment flux contribution to the channel is comparatively high. This being said, this relationship does not always hold true. Further downstream along the River Abuan, 1 km sections of channel with a high percentage change in ACW experience no landslide sediment flux contribution due to a lack of landslide occurrence whilst unit stream power reaches a maximum of 97,674.1 W/m.

Following a landslide, the proportion of sediment generated depends on the location, size of the scour and nature of the geology (Page et al., 1999).

Sediment supplied is also a reflection of the topographic and geologic properties of the mountain basin (Hovius et al., 1997). Landslides found near riverbanks are more likely to input a larger amount of sediment than landslides that occur at a lesser proximity to channels (Page et al., 1999). Landslides following Typhoon Lawin are concentrated on riverbanks with a high landslide density along the mid-course of the Abuan River and along tributary rivers (Figure 3.1). In comparison, landslides following Typhoon Kammuri are more densely populated in the upper course of the River Abuan with a lesser density of landslides occurring in close proximity to tributary rivers (Figure 3.1). This provides an explanation as to the greater percentage of channel widening observed following Typhoon Lawin compared to Typhoon Kammuri (Figures 3.9 and 3.10).

Therefore, the role of landslides in close proximity to river channels and consequent sediment cascades has a localised impact on changes to channel geomorphology. An important aspect of large landslides is their effect on the valley floor and riverbank morphology altering the long profile of a river.

Mobilised landslide sediment has the ability to scour the channel causing over deepening and widening of the channel. The erosional potential is great enough to alter the relief of the channel and even create stepped profiles (Korup, 2010). This research focuses on active channel width as without a DEM following the event, changes in the long profile of the river cannot be quantified and therefore am unable to fully validate modelled outputs. This presents an area of potential further research to investigate the effects of landslide events on the evolution of the long profile of river networks.

In addition to the erosional potential of landslide sediment input, large amounts of excavated debris carried in suspension may be deposited. This occurs when drag exceeds shear stress decreasing the flow velocity which interrupts fluvial bedrock incision (Shang et al. 2003). Landslide events have the ability to dramatically alter river dynamics leading to a more dynamic equilibrium in landform evolution processes rates. The natural equilibrium of the river is consequently dramatically altered through the abrupt introduction of landslide sediment (Korup, 2009). In addition, large sediment deposits also have the ability to create landslide dams which limit fluvial transport causing large aggradation upstream which inhibits incision into the bedrock. Changes are therefore not uniformed downstream and only when the dam fails can the accumulated sediment be transported further downstream. Consequently it can be inferred that landslides have a localised effect. The geomorphic efficiency to cause changes in ACW is dependent on the rate at which sediment is produced and transported to the channel based on the magnitude and frequency of the event (Korup, 2009).

A study site was selected along a major tributary river to the River Abuan to allow for further investigation into the role of landslide sediment cascades on driving lateral channel change (Figure 1.8). As seen via the magnified view of the study site in Figure 3.13, despite channel widening consistently greater than 50%, unit stream power calculated was relatively low compared to the rest of the channel network (Figure 3.13). The study site stretches over ~4 km selected as a suitable reach to model the effect of landslide sediment fluxes on changes in channel geomorphology following a typhoon event.

4.3 Effectiveness of r.avaflow to simulate the effects of typhoon induced landslides on channel geomorphology

4.3.1 Modelled with the inclusion of landslides and runouts

Manual mapping and comparison to changes in ACW as well as stream power, indicates there are additional processes driving changes in channel geomorphology. Results presented are similar to previous studies investigating the relationship between landslides and channel widening by Bennett et al. (submitted) and Panici et al. (in review). Findings in this research supports the prevalence of sediment delivered as a result of landslides to be a key driver of observed changes in channel geomorphology. Investigation demonstrates that hydraulic variables alone cannot fully explain changes observed, whereby changes in stream power do not always directly correlate with channel widening observed.

Simulated channel extents delineated from outputs of topographic change modelled within baseline parameters using r.avaflow (Figure 3.14) show the greatest consistency with that manually delineated from satellite imagery following Typhoon Lawin (Figure 3.16). Although the majority of the channel

was accurately simulated, small differences occur and therefore computational outputs do not fully capture observations made. Despite these localised discrepancies, this simulation has been presented as the best scenario to understand topographic changes across the study site following Typhoon Lawin with the current data available with only slight over and under estimations of ACW.

Modelled results along the study site support the correlation between sediment input and channel widening. Along the majority of the study site selected for modelling, results support that of Panici et al. (in review) that sediment delivery from landslides correlates to channel widening. Erosion dominated upstream of the section of river modelled and was found to be of a greater depth than recorded by Panici et al. (in review) in the neighbouring region of the Philippines (Figure 1.7). Solid and fine-solid phase contributions are modelled to be of a greater depth by the end of the simulation (Figure 3.17). There is an inverse relationship between all of the points of interest such that once velocity has slowed down, depth will increase. This indicates an initial impulsive flow which then slows down to become deeper over time. Increased sediment in conjunction with decreased velocity has resulted in the high levels of deposition modelled downstream (Figure 3.14), as the flow is unable to transport sediment in suspension. The solid phase depth contribution is found to be similar, yet more stable over time than in the Upper Agno catchment of the Liang River modelled by Panici et al. (in review). Greater depths of erosion experienced may be as a result of differences in the hydraulic forcings or geology. With low bank stability the shear stress of debris floods is greater than the cohesive strength of the soil and therefore lateral erosion occurs causing channel widening observed (Pitlick et al., 2013). With a lack of DEM following the event

it is not possible to validate the depths simulated. Therefore, without the ability to further investigate the geology of the Abuan River, differences in geology can only be hypothesised as the reasoning for the differences in depths of erosion simulated between these studies.

In contrast to Panici et al. (in review), across this section of the Abuan River catchment modelled, widening of the channel is predominantly attributed to deposition as opposed to erosion within the Upper Agno catchment of the Liang River (Figure 1.7). Moving downstream, deposition is modelled to increasingly drive changes in ACW. Any erosion simulated is of a shallower depth and is predominantly found on the outside of meanders (Figure 3.14) which follows a similar spatial pattern to the findings of Panici et al. (in review). Greater deposition is linked to the lower velocities experienced downstream as are not high enough to transport sediment in suspension. Deposition of landslide sediment between the observation points on the banks drives lateral channel migration. Sediment deposition depth of each phase varies over time and spatially. Sediment is contributed from multiple different landslides at varying proximities to the channel. Therefore, although these are all modelled to be released at the same time, for each individual landslide the time taken for sediment to reach the channel varies considerably. Landslides are unlikely to interact with each other, as can be inferred from Figure 3.17. It can be deduced that the high levels of deposition modelled and sediment pulses are of a direct consequence of local landslide sediment input as sediment flow is not feeding on from P3 to P4, hence the lowered velocities (Figure 3.17). P4 has the greatest total sediment depth modelled which occurs later on in the simulation. This may have been caused as a result of different processes, such as reduced channel gradient due to deposition further upstream causing potential bulking or

backing up of sediment and water flow. The downstream observation point (P4) experiences the greatest flow velocity of all the observation points. The extensive deposition upstream will temporarily reduce the sediment load of the flow increasing the velocity of the river (Hancock et al., 1998). The higher velocity of the water increases the erosional potential, which in conjunction with destabilised embankments from landslide occurrence leads to the erosion simulated at the end of the study site (Figure 3.14). Without the ability to conduct fieldwork and the lack of DEM following the event, it is difficult to distinguish the exact processes causing the observed channel change, however this provides a potential explanation. Despite these more conclusive findings of the role of landslide sediment in channel widening, high channel widening can also be observed when sediment contributions are at their lowest along the channel modelled (Figure 3.13). Unit stream power is also observed to be high, however remains comparatively low to that experienced across the River Abuan network. Therefore as with Panici et al. (in review), the relationship between landslides and channel change is not as clear as the conclusive findings of Bennett et al. (2017). It can be understood from this study that landslide sediment is a contributing factor to changes in channel geomorphology. The effect is however localised such that changes in channel geomorphology may be attributed to both erosion and deposition along the river network.

These findings provide an additional step along previous studies to improve understanding. The role of sediment is increasingly being studied and a recent study by Brenna et al. (2023) who investigates the drivers of channel widening in mountain basins. Similarly to this investigation, channel widening observed from analysis of satellite imagery across the Cordevole River catchment in the Dolomites, Italy could not be fully explained by stream power. With greater data

availability and higher accessibility for fieldwork, Brenna et al. (2023) assessed the degree of channel confinement and channel width ratios from before to after the event. As found in the Abuan River catchment, sediment in debris floods acts as a driver of lateral channel change. Although sediment was found to promote intense widening during extreme weather events, similarly to this investigation, cascades do not always cause major geomorphologic changes. This area of research is still in its infancy. Continued investigation is required into new locations and across different scales to further understand the controls of geomorphic processes in mountainous catchments following extreme weather events.

4.3.2 Simulations without the inclusion of landslides

Whilst results presented using baseline parameters indicate that sediment acts as a driver of lateral channel change, inconsistencies exist and therefore the relationship cannot be clearly defined. To better understand the impact of landslide sediment on changes in ACW, a model test run was simulated without the inclusion of landslides and runouts (Figure 3.18). If changes in ACW observed could be modelled without the presence of landslides, it could therefore be inferred that landslide sediment input is not a driving factor of geomorphological change following a typhoon event.

Without landslides, the topographic change of modelled channel extents is not quantitatively comparable to post-event delineated channel widths (Figure 3.19). It can be inferred from this that fluvial processes of both erosion and deposition contribute to changes in ACW observed. It is evident that following Typhoon Lawin, heavy rainfall and subsequent increased channel conveyance drives changes in ACW (Figures 3.6 and 3.7). Fluvial processes alone cannot

however fully account for the channel changes observed and this therefore confirms the role of landslide sediment. Similarly to Brenna et al. (2023), in areas of ordinary flood water flow the channel widening was considerably smaller, by at least 2 to 3 orders of magnitude.

When modelled with landslides, changes in ACW along the channel are more accurately simulated with only slight under or predominantly overestimations. Therefore, results presented in Figure 3.18, support the findings of Bennett et al. (2017) that there is a relationship between landslide occurrence and observed channel widening. Sediment delivery from landslides plays a vital role and therefore the alternate hypothesis can be accepted.

4.3.3 Sensitivity analysis

A sensitivity analysis has been conducted on the key parameters and inputs identified within r.avaflow to test the accuracy of the model outputs generated despite limited data availability. This will help to ensure that modelled outputs were not simulated by chance. All sensitivity scenario runs have been compared to the baseline scenario (Test 1), from which one parameter has been changed presented in Figure 3.20. The assessment of the robustness of the model is similar to Panici et al. (in review) (Figure 1.8), however differs slightly by testing some of the same as well as alternate parameters.

Test 2 demonstrates a change in the ratio between solid and fine-solid sediment, switching to a higher concentration of solid sediment rather than fine-solid modelled using the baseline parameters of Test 1 (Table 2.4). This parameter has been selected as fieldwork was unachievable for this research. Therefore analysis will help to validate the input sediment ratio selected which was based on a previous study by Panici et al. (in review) conducted in a

different region of the Philippines. Results demonstrate similar values maximum depths of both erosion and deposition found to have little spatial variance from Test 1 (Figure 3.20 and Table 3.6). Despite slight differences in the over and underestimation of changes in ACW modelled (Figure 3.21), overall changing the ratio of the sediment phases is found to have a small impact on overall results. Low parameter sensitivity validates the use of Panici et al. (in review) ratio of solid to fine-solid sediment input to model this study site.

The role of landslide sediment and differences in behaviour between solid and fine-solid sediment has been addressed within this research. To validate the incorporation of fine-solid, Test 3 investigates the changes to model outputs when only the solid component is considered as opposed to a multi-phase model. Results demonstrate notable differences in the depths of both erosion and deposition across the catchment (Figure 3.20). In addition, the modelled outputs demonstrate a greater over and underestimation compared to when run with baseline parameters of Test 1. It can be concluded that the combination of parameters in Test 3, only accounting for the solid phase, demonstrates a low consistency with the observed changes in lateral channel extent (Figure 3.21). Results presented support Panici et al. (in review) of high sensitivity (Table 3.6), validating the incorporation of the different sediment phases. This is critical to include within the model to effectively simulate the different behaviours and interactions between the viscous and non-viscous flow dynamics of each sediment phase.

Frictional parameters in Test 1 were based on the previous study by Panici et al. (in review). To assess the validity of using these values in a different region of the Philippines studied here, Test 4 demonstrates a simulation run with

default parameters set for r.avaflow (Mergili, 2014-2023). These values are all smaller than that modelled with the baseline parameters of Test 1 (Table 3.6). Values of topographic change modelled for both erosion and deposition are comparable to that modelled with the baseline parameters (Figure 3.20). In contrast, Test 4 presents a greater over and underestimation of changes in ACW compared to Test 1 (Figure 3.21). Overall results suggest that for this type of investigation, changes in the internal friction coefficient are negligible demonstrating moderate sensitivity in agreement with Panici et al. (in review).

Investigation by Panici et al. (in review.) into the sensitivity of model parameters, found that changes in entrainable depth had a relatively small impact on overall model results. To validate the use of this empirical formula, sensitivity analysis was conducted in hope of supporting previous findings in Test 5. Topographic changes modelled demonstrate a slight decrease in the depths of both erosion and deposition experienced (Figure 3.20) which results in both the further under and overestimation of the channel compared to Test 1 (Figure 3.21). Similarly to Panici et al. (in review), despite these differences, the simulated change in the maximum entrainable depth proved to be only somewhat sensitive. Despite the uncertainty associated with calculating landslide and runout depths using an empirical formula (Larsen et al., 2010) and estimations of entrainment depths, low sensitivity to this parameter validates depth values input.

Overall it can be concluded that there is consistency between sensitivity analysis tests and baseline test runs compared to changes in the post-typhoon channel observed. Spatial patterns of topographic change and consequent modelled channel widths follow the same trends across all test runs. Larger

discrepancies are only present when the model only accounts for the solid phase of sediment, highlighting the importance of using a multi-phase model (Table 3.6). Model sensitivity of adjustments in parameters that were also analysed by Panici et al. (in review) concluded comparable outcomes to that presented (Figure 1.8). Therefore, despite associated uncertainty, it can be concluded that baseline parameters selected are appropriate in modelling the impact of landslide sediment on changes in channel geomorphology following Typhoon Lawin.

4.4 Additional research considerations, limitations and improvements

4.4.1 Seasonal variability

Changes within ecosystems observed from satellite imagery over time can be considered as seasonal, gradual and abrupt changes (Verbesselt et al., 2010). Satellite imagery has long been used as a data source to remotely detect and assess changes in the land surface over time (Coppin et al., 2002). In order to analyse the impact of individual events, an appropriate time window between data sources must be obtained. For Typhoon Lawin, within the month time frame of the satellite imagery obtained (Table 2.1), no other extreme weather events have been recorded. Therefore, mapped landslides and delineated changes in channel width can be said to be triggered as a direct consequence of Typhoon Lawin with low associated uncertainty (Figure 3.1, blue). As for Typhoon Kammuri, due to data availability a greater time window of 5 months was analysed (Table 2.1). Once again, no further landslide events were recorded during this time frame. Therefore there is low associated uncertainty with landslides mapped by collaborators of the SCaRP project triggered by Typhoon Kammuri.

In assessing the suitability of the satellite imagery obtained, differences in seasonality between the images must also be considered. This is more important for Typhoon Kammuri specifically as images obtained are from different months and different seasons of the year. In the Philippines, the climate and consequently seasons are heavily influenced by the northeast monsoon period from December to April. In addition, the southwest monsoon period from May to November also aids in determining the wet and dry seasons (Perez and Comiso, 2014). The Abuan River catchment is located in the northeast of the Luzon, the northernmost island of the Philippines and wettest during December (Araza et al., 2021). The degree of seasonality in the Philippines is highly dependent on the landcover, whether that be agriculture, grassland, forested or urban (Perez and Comiso, 2014). Patterns demonstrate that across the Philippines vegetation is highest during the wet season. This can be assessed using the normalised difference vegetation index (NDVI) which indicates the vegetation's photosynthesis capacity (Tucker and Sellers, 1986). Patterns vary across areas of the Philippines, however even in areas of high NDVI, values only slightly fluctuate annually (Perez and Comiso, 2014). Areas of high NDVI represent areas of lush, forested vegetation that can be found across the Abuan River catchment. Therefore, despite satellite images being obtained from different months, images obtained can be deemed appropriate for analysis and comparison of channel as changes in vegetation only fluctuate slightly.

4.4.2 Data availability and lack of fieldwork analysis.

This study has provided an insight into the influence of landslide sediment input on changes in channel geomorphology following a typhoon event. Analysis presented is limited by the availability and type of data used. Remotely sensed

data sources have been utilised throughout this investigation as fieldwork was not feasible with the resources available within the timeframe research was conducted. Methods used to assess the impact of landslides, increasingly utilise remotely sensed data, however previous studies have supported this with field data (Bennet et al., submitted; Panici et al., in review). In field analysis of soil properties would help to improve the understanding of processes acting on hillslopes to better inform input parameters used within the model. In addition, this would aid in distinguishing between fluvial and landslide sedimentary deposits observed from satellite imagery to improve understanding of the dominant processes driving changes in ACW.

Although this research provides a framework to model changes in channel morphology following a typhoon-induced landslide event with low data availability, high uncertainty is associated with modelled results. To reduce the associated uncertainty and further understand the relationship between landslide sediment input and changes in ACW, a DEM following the typhoon event should be sourced. This would help to improve the accuracy of model inputs, such as the depth of landslides, runouts and maximum entrainable areas etc. In addition, results of modelled topographic change could be compared to the post-event DEM to substantiate the dominance of deposition as opposed to erosion modelled driving changes in ACW observed.

4.4.3 Limiting factors and associated uncertainty of ACW

Channel adjustment is a result of the difference between driving and resistive forces (Surian et al., 2009), however there may be additional external factors that determine the extent of channel change. Channels change in response to both natural and anthropogenic factors influencing the regulation and stability of

the channel over time (Zhang et al., 2022). Understanding of these factors informs the degree to which channel evolution may either be facilitated or impeded temporally (Taylor et al., 1993). Stream power and landslide sediment fluxes have been identified as a facilitating factor of lateral channel change, however their role is not spatially uniformed across the catchment. Therefore, there may be localised factors limiting changes in channel geomorphology as is dependent on a combination of factors including channel confinement, slope, gradient, geology, vegetation cover, sediment supply and flow regime (Bertrand and Liébault, 2019, Bisson et al., 2017, Grant et al., 2003).

Luzon, the island in which the Abuan River catchment is situated, generates large spatial differences in morphological characteristics such as channel gradient, drainage density, topography and confinement of river channels (Dingle et al., 2019). As the headwaters of the Abuan River catchment are found in the Sierra Madre mountains, annual typhoons excavate and transport large amounts of sediment which drives bed aggradation and bank erosion downstream. Therefore, moving downstream channels are of a lower gradient and extensive floodplains have developed (Dingle et al., 2019). Across the river channel network river channels are meandering (Figure 1.9 and 1.11). The morphology of the upper River Abuan river network is however difficult to characterise following the typhoon due to the remote location with fieldwork unable to be conducted. Boothroyd et al. (2023) characterised Filipino river channel networks using remotely sensed techniques also adopted here to provide a nationwide database of morphological data. This included, but was not limited to characteristics such as relief, slope, stream order, drainage area and compactness. Despite the ability to quantify certain morphological characteristics, without a DEM following the event simulated results cannot be

easily compared to that observed. In addition, these methods are unable to quantify the geologic characteristics of the catchments useful in understanding the processes acting along the slope. As this research aims to characterise more than just fluvial processes, the inability to fully identify morphological characteristics following the typhoon event presents a limitation in validating the mechanisms of channel change simulated later in this thesis. From visual interpretation alone it is difficult to distinguish type of sediment potentially driving channel widening. Variation in the sediment can be visually depicted from Google Earth imagery based on the size and differences in colour (Figure 1.11). Imagery is however not of a high enough resolution to identify the type of sediment to validate the processes driving channel change, i.e. whether these are fluvial deposits, landslide debris deposits or the exposure of bedrock due to high rates of erosion. In addition, cloud cover across the study site further limits the ability to identify this. Therefore, when assessing changes in channel geomorphology following a landslide event, simulated results have been compared with delineated observed data and suggestions for further research are provided. This research aims to provide a new conceptual understanding using only limited data resources, hence must consider associated uncertainty and limitations throughout.

4.4.4 Channel confinement

Channel confinement can be defined as the percentage of the length of a river channel network that abuts a confining margin (Brierley and Fryirs, 2013). This refers to a channel that is confined on either one or both sides of the channel embankment. The confinement of a river channel includes both the restriction or limitation of the lateral movement of flow (Fryirs et al., 2016). In conjunction with slope gradient, discharge and sediment regime, the degree of channel

confinement is considered as a primary control on channel geomorphology. Differences in channel confinement influence the capacity of a river channel to adjust whether that be laterally or vertically along the river profile. Quantification of channel confinement can therefore be useful in determining the range of river processes that occur on valley floors influencing changes in channel geomorphology.

The degree of channel confinement is strongly influenced by the surrounding geology of the area. Unconfined rivers tend to be alluvial which are more highly laterally mobile comprising of gravel and cobbles resulting in unstable river beds and banks (Eaton et al., 2010). In contrast, channels with a high degree of confinement are bedrock rivers and are hence more stable resulting in inhibited lateral migration of the channel (Bizzi and Lerner, 2015). The degree of channel confinement can also be altered through anthropogenic activity and the scale of human impact on geomorphic systems is larger now than in any point in history (Poepl et al., 2017). Anthropogenic factors may either be classified as direct, such as the construction of dams or channelisation, or indirect, such as changes in land cover or vegetation type (Goudie, 2006, Gregory, 2006)

To determine the degree of valley and channel confinement numerous data sources are required. Confinement can be inferred from a DEM, however additional information is necessary to support analysis that is unattainable without fieldwork or would otherwise have a very high level of uncertainty associated. Through the interpretation of satellite imagery, landcover has been determined across the catchment as primarily forested with small areas of urban areas, grassland and cultivated land downstream of the River Abuan catchment (Figure 1.10). With such dense forest cover, the catchment area is

extremely remote and this coupled with steep hillslopes makes much of the catchment inaccessible for fieldwork analysis. It can therefore be determined that processes acting within the landscape are natural with no anthropogenic change influencing the degree of channel confinement.

Detailed information is required about the geology often obtained through field techniques and in-person assessments (Bisson et al., 2017) which have not been achieved for this study. Geological data currently available for the Abuan River catchment as a result is too vague (Figure 1.10) and would not support the quantification of the degree of valley confinement. Within this investigation despite the fact sections of the river network may be confined influencing patterns of changes in ACW, it cannot be quantified so the effect cannot be determined. This therefore provides an area for further investigation into the ability to remotely determine the degree of channel confinement across river networks which would aid the analysis of this study.

Changes in channel geomorphology are determined by a combination influencing factors. Channel confinement may act as a limiting factor across some sections of the river channel and its inclusion in analysis would enhance understanding of changes in ACW. This being said results and findings presented can be deemed appropriate as individually assess the role of landslide sediment flux and stream power. These are found to have localised effects and therefore along sections may exert a greater influence than the potential degree of channel confinement, hence the observed sections of channel widening.

4.4.5 Assumptions and uncertainty associated with sediment input from landslides

Modelled outputs demonstrate that landslide sediment flux are a localised driver of lateral channel migration as a result of Typhoon Lawin. Sediment input has been increasingly considered by geomorphologists to link how sediment is transferred from different stores across the landscape (Poepl et al., 2017). This investigation is based on the assumption that large amounts of sediment originate from landslide scours which are understood to be a dominant mechanism of sediment transfer in mountain drainage basins (Brardinoni et al., 2009). Heavy rainfall induced by the extreme weather event also causes an increase in river discharge and enhances fluvial processes across the catchment. Active channel has been delineated along the margin of the channel and continuous riparian vegetation found on the riverbank (Donovan et al., 2019, Nelson et al., 2013, Rowland et al., 2016). Stripping of vegetation at the channel margins may instead be as a result of increased fluvial erosion from increased rainfall causing the high discharge values calculated (Table 3.4).

In some catchments, lateral changes in ACW may therefore instead be attributed to the increased erosion and deposition of fluvial action as opposed to landslide sediment input. This also varies within catchments as along sections of the River Abuan the channel widens without the presence of landslides and instead is attributed to high stream power (Figure 3.9). It has been determined from Test 1 and Test 0 that across the study site it is in fact a combination of both fluvial processes and landslide sediment input. Although results demonstrate that lateral channel change is predominantly driven by landslide sediment induced processes, the effect is localised and varies across the catchment.

The amount of sediment delivered is difficult to quantify as not all landslides will effectively supply sediment to the river system (Chen et al., 2018). The ability to deliver sediment is dependent on the topography, regolith, land use, distance to the channel and hillslope hydrology (Rickli and Graf, 2009). Uncertainty exists in the volume of sediment delivered from landslides due to the lack of DEM availability following Typhoon Lawin. Estimations using the empirical equation proposed by Larsen et al. (2010), indicate a large volume of sediment generation (Table 3.1, Figure 3.13). Further assumptions have been made that sediment generated reaches the river channels thereby influencing changes in lateral channel migration. These factors have been carefully considered when analysing results, hence the study site selected with steep slopes which generated numerous runouts from landslides found within a ~500 m radius of the channel. Following Typhoon Lawin, results presented demonstrate that areas of high landslide density (Figure 3.3) are frequently attributed to sections of river with high channel widening despite the values of stream power calculated (Figure 3.12). Modelled results demonstrate that landslide sediment flux as a result of landslides is a contributing factor to channel widening observed across the Abuan River channel network, despite uncertainties and assumptions.

4.4.6 Topographic change of lateral channel extents

Lateral channel change is influenced by a number of factors including sediment supply and discharge regime (Bisson et al., 2017). This indicates once again change is driven by a combination of fluvial and landslide driven processes following a typhoon event. Sediment deposits observed via satellite imagery are of different sizes and distributions. Areas of interest have been magnified and differences in sediment composition is particularly apparent in AOI number 3

(Figures 3.5 – 3.7), found along the meandering mid-course of the River Abuan. Landslide deposits are comprised of both coarse and fine sediments containing fragments of mudstone, boulder clasts, shale, sandstone and clays in the runouts (Catane et al., 2012, Tsou et al., 2011). Sediment delivered from landslides tends to be poorly sorted in comparison to fluvial deposits that are usually often more rounded. Although the distribution of grain size is important to understand the dynamics of debris flows (Johnson et al., 2012), it is not always considered and without field data cannot be determined for this research. Landslides are comprised of a range of sediment types and once deposited these cannot easily be distinguished from fluvial deposits. Therefore, fieldwork would need to be conducted to fully identify deposits observed from the satellite imagery.

Changes in lateral channel migration can be attributed to either erosional or depositional processes acting downstream. Modelled outputs run with the baseline scenario inputs demonstrate erosion upstream with the amount of deposition increasing moving downstream (Figure 3.14). Overall, deposition is modelled to dominate in the catchment with depths considerably greater than that eroded. Although depths of deposition are high, at the downstream confluence where it's modelled to be at its greatest, analysis of the pre-event channel demonstrates the channel is deeper indicating this is not unrealistic (Appendix E, Figure E). Found approximately 3500 km downstream, at this confluence the pre-event channel bank elevation ranged by 21.3m which is over 2 m greater than the highest deposition modelled. Therefore, despite high deposition depths, this would not cause a blockage or dam as seen in previous studies, instead channel discharge could continue to flow downstream.

By conducting fieldwork, changes may be more specifically attributed to either deposition, erosion or a combination of both processes. The presence of vegetation buried in deposits would indicate changes in ACW are linked to a combination of both processes, however with the remote location this may be difficult to observe in the field. Alternatively, higher resolution satellite imagery may allow for a more conclusive analysis of the type of deposit or whether changes observed are in fact the exposure of bedrock due to high erosion. Observations have been made from the satellite imagery currently available analysed alongside modelled outputs. From this, despite associated uncertainty, it can be inferred with that changes in ACW calculated result from predominantly high depths of deposition as opposed to erosion.

4.5 Model Limitations

4.5.1 Upstream sediment input

Previous studies conducted on the influence of sediment input from landslide sediment cascades have investigated the head of channels and their contributing tributaries (Bennett et al., submitted; Panici et al., in review). This research differs as the study site selected is found over 10 km downstream of the source of the tributary river to the River Abuan (Figure 1.12). Therefore, the study site does not reflect a closed channel system as changes in lateral channel migration may be influenced by external upstream contributions of sediment input.

In the short term after an event, sediment within the channel is considered to be determined by upstream disturbances in runoff and erosion of which the effects may be experienced downstream over time (Sutherland et al., 2002). Sediment delivery to the channel is also buffered by temporary storage on hillslopes,

spatial variability of storms and variation of land use or vegetation type (Glade, 2003). In addition, fluvial transport rates also play a role in determining how far sediment derived in the upstream catchment is transported downstream.

Therefore, without further investigation and field work, it is difficult to analyse and quantify the impact of upstream sediment as it propagates downstream.

This presents a limitation in this research as the upstream sediment contribution has not been considered. Results suggest a potential lag in the upstream section where erosion dominates (Figure 3.17). With the presence of landslides upstream, the full impact sediment supplied is not considered as the effects could propagate downstream. Having said this, landslide sediment fluxes have been identified to cause primarily a localised change in ACW, with lateral channel migration more commonly identified as a result of deposition. Therefore, it can be inferred that although sediment is mobilised and transported downstream, high levels of localised deposition suggest that landslide sediment flux upstream has a minimal effect on changes in ACW further downstream. There is however a high associated uncertainty. Research into additional study areas would be required to improve the confidence in findings, however, goes beyond the scope of this investigation. Thus, this presents an area for further investigation into the propagation of landslide sediment fluxes downstream. Additional research would be desirable to improve associated confidence in results presented and enhance the overall understanding of key drivers of changes in channel geomorphology following a typhoon event.

4.5.2 Model inputs

Without the presence of a DEM after the extreme weather event the depth of landslides and runouts have been calculated using the empirical formula by Larsen et al. (2010). This presents a limitation as there is high uncertainty associated with the depths of both the solid and fine-solid phase of sediment input. Additionally, there was no scaling relationship for maximum entrainable depth and this was consequently estimated based on previous studies as well as observations made from various output runs.

4.5.3 Suitability of r.avaflow

Even when using the most suitable model, results produced are a generalised and distorted view of reality (Mergili and Pudasaini, 2014-2023). A thorough understanding of the model allows for a more comprehensive understanding of the impact of landslide sediment cascades. All code, tools and manuals available for r.avaflow although created for the purpose to aid the user can contain inaccuracies. Therefore before using the model, an in depth understanding of its functionality helped to better inform inputs and parameter used which improved confidence in model outputs. Initial model outputs have been analysed and compared to measurements from satellite observations. Based on numerous modelled results, inputs and parameters have been carefully adjusted accordingly.

Since conducting this research, a new and updated version of the r.avaflow model has been released. Compatible with Windows, this version of the model is more user friendly and therefore less time consuming which increases the accessibility of further research into this study area. R.avaflow 2.4 used for this investigation, integrates all the necessary complementary functions of

entrainment, deposition and phase transformations required to simulate the complexity of cascading sediment flows. More significant improvements can be observed between the version used for this study and r.avaflow 2.3 or earlier as outlined by Mergili and Pudasaini (2014-2023). Despite recent advances, r.avaflow 2.4 is considered fit for purpose as includes only slight adjustments compared to version 3 and incorporates additional parameters outside of the key parameters altered for this investigation.

4.6 Future Research

4.6.1 Consideration of the influence of previous landslides on follow-up landslides

Episodic landslides reduce soil depth and rates of bedrock removal increase in connection with the frequency of landslides (Larsen et al., 2010). Despite annual Northern Pacific typhoon seasons, not all extreme weather events incurred make landfall or cause landslide events in the region. Research has been conducted into the impact of relic landslides and their influence on changing the likelihood of follow-up landslides. Parker et al. (2016) defines instability as dependent on slope and colluvium thickness and in agreement with Larsen et al. (2010) suggests that the removal of soil and colluvium following a landslide causes a decrease in likelihood of follow-up landslides. In addition, the removal of soil would cause slopes to stabilise and therefore there would not be enough sediment to generate a landslide.

Contrastingly, Samia et al. (2017) found that prior landslides cause a greater likelihood of subsequent landslides, however does so at a decreasing rate as sediment stabilises over a ten year time period. Previous investigation conducted in Biliran, Philippines, supported the finding of Parker et al. (2016)

that previous landslide occurrence in the areas studied did not impact the location, size or magnitude of landslides following subsequent typhoon events. Landslides following Typhoon Lawin dominate in the west whereas are more frequently found in the east following Typhoon Kammuri. As seen in Figure 3.1a landslides occur following both events in the centre of the catchment along the mid-course of the Abuan River. Despite this, as landslides investigated here are deemed not be episodic in nature, the occurrence of landslides following Typhoon Lawin is assumed to have little or no influence on the size occurred as a result of Typhoon Kammuri. This presents an area of further study to understand and validate the assumption of the influence of previous landslide occurrence on the size as well as magnitude of follow-up landslides. Conducting this research would improve understanding of sediment availability and dominant controls of sediment production across the catchment over time.

4.6.2 Additional study sites

Although considered in previous studies, this area of research is in its infancy and additional studies conducted across varying regions would help support current findings and enhance understanding. Previous studies have investigated a pristine mountainous environment in Colorado (Bennett et al., 2017, Figure 1.6) and a Filipino catchment heavily influenced by mining with the presence of tailing dams (Panici et al., in review, Figure 1.7). This research broadens existing understanding by focusing on a new location of a remote predominately forested river catchment. The influence of landslide sediment is presented to have a localised effect on lateral channel change and therefore investigation into new catchments would further enhance understanding.

For example, landslide hazard increasingly poses a threat to built-up environments where damage is considered to have the most detrimental effect

on local communities which increases their vulnerability (Saldivar-Sali and Einstein, 2007). It is also understood that human disturbance as a result of land use change, may be more detrimental to landslide induced hazard than climate change (Anderson and Holcombe, 2006, Borgatti and Soldati, 2010, Crozier, 2010). In the Philippines, poverty and landlessness are driving upland migration, cultivating previously forested areas to ensure subsistence food supplies are met (Gregory, 2006). With the ever-increasing pressure of urbanisation, study areas such as the Abuan River catchment, may not always remain forested. Research across different land use types will improve the ability to estimate channel change in response landslide sediment input. By understanding potential changes in channel geomorphology this will help to better predict the impact of landslides and aid in mitigation efforts thereby reducing the vulnerability of local communities.

In addition, the presence of limitations within this research provides purpose for further investigation to reduce the associated uncertainty within results presented. A small study area has been modelled to understand the influence of landslide sediment cascades which demonstrate a localised influence on changes in channel geomorphology. Further research across a greater extent would better inform understanding and therefore mitigation efforts to help reduce the impact of future catastrophic typhoon induced landslide events. Research presented therefore provides a foundation on which to build further research and broaden the understanding of complex landscape interactions with limited data sources.

4.6.3 Fieldwork data collection

When estimating landslide volumes using the empirical formula, Larsen et al. (2010) emphasises the sensitivity of the scaling exponent (γ), such that a

difference of 0.1 can overestimate of the volume of material transported by landslides by several orders of magnitude. Therefore, changes in γ are highly sensitive and when selecting an appropriate factor, consideration was taken to avoid over estimation of landslide volumes and reduce the associated uncertainty. Without the ability to conduct fieldwork and lack of DEM following these typhoon events, a greater uncertainty is associated with the magnitude of landslides reported compared to the frequency. This presents an area for further research, as if fieldwork were to be conducted it would inform a more precise understanding of the geology of the area better informing the value of γ . Additionally, further study and analysis would allow the comparison of different scaling methods to best quantify landslide volume following each of the typhoon events studied. Alternatively, over time resources and methods may allow for the creation of an updated DEM to inform a more reliable quantification of landslide volumes.

4.6.4 Application of data

Data provided in this investigation can be used to support other areas of research. This research supports the ScaRP project and despite studies of landslide susceptibility already being conducted in the region, the input of a greater number of landslide inventories can contribute to a more accurate susceptibility analysis. Therefore, the landslide inventory created for this research will be shared with collaborators of the ScaRP project to update existing hazard maps. As this supports an area of research in its infancy conducted at a new study site, data sourced, obtained and analysed can also be shared for use in further study to better inform the impact of landslide sediment cascades on changes in channel geomorphology.

5. Conclusion

This research aimed to further the understanding of how landslide sediment cascades influence changes in channel geomorphology following a typhoon event using only remotely sensed data and numerical modelling. Research focuses on the Abuan River catchment found in the northernmost island of Luzon, Philippines. Research presented follows on from Bennett et al.

(submitted) who suggested a relationship between landslides and channel widening which has also since been investigated by Panici et al. (in review).

This research builds on the findings of these two previous studies by investigating a more remote study area with less data availability.

Landslides as a result of Typhoon Lawin were mapped to be of a greater frequency than the landslides of comparatively greater magnitude following Typhoon Kammuri. Both events covered a large spatial extent across the River Abuan catchment, found predominantly in the northwest and northeast respectively in densely forested mountainous areas. Assessment of the Abuan River channel network demonstrated large amounts of channel widening. Due to data suitability, a higher associated confidence in the mapping of channel extents and frequency of landslides is associated with Typhoon Lawin compared to Typhoon Kammuri. With a lesser associated uncertainty, further analysis to investigate the effects of landslide sediment cascades on changes in channel geomorphology focused on the former typhoon event in 2016.

Controlling factors of changes in channel geomorphology typically assessed within the literature could not fully explain the channel widening experienced following the extreme weather event. Existing studies focus on hydraulic variables, such as stream power which was investigated in this research. In

addition, the degree of lateral channel confinement is often considered, though was not assessed. Although stream power was high during Typhoon Lawin, when analysing sections of greatest channel widening, values calculated were comparatively low. Previous investigations into extreme weather events often neglected the role of landslides and focused instead on flood river dynamics. As changes in channel geomorphology could not be wholly attributed to stream power following Typhoon Lawin, it could be inferred there were additional processes driving changes observed. Comparison between factors of stream power and landslide sediment input along the Abuan River were however found to be inconclusive. Therefore, a study site was selected with large channel widening, high sediment input and comparatively low stream power to try to simulate geomorphic change.

R.avaflow was selected as a multi-phase computational modelling tool to simulate the effects of landslide sediment in lateral channel change in response to the typhoon event. With only limited data available, empirical formulas were used to derive landslide depths as well as sediment volumes and additional parameters were estimated based on previous studies or successive model outputs. The use of a multiphase model allows for the inclusion of landslide sediment to enhance existing understanding of channel change following an extreme weather event. Landslide sediment was identified to have a localised effect on channel widening and the influence of landslide sediment varied downstream. The model predicted a dominance of deposition driving channel widening downstream of the study site with a higher proportion of erosion upstream. Without the existence of topographic data following the typhoon event, spatial patterns of erosion and deposition cannot be as easily validated. This being said, simulated channel change presented was consistent with that

observed from the manual delineation of channel extent using satellite imagery, deeming results appropriate for analysis with the limited resources available. Results were largely in agreement with the findings of Panici et al. (in review) that the inclusion of landslide sediment input could accurately simulate widening observed (Figure 1.7).

To enhance understanding, a model run was conducted without the inclusion of landslides and runouts. Simulated results demonstrate minimal topographic change and therefore a significant underestimation of channel change compared to that observed. This validates the inclusion of landslide sediment as a driver of lateral channel change. Hydraulic processes from flood water generated by the typhoon simulated small amounts of change, however, could not fully account for lateral channel change following the event. Therefore, it is understood to be a combination of fluvial and landslide driven processes that influence lateral channel change following an extreme weather event. This research consequently supports the findings of Bennett et al. (2017) and Brenna et al. (2023) that sediment input from landslide sediment cascades can be considered as additional factor which drives changes in channel geomorphology. Sensitivity analysis was conducted validating the choice of parameters, confirming the results presented and were consistent with the findings of Panici et al. (in review). In particular, when modelling the scenario using a single phase model output results were less consistent and overestimated the channel width compared to that observed (Figure 1.8). This validated the use of a multi-phase computational model to include both solid and fine-solid sediment to account for their differences in behaviour as well as the interactions between phases over time.

Limitations however exist due to the data availability and inability to conduct fieldwork. In this investigation, total as well as unit stream power and the role of sediment have been considered. However there are additional controlling factors that influence changes in channel geomorphology. For example, the degree of channel confinement, geology and vegetation cover, that were unattainable with the resources available which provides an area for further research. Within the model, the influence of sediment from landslides further upstream of the modelled channel reach is not considered. In addition without a DEM following the event, sediment depths from landslides included are based on empirical formulas increasing the associated uncertainty. Topographic changes modelled also cannot be validated without a DEM following the typhoon event which would enhance the understanding of how landslide sediment influences changes in channel geomorphology. Further research could be conducted into additional study areas with differing land cover types and the ability to conduct fieldwork would help to overcome the limitations presented.

This investigation builds on existing research to understand the role of landslide sediment driving changes in channel geomorphology over time. Figure 5.1 presents a schematic flow diagram of the proposed assessment of changes in channel geomorphology. When investigating the effects of extreme weather events on changes in geomorphology, research previously focused solely on fluvial processes. These findings present a new conceptual framework that enhances that previously used to include the role of sediment cascades induced by an extreme weather event. Research supports existing studies using only limited remotely sensed data and utilised empirical relationships to estimate unobtainable data required. Methods used demonstrate that results can be

deemed appropriate for analysis without the requirement of fieldwork. This improves on the current understanding whilst enabling others to delve deeper into this area of research in its infancy. Due to different limitations and uncertainties, this research informs potential future- research topics to build on findings presented. For example the inclusion of channel confinement statistics or addition of fieldwork studies to help validate simulated results. It furthers the understanding of the complexity of interactions between landslides and channel networks, with implications for landslide-flood hazard assessment.

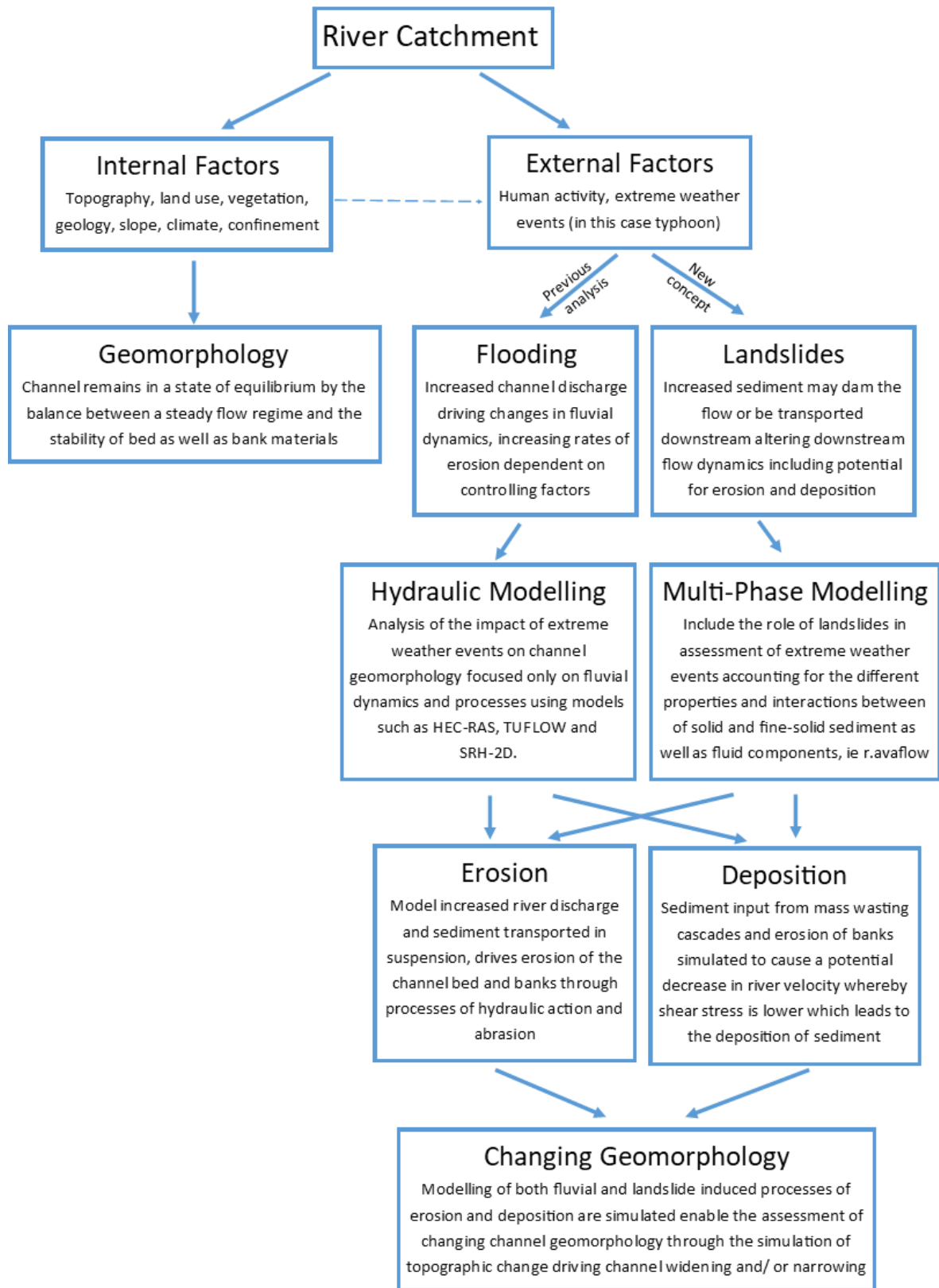


Figure 5.1 – schematic flow diagram demonstrating the new proposed framework in assessing changes in channel geomorphology following an extreme weather event to include the role of landslide sediment.

6. Appendices

6.1 Appendix A

Table A: Table showing the parameters selected when creating DEM in DSM-OPT service created by CRNS EOST (2020).

Name	Value
dsmopt_zoomf	1
dsmopt_ortho_singles	true
dsmopt_ortho_mosaic	false
dsmopt_reproject	true
dsmopt_reproj_epsg	32651
dsmopt_do_align	true
dsmopt_mask_water_bodies	false
dsmopt_szw	2
dsmopt_regul	0.025
dsmopt_z_uncertainty_ratio	0.3
dsmopt_zpas	0.4
dsmopt_default_correlation	0.2

6.2 Appendix B

Table B: Total and average intensity of rainfall on the day Typhoon Lawin made landfall at each satellite rainfall cell location.

Point	Long/Lat	Rainfall	
		Total (mm)	Intensity (mmhr ⁻¹)
1	17.05N 121.95E	377.5	7.9
2	17.15N 121.95E	353.5	7.4
3	17.25N 121.95E	392.4	8.2
4	17.35N 121.95E	426.7	8.9
5	17.35N 122.05E	370.8	7.7
6	17.25N 122.05E	353.5	7.4
7	17.15N 122.05E	390.9	8.1
8	17.05N 122.05E	400.0	8.3
9	17.05N 122.15E	387.0	8.1
10	17.15N 122.15E	440.4	9.2
11	17.25N 122.15E	426.3	8.9
12	17.35N 122.15E	411.0	8.6
13	17.35N 122.25E	463.3	9.7
14	17.25N 122.25E	381.2	7.9
15	17.15N 122.25E	425.1	8.9
16	17.05N 122.25E	398.6	8.3
17	17.05N 122.35E	427.5	8.9
18	17.15N 122.35E	414.5	8.6
19	17.25N 122.35E	395.7	8.2
20	17.35N 122.35E	389.7	8.1

6.3 Appendix C

Table C: Changes in ACW comparing pre- and post- channel width following Typhoon Lawin and Typhoon Kammuri.

Downstream Distance (km)	Lawin ACW				Kammuri ACW			
	Pre	Post	Δ	% Δ	Pre	Post	Δ	% Δ
1	56.9	65.2	8.3	14.6	54.9	52.1	-2.8	-5.1
2	27.5	27.2	-0.3	-1.0	23.0	24.4	1.4	6.1
3	25.1	26.0	0.9	3.5	21.4	20.4	-1.0	-4.6
4	30.2	31.9	1.8	5.8	24.2	35.8	11.6	48.1
5	32.9	39.4	6.5	19.9	29.9	42.7	12.9	43.2
6	47.9	44.7	-3.2	-6.7	32.4	40.7	8.3	25.5
7	27.6	27.2	-0.4	-1.5	19.9	29.6	9.7	48.8
8	36.1	45.2	9.1	25.2	33.3	60.2	26.9	80.8
9	24.0	34.7	10.8	44.9	17.8	22.4	4.7	26.3
10	19.7	26.9	7.2	36.3	49.6	54.1	4.5	9.1
11	28.6	26.3	-2.3	-8.0	50.6	52.8	2.2	4.4
12	42.1	53.2	11.1	26.4	37.9	50.1	12.1	32.0
13	43.9	62.4	18.5	42.1	41.2	46.5	5.3	13.0
14	47.3	40.5	-6.8	-14.3	43.5	40.6	-3.0	-6.8
15	48.0	40.0	-7.9	-16.5	27.7	31.2	3.6	12.9
16	47.2	48.8	1.6	3.5	54.9	52.1	-2.8	-5.1
17	26.9	26.6	-0.3	-1.0	57.0	61.5	4.6	8.0
18	56.9	65.2	8.3	14.6	60.1	57.6	-2.5	-4.1
19	61.5	66.4	5.0	8.1	57.7	57.2	-0.5	-0.8
20	59.3	61.8	2.5	4.2	59.1	63.0	3.9	6.6
21	54.4	61.3	6.9	12.7	58.4	47.8	-10.7	-18.2
22	59.3	69.6	10.3	17.4	49.7	44.3	-5.5	-11.0
23	54.3	57.7	3.3	6.2	41.6	40.5	-1.1	-2.7
24	51.0	58.8	7.8	15.3	69.3	75.8	6.5	9.4
25	59.7	60.6	0.9	1.5	68.4	79.5	11.1	16.3
26	73.4	75.5	2.1	2.9	76.9	77.7	0.8	1.0
27	72.5	75.8	3.3	4.5	71.5	68.4	-3.1	-4.3
28	74.9	80.2	5.3	7.0	69.2	72.4	3.2	4.6

29	74.4	83.0	8.6	11.6	90.5	85.9	-4.6	-5.1
30	64.1	73.1	8.9	13.9	78.5	103.6	25.1	32.0
31	89.5	97.2	7.7	8.6	56.6	51.3	-5.2	-9.3
32	83.6	102.1	18.5	22.1	66.7	75.8	9.1	13.6
33	67.9	64.5	-3.4	-5.0	74.4	88.7	14.3	19.2
34	74.5	88.5	14.0	18.8	60.4	65.8	5.4	8.9
35	77.7	96.1	18.4	23.7	98.2	107.2	9.1	9.2
36	79.7	80.1	0.4	0.5	72.0	93.7	21.8	30.2
37	66.9	60.1	-6.8	-10.1	66.6	81.8	15.2	22.8
38	98.9	100.9	2.1	2.1	74.9	99.4	24.5	32.8
39	74.8	82.5	7.8	10.4	66.1	86.0	19.9	30.1
40	72.3	82.4	10.0	13.9	71.0	97.1	26.1	36.7
41	78.3	85.6	7.2	9.2	83.6	99.0	15.4	18.4
42	70.8	77.9	7.1	10.1	85.7	98.4	12.7	14.8
43	76.4	85.7	9.3	12.2	99.4	164.5	65.1	65.5
44	89.4	88.3	-1.1	-1.3	99.6	141.6	41.9	42.1
45	88.2	91.8	3.6	4.1	104.6	141.1	36.5	34.9
46	83.6	91.5	7.9	9.5	102.8	154.7	51.9	50.5
47	117.7	164.6	46.9	39.8	110.8	143.5	32.6	29.5
48	82.0	88.8	6.7	8.2	87.4	106.1	18.7	21.4
49	107.6	140.3	32.6	30.3	127.4	146.9	19.6	15.4
50	98.3	122.9	24.6	25.1				
51	101.2	120.2	19.1	18.9				
52	111.3	142.6	31.4	28.2				
53	101.0	111.0	10.1	10.0				
54	104.0	140.0	36.0	34.7				
55	83.4	99.2	15.8	19.0				
56	136.7	121.0	-15.8	-11.5				

6.4 Appendix D

Table D – table summarising channel widths downstream along section of Abuan River network modelled comparing observed to simulated channels from Tests 0-5.

Distance downstream (m)	Active Channel Width (m)						
	Observed	Test 1	Test 2	Test 3	Test 4	Test 5	Test 0
0	44.0	45.1	66.0	65.3	63.4	65.3	17.3
150	58.9	61.6	65.3	67.8	64.4	63.0	23.0
300	45.5	45.4	61.7	63.9	64.8	64.8	15.8
450	34.2	42.7	47.8	45.8	49.8	47.8	33.9
600	40.7	38.9	46.2	45.0	48.0	44.2	29.7
750	50.0	53.0	58.6	55.6	53.1	53.3	20.1
900	67.9	71.0	77.2	78.5	79.5	79.1	43.3
1050	43.6	43.5	50.0	48.1	49.3	49.7	49.9
1200	42.5	43.3	31.3	30.9	30.8	30.8	38.6
1350	42.1	44.7	47.5	44.6	43.9	46.4	41.9
1500	55.9	54.3	72.9	72.1	73.8	73.2	58.0
1650	36.4	39.9	50.9	54.4	51.2	50.0	27.8
1800	53.0	53.7	56.5	60.1	59.7	57.0	37.6
1950	28.0	28.6	49.6	51.8	49.9	43.7	29.2
2100	32.5	31.8	41.2	42.5	40.6	41.0	30.6
2250	44.5	45.4	56.3	59.0	58.7	56.5	43.8
2400	36.9	40.8	47.6	47.4	46.9	47.3	61.4
2550	44.7	49.3	54.7	55.6	55.1	53.9	42.2
2700	43.0	42.7	58.0	60.0	57.0	56.8	45.8

2850	60.8	57.2	44.7	45.9	45.2	53.1	52.8
3000	53.9	53.8	63.1	64.5	65.1	63.1	67.7
3150	46.0	51.7	36.3	34.6	36.6	44.5	40.3
3300	73.6	80.5	66.1	66.1	61.5	50.6	53.9
3450	60.9	62.1	47.9	55.0	55.0	57.2	44.3
3600	58.9	58.6	53.7	60.8	56.5	49.6	49.2
3750	45.3	47.8	40.9	43.8	40.4	42.6	49.8
3900	57.4	59.3	40.6	39.7	41.4	39.6	61.3

6.5 Appendix E

Cross section of the pre-event river channel found at the confluence of the downstream tributary to the main channel modelled in the study site where deposition was modelled to be at its greatest.

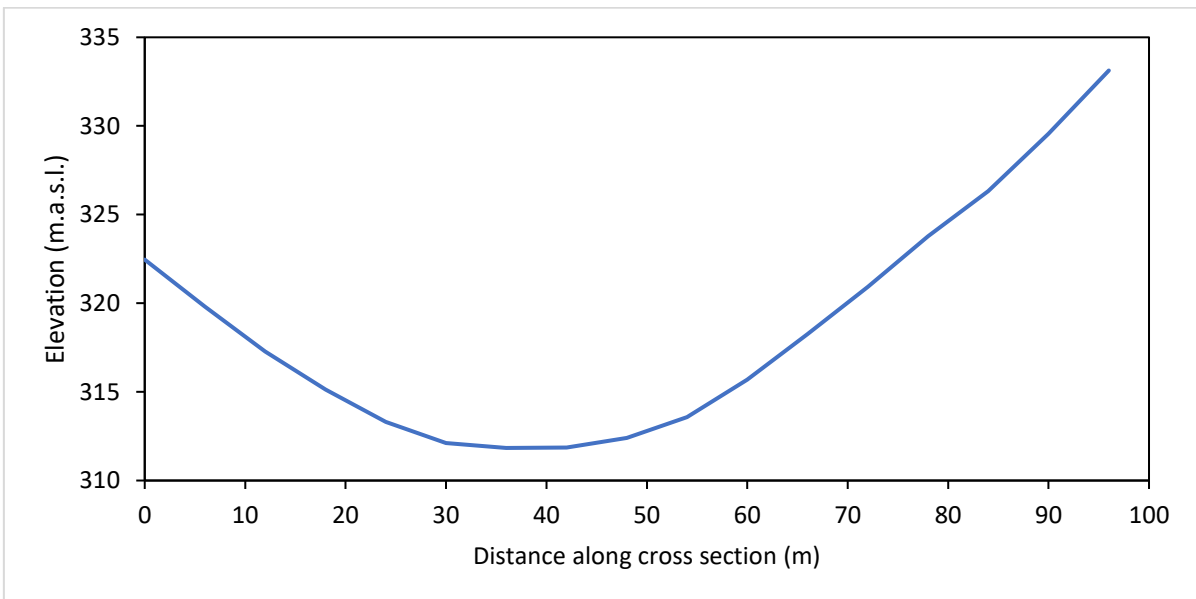


Figure E: data obtained from pre-event DEM quantifying change in elevation across cross section found ~3500 km downstream along the channel modelled.

7. Bibliography

4dixplorer. n.d. Our Software: LS3D [Online]. Available:

http://www.4dixplorer.com/software_ls3d.html [Accessed 25th April 2022].

Abancó, C., Bennett, G. L., Matthews, A. J., Matera, M. A. & Tan, F. J. 2020.

The role of geomorphology, rainfall and soil moisture in the occurrence of landslides triggered by 2018 Typhoon Mangkhut in the Philippines.

Natural Hazards and Earth System Sciences Discussions, 1-32.

Acosta, L. A., Eugenio, E. A., Macandog, P. B. M., Magcale-Macandog, D. B.,

Lin, E. K.-H., Abucay, E. R., Cura, A. L. & Primavera, M. G. 2016. Loss and damage from typhoon-induced floods and landslides in the

Philippines: community perceptions on climate impacts and adaptation options. International Journal of Global Warming, 9, 33-65.

Agency, E. 2021. Understanding river channel sensitivity to geomorphological changes [Online]. Available:

https://assets.publishing.service.gov.uk/media/606ddd86e90e074e53c33dbf/Understanding_how_river_channels_change_-_method_report.pdf [Accessed 27 October 2022].

Aleotti, P. & Chowdhury, R. 1999. Landslide hazard assessment: summary

review and new perspectives. Bulletin of Engineering Geology and the environment, 58, 21-44.

Anderson, M.G. and Calver, A., 1977. On the persistence of landscape features

formed by a large flood. Transactions of the Institute of British Geographers, pp.243-254.

- Anderson, M. G. & Holcombe, L. 2006 Sustainable landslide risk reduction in poorer countries. Proceedings of the Institution of Civil Engineers-Engineering Sustainability. Thomas Telford Ltd, 23-30.
- Araza, A., Perez, M., Cruz, R. V., Aggabao, L. F. & Soyosa, E. 2021. Probable streamflow changes and its associated risk to the water resources of Abuan watershed, Philippines caused by climate change and land use changes. Stochastic environmental research and risk assessment, 35, 389-404.
- Baggio, T., Mergili, M. & D'agostino, V. 2021. Advances in the simulation of debris flow erosion: The case study of the Rio Gere (Italy) event of the 4th August 2017. Geomorphology, 381, 107664.
- Bagnardi, M., González, P. J. & Hooper, A. 2016. High-resolution digital elevation model from tri-stereo Pleiades-1 satellite imagery for lava flow volume estimates at Fogo Volcano. Geophysical Research Letters, 43, 6267-6275.
- Bagnold, R. A. 1960. Sediment discharge and stream power: a preliminary announcement, United States Department of the Interior, Geological Survey.
- Balderama, O., Alejo, L. & Tongson, E. 2016. Calibration, validation and application of CERES-Maize model for climate change impact assessment in Abuan Watershed, Isabela, Philippines. Climate, Disaster and Development Journal, 2, 11-20.
- Balderama, O., Bareng, J. L. & Rosete, E. 2019. Application of SWAT Model to Assess Impact of Climate and Land Use Changes to Sedimentation in the Abuan Watershed, Philippines.

- Balderama, O. F. 2022. Climate Change Adaptation Practices Towards Sustainable Watershed Management: The Case of Abuan Watershed in Ilagan City, Philippines. *Interlocal Adaptations to Climate Change in East and Southeast Asia*. Springer.
- Bankoff, G. 1999. A history of poverty: The politics of natural disasters in the Philippines, 1985–95. *The Pacific Review*, 12, 381-420.
- Barit, J. B., Choi, K. & Ko, D. W. 2022. Modeling the risk of illegal forest activity and its distribution in the southeastern region of the Sierra Madre Mountain Range, Philippines. *iForest-Biogeosciences and Forestry*, 15, 63.
- Begnudelli, L., Sanders, B.F. and Bradford, S.F., 2008. Adaptive Godunov-based model for flood simulation. *Journal of Hydraulic Engineering*, 134(6), pp.714-725.
- Benda, L. & Dunne, T. 1997. Stochastic forcing of sediment supply to channel networks from landsliding and debris flow. *Water Resources Research*, 33, 2849-2863.
- Beniston, M. 2005. The risks associated with climatic change in mountain regions. *Global change and mountain regions*. Springer.
- Benke, A. C. & Cushing, C. E. 2011. *Rivers of North America*, Elsevier.
- Bennett, G., Molnar, P., Eisenbeiss, H. & Mcardell, B. 2012. Erosional power in the Swiss Alps: characterization of slope failure in the Illgraben. *Earth Surface Processes and Landforms*, 37, 1627-1640.
- Bennett, G.L., Miller, S.R., Roering, J.J., Schmidt, D.A.. 2016. Landslides, threshold slopes and the survival of relict terrain in the wake of the Mendocino Triple Junction, *Geology*. doi:10.1130/G37530.1

- Bertrand, M. & Liébault, F. 2019. Active channel width as a proxy of sediment supply from mining sites in New Caledonia. *Earth Surface Processes and Landforms*, 44, 67-76.
- Berzi, D., Jenkins, J. T. & Larcher, M. 2010. Debris flows: Recent advances in experiments and modeling. *Advances in geophysics*, 52, 103-138.
- Bisson, P. A., Montgomery, D. R. & Buffington, J. M. 2017. Valley segments, stream reaches, and channel units. *Methods in Stream Ecology*, Volume 1. Elsevier.
- Bizzi, S. & Lerner, D. N. 2015. The use of stream power as an indicator of channel sensitivity to erosion and deposition processes. *River Research and Applications*, 31, 16-27.
- Bladé, E., Gómez-Valentín, M., Dolz, J., Aragón-Hernández, J.L., Corestein, G. and Sánchez-Juny, M., 2012. Integration of 1D and 2D finite volume schemes for computations of water flow in natural channels. *Advances in Water Resources*, 42, pp.17-29.
- Borgatti, L. & Soldati, M. 2010. Landslides as a geomorphological proxy for climate change: a record from the Dolomites (northern Italy). *Geomorphology*, 120, 56-64.
- Bracken, L. J., Turnbull, L., Wainwright, J. & Bogaart, P. 2015. Sediment connectivity: a framework for understanding sediment transfer at multiple scales. *Earth Surface Processes and Landforms*, 40, 177-188.
- Brardinoni, F. & Church, M. 2004. Representing the landslide magnitude–frequency relation: Capilano River basin, British Columbia. *Earth Surface Processes and Landforms: The Journal of the British Geomorphological Research Group*, 29, 115-124.

- Brardinoni, F., Hassan, M. A., Rollerson, T. & Maynard, D. 2009. Colluvial sediment dynamics in mountain drainage basins. *Earth and Planetary Science Letters*, 284, 310-319.
- Brenna, A., Marchi, L., Borga, M., Zaramella, M. & Surian, N. 2023. What drives major channel widening in mountain rivers during floods? The role of debris floods during a high-magnitude event. *Geomorphology*, 430, 108650.
- Brierley, G. J. 2010. Landscape memory: the imprint of the past on contemporary landscape forms and processes. *Area*, 42, 76-85.
- Brierley, G. J. & Fryirs, K. A. 2013. *Geomorphology and river management: applications of the river styles framework*, John Wiley & Sons.
- Buser, O. & Bartelt, P. 2009. Production and decay of random kinetic energy in granular snow avalanches. *Journal of Glaciology*, 55, 3-12.
- Catane, S. G., Abon, C. C., Saturay Jr, R. M., Mendoza, E. P. P. & Futralan, K. M. 2012. Landslide-amplified flash floods—the June 2008 Panay Island flooding, Philippines. *Geomorphology*, 169, 55-63.
- Catto, J. L. & Dowdy, A. 2021. Understanding compound hazards from a weather system perspective. *Weather and Climate Extremes*, 32, 100313.
- Chang, C. 2020. Improved three-week weather forecasts could save lives from disaster.
- Chen, C.-W., Oguchi, T., Hayakawa, Y. S., Saito, H., Chen, H., Lin, G.-W., Wei, L.-W. & Chao, Y.-C. 2018. Sediment yield during typhoon events in relation to landslides, rainfall, and catchment areas in Taiwan. *Geomorphology*, 303, 540-548.

- Chen, H., Zhang, L. M., Gao, L., Yuan, Q., Lu, T., Xiang, B. & Zhuang, W. 2017. Simulation of interactions among multiple debris flows. *Landslides*, 14, 595-615.
- Chigira, M., Tsou, C.-Y., Matsushi, Y., Hiraishi, N. & Matsuzawa, M. 2013. Topographic precursors and geological structures of deep-seated catastrophic landslides caused by Typhoon Talas. *Geomorphology*, 201, 479-493.
- Clapuyt, F., Vanacker, V., Christl, M., Van Oost, K. & Schlunegger, F. 2019. Spatio-temporal dynamics of sediment transfer systems in landslide-prone Alpine catchments. *Solid Earth*, 10, 1489-1503.
- Coppin, P., Lambin, E., Jonckheere, I. & Muys, B. 2002. Digital change detection methods in natural ecosystem monitoring: A review. *Analysis of multi-temporal remote sensing images*, 3-36.
- Corominas, J. & Moya, J. 2008. A review of assessing landslide frequency for hazard zoning purposes. *Engineering geology*, 102, 193-213.
- Croke, J., Mockler, S., Fogarty, P. & Takken, I. 2005. Sediment concentration changes in runoff pathways from a forest road network and the resultant spatial pattern of catchment connectivity. *Geomorphology*, 68, 257-268.
- Crozier, M. J. 2010. Deciphering the effect of climate change on landslide activity: A review. *Geomorphology*, 124, 260-267.
- Davies, T. R. & Korup, O. 2010. Sediment cascades in active landscapes. *Sediment Cascades: An Integrated Approach*, edited by: Burt, TP and Allison, RJ, John Wiley and Sons, Ltd, Chichester, UK, 89-115.
- De Beurs, K. & Henebry, G. 2005. A statistical framework for the analysis of long image time series. *International Journal of Remote Sensing*, 26, 1551-1573.

- Dietrich, A. & Krautblatter, M. 2019. Deciphering controls for debris-flow erosion derived from a LiDAR-recorded extreme event and a calibrated numerical model (Roßbichelbach, Germany). *Earth Surface Processes and Landforms*, 44, 1346-1361.
- Dingle, E. H., Paringit, E. C., Tolentino, P. L., Williams, R. D., Hoey, T. B., Barrett, B., Long, H., Smiley, C. & Stott, E. 2019. Decadal-scale morphological adjustment of a lowland tropical river. *Geomorphology*, 333, 30-42.
- Donovan, M., Belmont, P., Notebaert, B., Coombs, T., Larson, P. & Souffront, M. 2019. Accounting for uncertainty in remotely-sensed measurements of river planform change. *Earth-science reviews*, 193, 220-236.
- Durkee, E. F. & Pederson, S. L. 1961. Geology of northern Luzon, Philippines. *AAPG Bulletin*, 45, 137-168.
- Earth, G. 2023. Explore New Satellite Imagery.
- East, A.E., Logan, J.B., Mastin, M.C., Ritchie, A.C., Bountry, J.A., Magirl, C.S., and Sankey, J.B. 2018. Geomorphic evolution of a gravel-bed river under sediment-starved versus sediment-rich conditions: River response to the world's largest dam removal. *Journal of Geophysical Research: Earth Surface*, 123, 3338– 3369.
- Eaton, B., Millar, R. G. & Davidson, S. 2010. Channel patterns: Braided, anabranching, and single-thread. *Geomorphology*, 120, 353-364.
- Eco, R., Aquino, D., Lagmay, A., Alejandrino, I., Bonus, A., Escape, C., Felix, R., Ferrer, P., Gacusan, R. & Galang, J. 2015. Landslide and debris flow susceptibility mapping of Leyte Province, Philippines using remote sensing, numerical modelling, and GIS. *Journal of the Philippine Geoscience and Remote Sensing Society*, 1, 1, 53-71.

- Eidsvig, U. M., Mclean, A., Vangelsten, B. V., Kalsnes, B., Ciurean, R. L., Argyroudis, S., Winter, M., Mavrouli, O. C., Fotopoulou, S. & Pitilakis, K. 2014. Assessment of socioeconomic vulnerability to landslides using an indicator-based approach: methodology and case studies. *Bulletin of engineering geology and the environment*, 73, 307-324.
- Elsner, J. B. & Liu, K.-B. 2003. Examining the ENSO-typhoon hypothesis. *Climate Research*, 25, 43-54.
- Everham, E. M. & Brokaw, N. V. 1996. Forest damage and recovery from catastrophic wind. *The botanical review*, 62, 113-185.
- Evio, B. & Bonito, S. 2017. Philippines: The Role of the Philippine Nurses Association in Disaster Preparedness and Response During Typhoon Haiyan. *The Role of Nurses in Disaster Management in Asia Pacific*. Springer.
- Fabregas, A. C., Arellano, P. B. V. & Pinili, A. N. D. 2020 Long-Short Term Memory (LSTM) Networks with Time Series and Spatio-Temporal Approaches Applied in Forecasting Earthquakes in the Philippines. *Proceedings of the 4th International Conference on Natural Language Processing and Information Retrieval*. 188-193.
- Fahnestock, R. K. 1978. Little Tahoma Peak rockfalls and avalanches, Mount Rainier, Washington, USA. *Developments in Geotechnical Engineering*. Elsevier.
- Fan, L., Lehmann, P. & Or, D. 2016. Effects of soil spatial variability at the hillslope and catchment scales on characteristics of rainfall-induced landslides. *Water Resources Research*, 52, 1781-1799.
- Ferguson, R., Church, M., Rennie, C. & Venditti, J. 2015. Reconstructing a sediment pulse: Modeling the effect of placer mining on Fraser River,

- Canada. *Journal of Geophysical Research: Earth Surface*, 120, 1436-1454.
- Finnegan, N. J., Roe, G., Montgomery, D. R. & Hallet, B. 2005. Controls on the channel width of rivers: Implications for modeling fluvial incision of bedrock. *Geology*, 33, 229-232.
- Finnegan, N. J., Sklar, L. S. & Fuller, T. K. 2007. Interplay of sediment supply, river incision, and channel morphology revealed by the transient evolution of an experimental bedrock channel. *Journal of Geophysical Research: Earth Surface*, 112.
- Froude, M. J. & Petley, D. N. 2018. Global fatal landslide occurrence from 2004 to 2016. *Natural Hazards and Earth System Sciences*, 18, 2161-2181.
- Fryirs, K. A., Brierley, G. J., Preston, N. J. & Kasai, M. 2007. Buffers, barriers and blankets: The (dis) connectivity of catchment-scale sediment cascades. *Catena*, 70, 49-67.
- Fryirs, K. A., Wheaton, J. M. & Brierley, G. J. 2016. An approach for measuring confinement and assessing the influence of valley setting on river forms and processes. *Earth Surface Processes and Landforms*, 41, 701-710.
- Gariano, S. L. & Guzzetti, F. 2016. Landslides in a changing climate. *Earth-Science Reviews*, 162, 227-252.
- Gartner, J. D., Dade, W. B., Renshaw, C. E., Magilligan, F. J. & Buraas, E. M. 2015. Gradients in stream power influence lateral and downstream sediment flux in floods. *Geology*, 43, 983-986.
- Gasparini, N. M., Tucker, G. E. & Bras, R. L. 1999. Downstream fining through selective particle sorting in an equilibrium drainage network. *Geology*, 27, 1079-1082.

- Glade, T. 2003. Landslide occurrence as a response to land use change: a review of evidence from New Zealand. *Catena*, 51, 297-314.
- Go, J. R. R. 2017. Of choices, changes, and challenges: The Philippines in 2016. *Philippine Political Science Journal*, 38, 48-73.
- Goguel, J. 1978. Scale-dependent rockslide mechanisms, with emphasis on the role of pore fluid vaporization. *Developments in geotechnical engineering*. Elsevier.
- Goudie, A. S. 2006. Global warming and fluvial geomorphology. *Geomorphology*, 79, 384-394.
- Grafil, L. & Castro, O. 2014. Acquisition of IfSAR for the production of nationwide DEM and ORI for the Philippines under the Unified Mapping Project. *Infomapper*, 21, 40-43.
- Gran, K. B. & Czuba, J. A. 2017. Sediment pulse evolution and the role of network structure. *Geomorphology*, 277, 17-30.
- Grant, G. E., Schmidt, J. C. & Lewis, S. L. 2003. A geological framework for interpreting downstream effects of dams on rivers. *Water Science and Application*, 7, 209-225.
- Gregory, K. J. 2006. The human role in changing river channels. *Geomorphology*, 79, 172-191.
- Grigorian, S., Eglit, M. & Iakimov, I. L. 1967. New statement and solution of the problem of the motion of snow avalanche. *Snow, Avalanches & Glaciers*. Tr. Vysokogornogo Geofizich Inst, 12, 104-113.
- Guns, M. & Vanacker, V. 2014. Shifts in landslide frequency–area distribution after forest conversion in the tropical Andes. *Anthropocene*, 6, 75-85.
- Guthrie, R. & Evans, S. 2004. Analysis of landslide frequencies and characteristics in a natural system, coastal British Columbia. *Earth*

- Surface Processes and Landforms: The Journal of the British
Geomorphological Research Group, 29, 1321-1339.
- Guzzetti, F., Ardizzone, F., Cardinali, M., Rossi, M. & Valigi, D. 2009. Landslide volumes and landslide mobilization rates in Umbria, central Italy. *Earth and Planetary Science Letters*, 279, 222-229.
- Guzzetti, F., Malamud, B. D., Turcotte, D. L. & Reichenbach, P. 2002. Power-law correlations of landslide areas in central Italy. *Earth and Planetary Science Letters*, 195, 169-183.
- Haas, T. D. & Woerkom, T. V. 2016. Bed scour by debris flows: experimental investigation of effects of debris-flow composition. *Earth Surface Processes and Landforms*, 41, 1951-1966.
- Heim, A. 1932. *Bergsturz und menschenleben*, Fretz & Wasmuth.
- Hovius, N., Stark, C. P. & Allen, P. A. 1997. Sediment flux from a mountain belt derived by landslide mapping. *Geology*, 25, 231-234.
- Hsu, K. J. 1975. Catastrophic debris streams (sturzstroms) generated by rockfalls. *Geological Society of America Bulletin*, 86, 129-140.
- Hungr, O., Leroueil, S. & Picarelli, L. 2014. The Varnes classification of landslide types, an update. *Landslides*, 11, 167-194.
- Hutchinson, M. F. & Gallant, J. C. 2000. Digital elevation models and representation of terrain shape. *Terrain analysis: principles and applications*, 29-50.
- Hutter, K. & Schneider, L. 2010. Important aspects in the formulation of solid–fluid debris-flow models. Part I. Thermodynamic implications. *Continuum Mechanics and Thermodynamics*, 22, 363-390.
- Iverson, R. M. 1997. The physics of debris flows. *Reviews of geophysics*, 35, 245-296.

- Iverson, R. M. & Denlinger, R. P. 2001. Flow of variably fluidized granular masses across three-dimensional terrain: 1. Coulomb mixture theory. *Journal of Geophysical Research: Solid Earth*, 106, 537-552.
- Jaboyedoff, M., Choffet, M., Derron, M.H., Horton, P., Loye, A., Longchamp, C., Mazotti, B., Michoud, C. and Pedrazzini, A., 2012. Preliminary slope mass movement susceptibility mapping using DEM and LiDAR DEM. *Terrigenous mass movements: Detection, modelling, early warning and mitigation using geoinformation technology*, pp.109-170.
- Jakob, M. & Lambert, S. 2009. Climate change effects on landslides along the southwest coast of British Columbia. *Geomorphology*, 107, 275-284.
- Johnson, C., Kokelaar, B., Iverson, R. M., Logan, M., Lahusen, R. & Gray, J. 2012. Grain-size segregation and levee formation in geophysical mass flows. *Journal of Geophysical Research: Earth Surface*, 117.
- Johnson, R. 2016. Assessment of torrent erosion impacts on the eastern flank of Thirlmere Reservoir and A591 (Cumbria) following Storm Desmond 2015.
- Johnson, R. M. & Warburton, J. 2002. Flooding and geomorphic impacts in a mountain torrent: Raise Beck, Central Lake District, England. *Earth Surface Processes and Landforms*, 27, 945-969.
- Jones, J. N., Bennett, G. L., Abancó, C., Matera, M. A. & Tan, F. J. 2023. Multi-event assessment of typhoon-triggered landslide susceptibility in the Philippines. *Natural Hazards and Earth System Sciences*, 23, 1095-1115.
- Joyce, H. M., Hardy, R. J., Warburton, J. & Large, A. R. 2018. Sediment continuity through the upland sediment cascade: geomorphic response

- of an upland river to an extreme flood event. *Geomorphology*, 317, 45-61.
- Karsli, F., Atasoy, M., Yalcin, A., Reis, S., Demir, O. & Gokceoglu, C. 2009. Effects of land-use changes on landslides in a landslide-prone area (Ardesen, Rize, NE Turkey). *Environmental monitoring and assessment*, 156, 241-255.
- Kirschbaum, -. D. 2016. *Landslides: Landslide Pilot*.
- Kirschbaum, D. & Stanley, T. 2018. Satellite-based assessment of rainfall-triggered landslide hazard for situational awareness. *Earth's Future*, 6, 505-523.
- Kjekstad, O. & Highland, L. 2009. Economic and social impacts of landslides. *Landslides—disaster risk reduction*. Springer.
- Knapen, A., Kitutu, M. G., Poesen, J., Breugelmans, W., Deckers, J. & Muwanga, A. 2006. Landslides in a densely populated county at the footslopes of Mount Elgon (Uganda): characteristics and causal factors. *Geomorphology*, 73, 149-165.
- Knutson, T. R., McBride, J. L., Chan, J., Emanuel, K., Holland, G., Landsea, C., Held, I., Kossin, J. P., Srivastava, A. & Sugi, M. 2010. Tropical cyclones and climate change. *Nature geoscience*, 3, 157-163.
- Korup, O. 2005. Large landslides and their effect on sediment flux in South Westland, New Zealand. *Earth Surface Processes and Landforms: The Journal of the British Geomorphological Research Group*, 30, 305-323.
- Korup, O., Densmore, A. L. & Schlunegger, F. 2010. The role of landslides in mountain range evolution. *Geomorphology*, 120, 77-90.

- Kubota, H. & Chan, J. C. 2009. Interdecadal variability of tropical cyclone landfall in the Philippines from 1902 to 2005. *Geophysical Research Letters*, 36.
- Kumar, V., Gupta, V., Jamir, I. & Chatteraj, S. L. 2019. Evaluation of potential landslide damming: Case study of Urni landslide, Kinnaur, Satluj valley, India. *Geoscience Frontiers*, 10, 753-767.
- Kumar, V., Sharma, K.V., Caloiero, T., Mehta, D.J. and Singh, K., 2023. Comprehensive overview of flood modeling approaches: A review of recent advances. *Hydrology*, 10(7), p.141.
- Langhammer, J. 2010. Analysis of the relationship between the stream regulations and the geomorphologic effects of floods. *Natural Hazards*, 54, 121-139.
- Larsen, I. J., Montgomery, D. R. & Korup, O. 2010. Landslide erosion controlled by hillslope material. *Nature Geoscience*, 3, 247-251.
- Lecomte, D. 2020. International Weather Events 2019: Historic Heat, Hurricanes, and Fires. *Weatherwise*, 73, 24-31.
- Lee, S. & Evangelista, D. G. 2005. Landslide susceptibility mapping using probability and statistics models in Baguio City, Philippines. *ISPRS 31st International Symposium on Remote Sensing of Environment*, Saint Petersburg, Russia. 20-24.
- Legros, F. 2002. The mobility of long-runout landslides. *Engineering geology*, 63, 301-331.
- Leopold, L. B. & Maddock, T. 1953. *The hydraulic geometry of stream channels and some physiographic implications*, US Government Printing Office.
- Lewin, J. 2013. Enlightenment and the GM floodplain. *Earth Surface Processes and Landforms*, 38, 17-29.

- Li, G., West, A. J., Densmore, A. L., Hammond, D. E., Jin, Z., Zhang, F., Wang, J. & Hilton, R. G. 2016. Connectivity of earthquake-triggered landslides with the fluvial network: Implications for landslide sediment transport after the 2008 Wenchuan earthquake. *Journal of Geophysical Research: Earth Surface*, 121, 703-724.
- Liébault, F. & Piégay, H. 2002. Causes of 20th century channel narrowing in mountain and piedmont rivers of southeastern France. *Earth Surface Processes and Landforms: The Journal of the British Geomorphological Research Group*, 27, 425-444.
- Lipad. 2018. Pinacanauan De Ilagan 100 Year Flood Hazard Map [Online]. Available: https://lipad-fmc.dream.upd.edu.ph/layers/geonode%3Apinacanauan_de_ilagan_fh100yr_10m#more [Accessed 20th February 2022].
- Liu, W., Hu, Y.-X., He, S.-M., Zhou, J.-W. & Chen, K.-T. 2021. A Numerical Study of the Critical Threshold for Landslide Dam Formation Considering Landslide and River Dynamics. *Frontiers in Earth Science*, 9, 651887.
- Magilligan, F. J. 1992. Thresholds and the spatial variability of flood power during extreme floods. *Geomorphology*, 5, 373-390.
- Magilligan, F.J., Buraas, E.M. and Renshaw, C.E., 2015. The efficacy of stream power and flow duration on geomorphic responses to catastrophic flooding. *Geomorphology*, 228, pp.175-188.
- Malamud, B. D., Turcotte, D. L., Guzzetti, F. & Reichenbach, P. 2004. Landslide inventories and their statistical properties. *Earth Surface Processes and Landforms*, 29, 687-711.
- Mangeney-Castelnau, A., Bouchut, F., Vilotte, J., Lajeunesse, E., Aubertin, A. & Pirulli, M. 2005. On the use of Saint Venant equations to simulate the

- spreading of a granular mass. *Journal of Geophysical Research: Solid Earth*, 110.
- Mcardell, B. W., Bartelt, P. & Kowalski, J. 2007. Field observations of basal forces and fluid pore pressure in a debris flow. *Geophysical research letters*, 34.
- Mcardell, B. W. & Sartori, M. 2021. The illgraben torrent system. *Landscapes and landforms of Switzerland*, 367-378.
- Mcdougall, S. 2017. 2014 Canadian Geotechnical Colloquium: Landslide runout analysis—current practice and challenges. *Canadian Geotechnical Journal*, 54, 605-620.
- Mcdougall, S. & Hungr, O. 2005. Dynamic modelling of entrainment in rapid landslides. *Canadian Geotechnical Journal*, 42, 1437-1448.
- Melillo, M., Brunetti, M. T., Peruccacci, S., Gariano, S. L., Roccati, A. & Guzzetti, F. 2018. A tool for the automatic calculation of rainfall thresholds for landslide occurrence. *Environmental Modelling & Software*, 105, 230-243.
- Mergili, M. 2014-2023. r.avaflow - The mass flow simulation tool.
r.avaflow.direct Web interface.
- Mergili, M., Fischer, J.-T., Krenn, J. & Pudasaini, S. P. 2017. r. avaflow v1, an advanced open-source computational framework for the propagation and interaction of two-phase mass flows. *Geoscientific Model Development*, 10, 553-569.
- Mergili, M., Jaboyedoff, M., Pullarello, J. & Pudasaini, S. P. 2020. Back calculation of the 2017 Piz Cengalo–Bondo landslide cascade with r. avaflow: what we can do and what we can learn. *Natural Hazards and Earth System Sciences*, 20, 505-520.

- Mergili, M. & Pudasaini, S. 2019. r. avaflow–The open source mass flow simulation model.
- Mergili, M. & Pudasaini, S. P. 2014-2023. Current version: r.avaflow 3 Current release: 20230127 [Online]. Available: <https://www.landslidemodels.org/r.avaflow/> [Accessed 20 Spetember 2022].
- Meyer-Peter, E. & Müller, R. 1948. Formulas for bed-load transport. IAHSR 2nd meeting, Stockholm, appendix 2. IAHR.
- Meyrat, G., Mcardell, B., Ivanova, K., Müller, C. & Bartelt, P. 2022. A dilatant, two-layer debris flow model validated by flow density measurements at the Swiss illgraben test site. *Landslides*, 19, 265-276.
- Milliman, J. D. & Syvitski, J. P. 1992. Geomorphic/tectonic control of sediment discharge to the ocean: the importance of small mountainous rivers. *The journal of Geology*, 100, 525-544.
- Mondini, A. C., Chang, K.-T. & Yin, H.-Y. 2011. Combining multiple change detection indices for mapping landslides triggered by typhoons. *Geomorphology*, 134, 440-451.
- Montgomery, D. R. & Buffington, J. M. 1998. Channel processes, classification, and response. *River Ecology and Management: Lessons from the Pacific Coastal Ecoregion*, RJ Naiman and RE Bilby (Editors). Springer-Verlag, New York, New York, 13-42.
- Mouratidis, A. 2010. Use of satellite Geodesy in slope stability monitoring. National Observatory of Athens.
- Mueller, E. R. & Pitlick, J. 2013. Sediment supply and channel morphology in mountain river systems: 1. Relative importance of lithology, topography,

and climate. *Journal of Geophysical Research: Earth Surface*, 118, 2325-2342.

NASA. 2006. Historic Tropical Cyclone Tracks. [Online] Available:

<https://earthobservatory.nasa.gov/images/7079/historic-tropical-cyclone-tracks> [Accessed 13/10/2023]

Nasa. 2019. Kammuri – Northwestern Pacific Ocean [Online]. Available:

<https://blogs.nasa.gov/hurricanes/tag/kammuri-2019/> [Accessed 20 October 2021].

Ndrmmc. 2014. SitRep No. 108 Effects of Typhoon Yolanda (Haiyan) [Online].

National Disaster Risk Reduction and Management Council. Available:

[http://www.ndrrmc.gov.ph/attachments/article/1329/Effects_of_Typhoon_YOLANDA_\(HAIYAN\)_SitRep_No_108_03APR2014.pdf](http://www.ndrrmc.gov.ph/attachments/article/1329/Effects_of_Typhoon_YOLANDA_(HAIYAN)_SitRep_No_108_03APR2014.pdf) [Accessed 4th January 2021].

Ndrmmc. 2016. SitRep No. 08 re Preparedness Measures and Effects of Super Typhoon "LAWIN" (I.N. Haima) [Online]. National Disaster Risk Reduction and Management Council.

Available:http://ndrrmc.gov.ph/attachments/article/3259/SitRep_No_02_re_Preparedness_Measures_and_Effects_of_TD_Urduja_KAI-TAK_as_of_15DEC2017_0800H.pdf [Accessed 17th April 2022].

Ndrmmc. 2017. SitRep No. 02 re Preparedness Measures and Effects of Tropical Depression "Urduja" [Online]. National Disaster Risk Reduction and Management Council.

Available:http://ndrrmc.gov.ph/attachments/article/3259/SitRep_No_02_re_Preparedness_Measures_and_Effects_of_TD_Urduja_KAI-TAK_as_of_15DEC2017_0800H.pdf [Accessed 4th January 2021].

- Ndrmmc. 2020. Final Report regarding Preparedness Measures and Effects for Typhoon “TISOY” (I.N. “KAMMURI”) [Online]. National Disaster Risk Reduction and Management Council. Available: [http://www.ndrrmc.gov.ph/attachments/article/1329/Effects_of_Typhoon_YOLANDA_\(HAIYAN\)_SitRep_No_108_03APR2014.pdf](http://www.ndrrmc.gov.ph/attachments/article/1329/Effects_of_Typhoon_YOLANDA_(HAIYAN)_SitRep_No_108_03APR2014.pdf) [Accessed 17th April 2022].
- Nelson, N. C., Erwin, S. O. & Schmidt, J. C. 2013. Spatial and temporal patterns in channel change on the Snake River downstream from Jackson Lake dam, Wyoming. *Geomorphology*, 200, 132-142.
- Nolasco-Javier, D., Kumar, L. & Tengonciang, A. M. P. 2015. Rapid appraisal of rainfall threshold and selected landslides in Baguio, Philippines. *Natural hazards*, 78, 1587-1607.
- Nones, M. 2019. Dealing with sediment transport in flood risk management. *Acta Geophysica*, 67, 677-685.
- Nuth, C. & Kääb, A. 2011. Co-registration and bias corrections of satellite elevation data sets for quantifying glacier thickness change. *The Cryosphere*, 5, 271-290.
- Observatory, M. 2016. Typhoon Haima (Lawin) Report #4 20 October 2016, 3.00PM PHT [Online]. Available: https://www.observatory.ph/wp-content/uploads/2016/10/TCHaima_Report4_20Oct2016-3.00PM.pdf [Accessed 17th April 2022].
- Oguchi, T., Saito, K., Kadomura, H. & Grossman, M. 2001. Fluvial geomorphology and paleohydrology in Japan. *Geomorphology*, 39, 3-19.

- Page, M., Reid, L. & Lynn, I. 1999. Sediment production from Cyclone Bola landslides, Waipaoa catchment. *Journal of Hydrology (New Zealand)*, 289-308.
- Palaseanu-Lovejoy, M., Bisson, M., Spinetti, C., Buongiorno, M. F., Alexandrov, O. & Cecere, T. 2019. High-resolution and accurate topography reconstruction of Mount Etna from pleiades satellite data. *Remote Sensing*, 11, 2983.
- Parida, S., Tandon, S. & Singh, V. 2017. Controls on channel width in an intermontane valley of the frontal zone of the northwestern Himalaya. *Geomorphology*, 278, 12-27.
- Parker, R. N., Hales, T. C., Mudd, S. M., Grieve, S. W. D. & Constantine, J. A. 2016. Colluvium supply in humid regions limits the frequency of storm-triggered landslides. *Scientific Reports*, 6, 34438.
- Pastor, M., Haddad, B., Sorbino, G., Cuomo, S. & Drempevic, V. 2009. A depth-integrated, coupled SPH model for flow-like landslides and related phenomena. *International Journal for numerical and analytical methods in geomechanics*, 33, 143-172.
- Patel, D. P., Ramirez, J. A., Srivastava, P. K., Bray, M. & Han, D. 2017. Assessment of flood inundation mapping of Surat city by coupled 1D/2D hydrodynamic modeling: a case application of the new HEC-RAS 5. *Natural Hazards*, 89, 93-130.
- Pecchi, M., Marchi, M., Moriondo, M., Forzieri, G., Ammoniaci, M., Bernetti, I., Bindi, M. & Chirici, G. 2020. Potential impact of climate change on the forest coverage and the spatial distribution of 19 key forest tree species in Italy under RCP4.5 IPCC trajectory for 2050s.

- Perez, G. J. P. & Comiso, J. C. 2014. Seasonal and interannual variabilities of Philippine vegetation as seen from space. *Philippine Journal of Science*, 143, 147-155.
- Picarelli, L., Oboni, F., Evans, S., Mostyn, G. & Fell, R. 2005. Hazard characterization and quantification. *Landslide risk management*. CRC Press.
- Pitlick, J., Marr, J. & Pizzuto, J. 2013. Width adjustment in experimental gravel-bed channels in response to overbank flows. *Journal of Geophysical Research: Earth Surface*, 118, 553-570.
- Pitman, E. B. & Le, L. 2005. A two-fluid model for avalanche and debris flows. *Philosophical Transactions of the Royal Society A: Mathematical, Physical and Engineering Sciences*, 363, 1573-1601.
- Poeppl, R. E., Keesstra, S. D. & Maroulis, J. 2017. A conceptual connectivity framework for understanding geomorphic change in human-impacted fluvial systems. *Geomorphology*, 277, 237-250.
- Pradhan, B., Sezer, E. A., Gokceoglu, C. & Buchroithner, M. F. 2010. Landslide susceptibility mapping by neuro-fuzzy approach in a landslide-prone area (Cameron Highlands, Malaysia). *IEEE Transactions on Geoscience and Remote Sensing*, 48.
- Prosser, I. P., Hughes, A. O. & Rutherford, I. D. 2000. Bank erosion of an incised upland channel by subaerial processes: Tasmania, Australia. *Earth Surface Processes and Landforms: The Journal of the British Geomorphological Research Group*, 25, 1085-1101.
- Pudasaini, S. P. 2012. A general two-phase debris flow model. *Journal of Geophysical Research: Earth Surface*, 117.

- Pudasaini, S. P. & Krautblatter, M. 2021. The mechanics of landslide mobility with erosion. *Nature communications*, 12, 1-15.
- Pudasaini, S. P. & Mergili, M. 2019. A multi-phase mass flow model. *Journal of Geophysical Research: Earth Surface*, 124, 2920-2942.
- Pulhin, J. M., Shaw, R. & Pereira, J. J. 2010. Climate change adaptation and disaster risk reduction: key challenges and ways forward. *Climate Change Adaptation and Disaster Risk Reduction: An Asian Perspective*. Emerald Group Publishing Limited.
- Rabonza, M., Felix, R., Lagmay, A. M., Eco, R., Ortiz, I. J. & Aquino Chow, D. 2016. Shallow landslide susceptibility mapping using high-resolution topography for areas devastated by super typhoon Haiyan. *Landslides*, 13, 201-210.
- Ramos, A. M. & Nees, L. B. 2017. A MULTI-SECTORAL ANALYSIS OF THE RESPONSES TO SUPER TYPHOON HAIMA IN SANTA MARIA. *International course on water and water management in the Philippines*, 151.
- Rathburn, S., Bennett, G., Wohl, E., Briles, C., Mcelroy, B. & Sutfin, N. 2017. The fate of sediment, wood, and organic carbon eroded during an extreme flood, Colorado Front Range, USA. *Geology*, 45, 499-502.
- Reichenbach, P., Busca, C., Mondini, A. C. & Rossi, M. 2014. The Influence of Land Use Change on Landslide Susceptibility Zonation: The Briga Catchment Test Site (Messina, Italy). *Environmental Management*, 54, 1372-1384.
- Reichenbach, P., Rossi, M., Malamud, B. D., Mihir, M. & Guzzetti, F. 2018. A review of statistically-based landslide susceptibility models. *Earth-Science Reviews*, 180, 60-91.

- Reid, L. & Page, M. 2003. Magnitude and frequency of landsliding in a large New Zealand catchment. *Geomorphology*, 49, 71-88.
- Rhoads, B. L. 2020. *River dynamics: geomorphology to support management*, Cambridge University Press.
- Rickli, C. & Graf, F. 2009. Effects of forests on shallow landslides—case studies in Switzerland. *Forest Snow and Landscape Research*, 82, 33-44.
- Righini, M., Surian, N., Wohl, E., Marchi, L., Comiti, F., Amponsah, W. & Borga, M. 2017. Geomorphic response to an extreme flood in two Mediterranean rivers (northeastern Sardinia, Italy): Analysis of controlling factors. *Geomorphology*, 290, 184-199.
- Robinson, R. A. & Slingerland, R. L. 1998. Origin of fluvial grain-size trends in a foreland basin; the Pocono Formation on the central Appalachian Basin. *Journal of Sedimentary Research*, 68, 473-486.
- Rowland, J. C., Shelef, E., Pope, P. A., Muss, J., Gangodagamage, C., Brumby, S. P. & Wilson, C. J. 2016. A morphology independent methodology for quantifying planview river change and characteristics from remotely sensed imagery. *Remote Sensing of Environment*, 184, 212-228.
- Ruiz-Villanueva, V., Badoux, A., Rickenmann, D., Böckli, M., Schläfli, S., Steeb, N., Stoffel, M. & Rickli, C. 2018. Impacts of a large flood along a mountain river basin: the importance of channel widening and estimating the large wood budget in the upper Emme River (Switzerland). *Earth Surface Dynamics*, 6, 1115-1137.
- Ruiz-Villanueva, V., Díez-Herrero, A., Ballesteros, J. & Bodoque, J. 2014. Potential large woody debris recruitment due to landslides, bank erosion and floods in mountain basins: a quantitative estimation approach. *River Research and Applications*, 30, 81-97.

- Saldivar-Sali, A. & Einstein, H. H. 2007. A Landslide Risk Rating System for Baguio, Philippines. *Engineering Geology*, 91, 85-99.
- Salvatici, T., Tofani, V., Rossi, G., D'ambrosio, M., Tacconi, C., Stefanelli, Masi, E., Rosi, A., Pazzi, V., Vannoci, P., Petrolo, Catani, F., Ratto, S., Stevenin, H. & Casagli, N. 2018. Application of a physically-based model to forecast shallow landslides at regional scale. *Journal of Geotechnical and Geoenvironmental Engineering*, 144, 04018013.
- Samia, J., Temme, A., Bregt, A., Wallinga, J., Guzzetti, F., Ardizzone, F. & Rossi, M. 2017. Do landslides follow landslides? Insights in path dependency from a multi-temporal landslide inventory. *Landslides*, 14, 547-558.
- Santi, P. M., Dewolfe, V. G., Higgins, J. D., Cannon, S. H. & Gartner, J. E. 2008. Sources of debris flow material in burned areas. *Geomorphology*, 96, 310-321.
- Sargeant, S., Finlayson, A., Dijkstra, T., Flinn, B., Schofield, H., Morel, L. M., Twigg, J., Lovell, E., Stephenson, V. & Adhikari, B. 2020. The influence of the physical environment on self-recovery after disasters in Nepal and the Philippines. *International Journal of Disaster Risk Reduction*, 50, 101673.
- Savage, S. B. & Hutter, K. 1989. The motion of a finite mass of granular material down a rough incline. *Journal of fluid mechanics*, 199, 177-215.
- Schraml, K., Thomschitz, B., Mcardell, B., Graf, C. & Kaitna, R. 2015. Modeling debris-flow runout patterns on two alpine fans with different dynamic simulation models. *Natural Hazards and Earth System Science*, 15, 1483-1492.
- Schuster, R. L. 1996. LANDSLIDES: INVESTIGATION AND MITIGATION. CHAPTER 2-SOCIOECONOMIC SIGNIFICANCE OF LANDSLIDES.

- Schwanghart, W. & Scherler, D. 2014. TopoToolbox 2–MATLAB-based software for topographic analysis and modeling in Earth surface sciences. *Earth Surface Dynamics*, 2, 1-7.
- Sevieri, G. & Galasso, C. Typhoon fragility analysis and climate change impact assessment of Filipino cultural heritage asset roofs. Proceedings of the International Conference on Structural Dynamic, EUROODYN, 2020. European Association for Structural Dynamics (EASD), 4763-4776.
- Shaller, P. & Shaller, A. 1996. Review of Proposed Mechanisms for Sturzstroms (Long-Runout Landslides), Sturzstroms and Detachment Faults, Anza-Borrego Desert State Park California, PL Abbott and DC Seyrnour, Editors, 1996, South Coast Geological Society. Inc., Santa Ana, CA, 185-202.
- Shaw, R., Pulhin, J. M. & Pereira, J. J. 2010. Climate change adaptation and disaster risk reduction: An Asian perspective, Emerald Group Publishing Limited.
- Solomon, S., Qin, D., Manning, M., Chen, Z., Marquis, M., Averyt, K., Tignor, M. & Miller, H. 2007. IPCC fourth assessment report (AR4). Climate change, 374.
- Spotila, J. A., Moskey, K. A. & Prince, P. S. 2015. Geologic controls on bedrock channel width in large, slowly-eroding catchments: Case study of the New River in eastern North America. *Geomorphology*, 230, 51-63.
- Stark, C. P. & Hovius, N. 2001. The characterization of landslide size distributions. *Geophysical research letters*, 28, 1091-1094.
- Stephenson, V., Finlayson, A. & Miranda Morel, L. 2018. A risk-based approach to shelter resilience following flood and typhoon damage in rural Philippines. *Geosciences*, 8, 76.

- Stumpf, A., Malet, J.-P., Allemand, P. & Ulrich, P. 2014. Surface reconstruction and landslide displacement measurements with Pléiades satellite images. *ISPRS Journal of Photogrammetry and Remote Sensing*, 95, 1-12.
- Surian, N., Ziliani, L., Comiti, F., Lenzi, M. A. & Mao, L. 2009. Channel adjustments and alteration of sediment fluxes in gravel-bed rivers of North-Eastern Italy: potentials and limitations for channel recovery. *River research and applications*, 25, 551-567.
- Sutherland, D. G., Ball, M. H., Hilton, S. J. & Lisle, T. E. 2002. Evolution of a landslide-induced sediment wave in the Navarro River, California. *Geological Society of America Bulletin*, 114, 1036-1048.
- Takahashi, T. 1991. Debris flow. IAHR monograph series. Rotterdam: Balkema.
- Tarolli, P. 2014. High-resolution topography for understanding Earth surface processes: Opportunities and challenges. *Geomorphology*, 216, 295-312.
- Taylor, P. D., Fahrig, L., Henein, K. & Merriam, G. 1993. Connectivity is a vital element of landscape structure. *Oikos*, 571-573.
- Tebbens, S. 2020. Landslide scaling: a review. *Earth and Space Science*, 7.
- Thompson, C. & Croke, J. 2013. Geomorphic effects, flood power, and channel competence of a catastrophic flood in confined and unconfined reaches of the upper Lockyer valley, southeast Queensland, Australia. *Geomorphology*, 197, 156-169.
- Tseng, C. M., Lin, C. W. & Hsieh, W. D. 2015. Landslide susceptibility analysis by means of event-based multi-temporal landslide inventories. *Natural Hazards and Earth System Sciences Discussions*, 3, 1137-1173.

- Tsou, C.-Y., Feng, Z.-Y. & Chigira, M. 2011. Catastrophic landslide induced by typhoon Morakot, Shiaolin, Taiwan. *Geomorphology*, 127, 166-178.
- Tucker, C. J. & Sellers, P. 1986. Satellite remote sensing of primary production. *International journal of remote sensing*, 7, 1395-1416.
- Van Asch, T. W., Buma, J. & Van Beek, L. 1999. A view on some hydrological triggering systems in landslides. *Geomorphology*, 30, 25-32.
- Van Der Meide, M. & Pagaran, K. 2017. THE IMPACT OF TYPHOON HAIMA/LAWIN ON CORN FARMERS IN CABAGAN AND SANTA MARIA, ISABELA PHILIPPINES. *International course on water and water management in the Philippines*, 79.
- Varnes, D. J. 1978. Slope movement types and processes. *Special report*, 176, 11-33.
- Verbesselt, J., Hyndman, R., Newnham, G. & Culvenor, D. 2010. Detecting trend and seasonal changes in satellite image time series. *Remote sensing of Environment*, 114, 106-115.
- Voellmy, A. 1955. *Über die Zerstörungskraft von Lawinen*. Schweizerische Bauzeitung, Jahrg.,
- Von Boetticher, A., Turowski, J. M., Mcardell, B. W., Rickenmann, D. & Kirchner, J. W. 2016. DebrisInterMixing-2.3: a finite volume solver for three-dimensional debris-flow simulations with two calibration parameters—Part 1: Model description. *Geoscientific Model Development*, 9, 2909-2923.
- Wainwright, J., Turnbull, L., Ibrahim, T. G., Lexartza-Artza, I., Thornton, S. F. & Brazier, R. E. 2011. Linking environmental regimes, space and time: Interpretations of structural and functional connectivity. *Geomorphology*, 126, 387-404.

- Wang, L., Chang, M., Dou, X., Ma, G. & Yang, C. 2017. Analysis of river blocking induced by a debris flow. *Geofluids*, 2017.
- Whipple, K. X. 2004. Bedrock rivers and the geomorphology of active orogens. *Annu. Rev. Earth Planet. Sci.*, 32, 151-185.
- Williams, G. & Costa, J. 1988. Geomorphic measurements after a flood. *Flood Geomorphology*. John Wiley & Sons New York. 1988. p 65-77.
- Wobus, C. W., Tucker, G. E. & Anderson, R. S. 2006. Self-formed bedrock channels. *Geophysical Research Letters*, 33.
- Wohl, E., Cenderelli, D. A., Dwire, K. A., Ryan-Burkett, S. E., Young, M. K. & Fausch, K. D. 2010. Large in-stream wood studies: a call for common metrics. *Earth Surface Processes and Landforms: The Journal of the British Geomorphological Research Group*, 35, 618-625.
- Wolman, M. G. & Gerson, R. 1978. Relative scales of time and effectiveness of climate in watershed geomorphology. *Earth surface processes*, 3, 189-208.
- Wyżga, B. 1997. Methods for studying the response of flood flows to channel change. *Journal of Hydrology*, 198, 271-288.
- Yanites, B. J., Mitchell, N. A., Bregy, J. C., Carlson, G. A., Cataldo, K., Holahan, M., Johnston, G. H., Nelson, A., Valenza, J. & Wanker, M. 2018. Landslides control the spatial and temporal variation of channel width in southern Taiwan: Implications for landscape evolution and cascading hazards in steep, tectonically active landscapes. *Earth Surface Processes and Landforms*, 43, 1782-1797.
- Yang, C.T. and Stall, J.B., 1974. Unit stream power for sediment transport in natural rivers.

- Yap, S. L., Davies, S. J. & Condit, R. 2016. Dynamic response of a Philippine dipterocarp forest to typhoon disturbance. *Journal of Vegetation Science*, 27, 133-143.
- Yonson, R., Noy, I. & Gaillard, J. 2018. The measurement of disaster risk: An example from tropical cyclones in the Philippines. *Review of Development Economics*, 22, 736-765.
- Zhang, J., Wang, Z., Dong, Z., Zhou, Y., Li, Z., Cui, Y. & Zheng, S. 2022. Morphological response of the upper Yangtze Estuary to changes in natural and anthropogenic factors. *River Research and Applications*.
- Zhang, T., Yin, Y., Li, B., Liu, X., Wang, M., Gao, Y., Wan, J. and Gnyawali, K.R., 2023. Characteristics and dynamic analysis of the February 2021 long-runout disaster chain triggered by massive rock and ice avalanche at Chamoli, Indian Himalaya. *Journal of Rock Mechanics and Geotechnical Engineering*, 15(2), pp.296-308.
- Ziliani, L. & Surian, N. 2012. Evolutionary trajectory of channel morphology and controlling factors in a large gravel-bed river. *Geomorphology*, 173, 104-117.